KU Leuven
Biomedical Sciences Group
Faculty of Medicine
Department of Cellular and Molecular Medicine
Laboratory of Biosignaling and Therapeutics

Investigations towards understanding the molecular mechanisms that underlie PRL-3's role in tumorigenesis

Giulia VARSANO

Jury:

Promoter:	Prof. Dr. Mathieu Bollen
Co-promoter:	Dr. Maja Köhn
Chair:	Prof. Dr. Humbert De Smedt
Secretary:	Els Wellens
Jury members:	Prof. Dr. Geert Berx
	Dr. Carsten Schultz
	Prof. Dr. Anna Sablina
	Prof. Dr. Veerle Janssens

Dissertation presented in partial fulfillment of the requirements for the degree of Doctor of Biomedical Sciences

March 2014

Acknowledgments

This thesis is presented with respect and gratitude to Dr. Maja Köhn, for the continuous support of my PhD study and research, for her patience, motivation and enthusiasm. I would like also to thank my thesis committee members: Prof. Dr. Mathieu Bollen and Dr. Carsten Schultz for their insightful comments and Prof. Dr. Geert Berx, Prof. Dr. Anna Sablina, Prof. Dr. Veerle Janssens for accepting to be members of my examining committee. I also would like to thanks Dr. Jeroen Krijgsveld for his kindness and disponibility regarding Dutch translation.

My sincere thanks also go to current and former lab members, a special thank to Irina, Pablo, Karolina, Yansong and Birgit for all the fun we had together, for being willing to hear all my complaints, for waiting the afternoon to start a conversation.

I am thankful for and would like to acknowledge many others who helped me along the way: Yuri, for accepting me the way I am, for this journey together, although things don't always go the way we planned; Antonella who was there, everyday, she gave me all the wisdom and all the courage that I needed. I want to thank also all the precious friends with whom I shared these four years, especially Flavia, Claudia, Marzia, Andrea, Claudio, Maria, Rodolfo, Niccolo, Enrico, Erika, Tilman, Michele, Hossein, Alfredo, Matteo and Ilaria.

Finally, I would like to thank my family, especially my mother and father for always believing in me, for their continuous love and their support in my decisions.

I want to give thanks to the divine
Labyrinth of causes and effects
For the diversity of beings
That form this singular universe,
For love, which lets us see others
As God sees them,
For morning, that gives us the illusion of a new beginning,
For night, its darkness and its astronomy,
For the bravery and happiness of others,
For my country, sensed in jasmine flowers
Or in an old sword,
For music, that mysterious form of time.

Jorge Luis Borges.

Table of Contents

List of abbreviations

2D	Two-dimensional
3D	Three-dimensional
5-ptase	5-phosphatase
ADP	Adenosine diphosphate
AJs	Adherens junctions
AMIS	Apical membrane initiation site
Anx2	AnnexinA2
aPKC	Atypical protein kinase C
Arf	ADP-ribosylation factor
CD	Circular dichroism
CDC25	Cell division cycle 25
Cdc42	Cell division control protein 42
CDH22	Cadherin 22
Cep55	Centrosomal protein 55
CHO	Chinese hamster ovary
CR1	Conserved region 1
CRIB	Cdc42/Rac interactive binding
Csk	C-Src kinase
DAG	Diacylglycerol
diC8	Dioctanoyl
DLD-1	D.L. Dexter-1
DSP	Dual specificity phosphatase
ECM	Extracellular matrix
EF2	Elongation factor 2
EHS	Engelbreth-Holm-Swarm
EMT	Epithelial-mesenchymal transition
ERK1/2	Extracellular signal-regulated kinase 1/2
ERM	Ezrin/radixin/moesin
FAK	Focal adhesion kinase
FKBP38	FK506-binding protein 38
GDP	Guanosine 5′-diphosphate
GEF	Guanine nucleotide exchange factor
GFP	Green fluorescent protein
GST	Glutatione S-transferase
GTP	Guanosine-5'-triphosphate
HAD	Haloacid dehalogenase
HEK293	Human embryonic kidney 293
HUVEC	Human umbilical vein endothelial cells
IP3	Inositol(1,4,5)-triphosphate
JAMs	Junctional adhesion molecules
kDa	KiloDalton
Kifs	Kinesin superfamily proteins
MCF10A	Michigan cancer foundation-10A
MCF7	Michigan Cancer Foundation-7

MD	Molecular dynamics
MDCK	Madin-Darby canine kidney
MEF2C	Myocite enhancer factor 2C
MKLP1	Mitotic kinesin-like protein
MKP3	MAP kinase phosphatase 3
MTMR2	Myotubularin related protein 2
OMFP	3-O-methylfluorescein phosphate
p53	Protein 53
Par3	Partitioning defective 3 homolog
Par6	Partitioning defective 6 homolog
PB1	Phox and Bem1p 1
PCBP1	PolyC-RNA-binding protein 1
PDZ	Postsynaptic density 95/disc large/zonula occludens-1
PI3K	Phoisphoinositide-3-kinase
PIPKIγ	Phosphate 5 kinase type Iγ
PLC	Phospholipase C
PRL	Phosphatases of regenerating liver
pSer	Phosphoserine
PtdIns	Phosphoinositides
PtdIns(3,4,5)P3	Phosphatidylinositol (3,4,5)-triphosphate
PtdIns(4,5)P2	Phosphatidylinositol (4,5)-bisphosphate
PTEN	Phosphatase and tensin homolog
pThr	Phosphothreonine
PTP	Protein tyrosin phosphatase
PTP1B	Protein tyrosine phosphatase 1B
pTyr	Phosphotyrosine
Rabs	Ras-related in brain proteins
Rac	Ras-related C3 botulinum toxin substrate
Rho	Ras homologous
Sec	Secretion related proteins
SH2	Src Homology 2
SHIP2	SH2-containing inositol 5'-phosphatase
Smad3	Mothers against decapentaplegic homolog 3
Src	Rous sarcoma oncogene cellular homolog
t-SNAREs	Target synaptosome-associated protein receptor
TGFb	Transforming growth factor beta
TIAM1	T-cell lymphoma invasion and metastasis 1
TJs	Tight junctions
TLC	Thin Layer Chromatography
UTR	Untranslanted region
VEGF	Vascular endothelial growth factor
WT	Wildtype
YFP	Yellow fluorescent protein
ZO	Zona occludens

Chapter I: General introduction

I.1 Phosphatase of regenerating liver 3 (PRL-3)

I.1.1. Protein phosphorylation/dephosphorylation

Eukaryotic cells are able to coordinate rapid responses to external stimuli as well as to preserve internal homeostasis. The final cellular outcome is the result of an integrated network of fine-tuned intracellular signalling pathways that are mainly based on dynamic events of phosphorylation and dephosphorylation. These modifications can for example activate or inhibit protein enzymatic activity, change protein-protein interaction affinity and/or modify protein subcellular localization. Protein phosphorylation is a reversible posttranslational modification that occurs mainly on hydroxyl-containing residues: serine, threonine and tyrosine. Protein kinases are the enzymes that catalyze the covalent attachment of a phosphoryl group to a hydroxyl-containing side chain, whereas protein phosphatases catalyze the transfer of the phosphate from a phosphoprotein to a water molecule (Cohen, 2002). Notably, kinases and phosphatases are also involved in the regulation of signal transduction affecting the phosphorylation of non-protein substrates, such as inositol phospholipids (Majerus and York, 2009).

Protein phosphatases have been classified into mechanistically distinct superfamilies that do not share any structural similarities and apparently evolved independently (Alonso et al., 2004). Based on the mechanism of catalysis protein phosphatases can be classified in:

a) The serine/threonine phosphatases superfamily wherein the catalysis proceeds without a phosphoenzyme intermediate, with the direct hydrolysis of the phosphosubstrate; the process strictly requires the presence of metal ions in the enzyme active site. The substrate specificity of this superfamily is obtained by combinatorial interaction between catalytic and regulatory subunits rather than specific aminoacid sequence recognition (Brautigan, 2013).
b) The haloacid dehalogenase (HAD) superfamily in which the nucleophile aspartic acid in the active site is an absolute requirement for the activity (Seifried et al., 2013).
c) The protein tyrosin phosphatase (PTP) superfamily wherein the catalytic cysteine in the active site forms a phosphoenzyme intermediate in the reaction with the substrate. The PTP superfamily is the largest class with 96 catalytically active

members and all the members share the consensus catalytic signature motif His-Cys-X_5-Arg (X= any aminoacid) (Li et al., 2013; Tonks, 2006, 2013). The PTP superfamily will be discussed in detail in the following paragraphs.

I.1.2. Protein Tyrosin phosphatases (PTPs)

I.1.2.A. Mechanism of catalysis

In the PTP superfamily the dephosphorylation reaction proceeds with a two-step mechanism (Fig. I.1). The first step involves the nucleophilic attack of the phosphate group by the thiol group of the catalytic cysteine. This reaction is facilitated by the presence of a conserved aspartic acid from a flanking loop that functions as a general acid, protonating the leaving group of the substrate. In the second step the same aspartic acid residue acts as a general base activating a water molecule leading to the hydrolysis of the phosphocysteine intermediate. This second step, in almost all PTPs, is facilitated by the presence of a serine or threonine residue that follows the arginine in the His-Cys-X_5-Arg signature. The hydroxyl group of this conserved residue is important for the breakdown of the phosphoenzyme intermediate (Kolmodin and Aqvist, 2001).

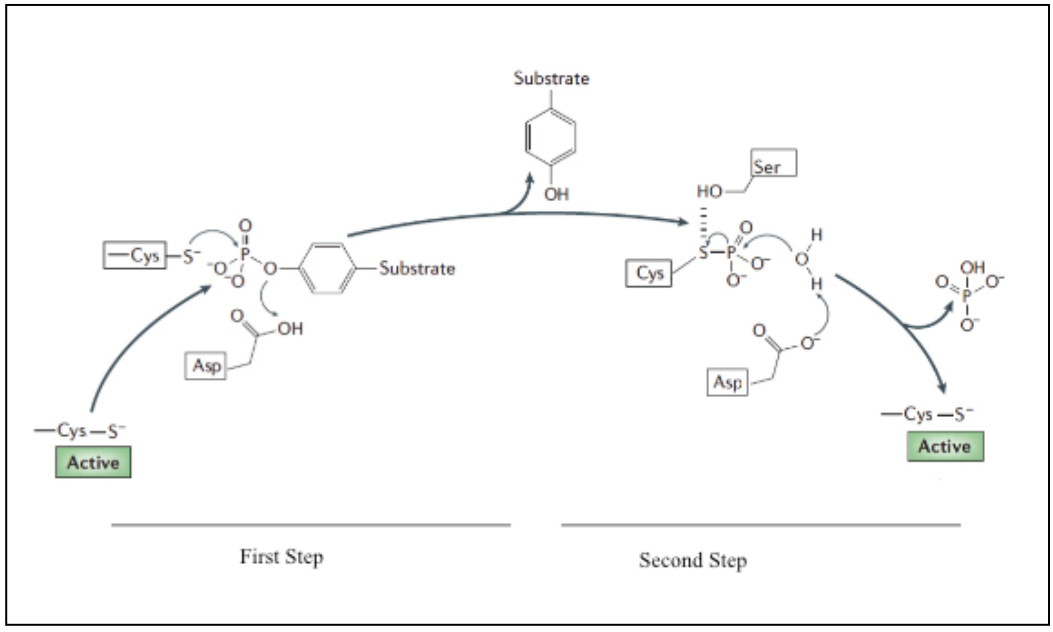

Figure I.1. PTPs catalytic mechanism. *A detailed description of the PTPs catalytic mechanism is reported in the main text. Black boxes highlight the critical catalytic residues. Adapted from Tonks (2006).*

I.1.2.B. PTP classification

Among the PTP superfamily two classes can be defined: the classical PTPs and the dual specificity phosphatases (DSPs) (Alonso et al., 2004; Tonks, 2006).

a) The classical PTP family comprises transmembrane as well as cytoplasmic enzymes characterized by phosphotyrosine (pTyr) specificity (Tonks, 2006). One of the best-characterized classical PTP is PTP1B. PTP1B is considered a prototype of this family, given that most of the findings on its structure, regulation and function have revealed principles valid for the whole classical PTP family (Tonks, 2003).

b) The DSPs family is a heterogeneous group of non-transmembrane phosphatases characterized by a shallow conformation of the catalytic pocket that allows them to accommodate a broad range of substrates. DSPs can dephosphorylate phosphoserine (pSer)/phosphothreonine (pThr) and pTyr residues as well as non-protein substrates. Some members of DSPs family, for example, show activity against phosphoinositides (Patterson et al., 2009; Pulido et al., 2013; Tonks, 2013). The most striking example of DSPs with a broad range of substrate specificity is the phosphatase PTEN (phosphatase and tensin homolog). The PTEN catalytic pocket is sufficiently large to accommodate the head group of phosphoinositides (PtdIns) as well as tyrosine-, threonine- and serine-phosphorylated phosphopepetides, with an unusual preference for highly acidic sequences (Song et al., 2012). *In vivo* experiments have confirmed PTEN activity against the phosphate in the 3' position of the inositol ring of PtdIns, mainly PtdIns(3,4,5)P_3 (see chapter I.2 for a detailed description of phosphoinositide molecules) (Maehama, 1998). Moreover, recently *in vivo* evidence of the protein phosphatase activity of PTEN has been provided, showing that the enzyme is able to dephosphorylate itself on the regulatory residues pSer and pThr (Tamguney and Stokoe, 2007; Zhang et al., 2012).

I.1.3. Phosphatases of regenerating liver (PRLs)

PRL phosphatases constitute a class of small (20 kDa), single domain phosphatases that belong to the DSP family. There are three members (PRL-1, PRL-2 and PRL-3) that share high sequence identity and key structural features unique to this family (Fig. I.2). PRLs contain the conserved catalytic PTP signature (His-Cys-X_5-Arg) but the active site is unusually hydrophobic and instead of the serine/threonine residue

that facilitates the breakdown of the phosphoenzyme intermediate an alanine is found in that position (Fig. I.1, Fig. I.2) (Al-Aidaroos and Zeng, 2010; Bessette et al., 2008; Rios et al., 2013; Stephens et al., 2005). All the three members contain a CAAX prenylation motif at the C-terminus (Where C is a cystein, A is an aliphatic aminoacid, and X is any aminoacid) that is uniquely characteristic to PRLs. The prenylation is essential for the anchoring of proteins to membrane compartments (Zeng et al., 2000). In close proximity to the farnesylation site, a stretch of basic aminoacids (polybasic sequence) facilitates the binding to the plasma membrane by interaction with negatively charged membrane phospholipids (Sun et al., 2007). Structural studies on PRL-1 and PRL-3 have also suggested a potential mechanism for *in vivo* regulation of PRL's activity based on the formation of an intramolecular disulfide bond between the catalytic cystein (Cys104) and the conserved cystein in position 49 (Fig. I.2) (Skinner et al., 2009). Notably, redox-regulation of the catalytic activity is not a PRL unique characteristic but has also been described for other DSP, such as PTEN (Boivin and Tonks, 2010).

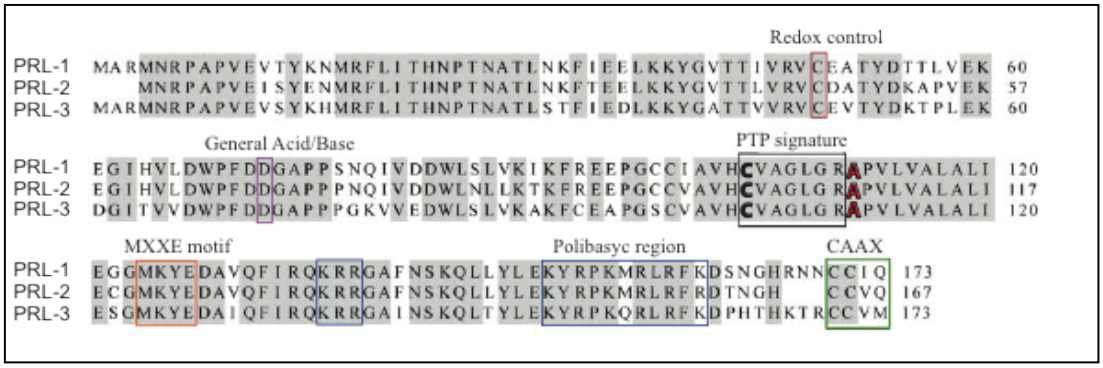

Figure I.2. PRLs sequence alignment. *Sequence alignment of human PRL-1, PRL-2 and PRL-3. Red box: cysteine involved in the redox-regulation of the catalytic activity (Cys 49 in PRL-3). Purple box: Aspartic acid involved in the mechanism of catalysis (Asp 72 in PRL-3). Black box: PTP signature motif, catalytic cysteine in bold (Cys 104 in PRL-3). The natural substitution Ser/Thr to Alanine is highlighted in red bold (Ala 111 in PRL-3). Orange box: Golgi targeting MXXE motif. Blue box: stretch of positive charge residues (polybasic sequence). Green box: CAAX prenylation motif. Adapted from B.J. Stephens (2005).*

Beyond sequence and structural similarities, PRLs share also the ability to promote cell proliferation, migration, invasion, tumor growth and metastasis (Al-Aidaroos and Zeng, 2010; Bessette et al., 2008; Stephens et al., 2005). Multiple lines of evidence are reinforcing the opinion that PRLs are a unique class of oncogenic phosphatases

that play a causative role in tumor metastasis (Guzińska-Ustymowicz and Pryczynicz, 2011) (see paragraph I.C.5. for a detailed description of PRL-3 in cancer metastasis).

Despite their similarities, PRLs exhibit a distinct pattern of tissue distribution. PRL-1 and PRL-2 are ubiquitously expressed in adult human tissues, although considerable variation in PRL-1 levels has been observed among different tissue types (Dumaual et al., 2006). In contrast, the expression of PRL-3 seems to be much more restricted. PRL-3 mRNA is largely confined to heart and skeletal muscle although, at the protein level, the expression was confirmed in rat fetal heart but neither in rat nor in human adult heart (Guo et al., 2006; Matter et al., 2001).

This thesis will mainly focus on PRL-3 and the next paragraphs will provide an overview on the current status of PRL-3 research.

I.1.3.A.The subcellular localization of PRL-3

The subcellular localization of PRL-3 is mainly governed by its C-terminal lipidation. It has been shown recently that the protein is subjected to a dual lipidation, i.e. farnesylation on the first and palmitoylation on the second cysteine of the CAAX box (Fig. I.2). The protein is mainly associated with the plasma membrane and intracellular punctuate structures that are suggested to be early endosomes (Nishimura and Linder, 2013; Zeng et al., 2000). Recently, it has also been reported that PRL-3 can associate with the Golgi apparatus and with the perinuclear endosomal compartments (Krndija et al., 2012). When the lipidation process is impaired, for example by application of prenylation inhibitors, the protein relocalizes to the nucleus; most probably the C-terminal polybasic sequence also acts as a nuclear localization signal. However a biological function of PRL-3 in the nucleus has not yet been demonstrated (Zeng et al., 2000).

I.1.3.B. The regulation of PRL-3

Multiple and sometimes contradictory scenarios for PRL-3 transcriptional, translational and post-translational regulation have been reported. These data are also often difficult to integrate considering the different experimental conditions and cell lines used. On the other hand, these findings, together with the extremely restricted pattern of expression, underline the idea of a fine-tuned regulation of PRL-3 levels and most likely activity, typical of oncogenes. Selected examples of PRL-3 regulation will be briefly discussed in the next paragraphs.

I.1.3.B.1. Transcriptional regulation

PRL-3 transcription is up-regulated in human umbilical vein endothelial cells (HUVEC) after stimulation with the growth factor VEGF (vascular endothelial growth factor) through the transcription factor MEF2C (myocyte enhancer factor 2C) (Xu et al., 2011). Additionally, it seems that PRL-3 itself, in lung cancer cell lines, is able to up-regulate VEGF expression, opening the possibility of a positive feedback loop of transcriptional regulation (Ming et al., 2009). Moreover, it has been reported that PRL-3 is a direct transcriptional p53 target gene, but contrary results have been obtained in different cell lines, suggesting a complex scenario of transcriptional regulation that is cell-type specific (Basak et al., 2008; Min et al., 2010). Recently, Jiang *et al*. (2011) reported the first example of PRL-3 negative transcriptional regulation. The authors demonstrate that TGFβ (transforming growth factor beta) signaling antagonizes PRL-3 expression via Smad3-dependent inhibition of PRL-3 promoter activity (Jiang et al., 2011). Interestingly, the authors propose that in tumors, for example from colorectal cancer, where the TGFβ signaling is often affected, the loss of the mentioned inhibitory effect could explain the elevated levels of PRL-3 (see below for a detailed description of the role of PRL-3 in cancer metastasis).

I.1.3.B.2. Post-transcriptional regulation

It has been shown that PRL-3 mRNA and protein levels often do not correlate. This is thought to be due to an inhibitory effect of the RNA binding protein PCBP1 (PolyC-RNA-binding protein 1) on PRL-3 mRNA translation. PCBP1 binds the the 5' untranslated region (UTR) of the PRL-3 transcript and suppresses its incorporation into the polyribosome (Wang et al., 2010).

I.1.3.B.3. Post-translational regulation

PRL-3 protein stability is also regulated. In MCF7 cancer cell lines for example, it has been shown that PRL-3 is targeted for degradation through the proteasome pathway as a result of the interaction with the protein FKBP38 (FK506-binding protein 38) (Choi et al., 2011).

Recently, it has also been reported that PRL-3 can be phosphorylated *in vitro* and *in vivo* by the tyrosin kinase Src. The primary site of phosphorylation is the conserved

Tyr53. The authors also provided a direct link between Tyr 53 phosphorylation on PRL-3 and the pro-invasion phenotype associated with PRL-3 overexpression (see paragraph I.1.3.d) (Fiordalisi et al., 2013). However, it is not clear by what mechanism phosphorylation affects the function of PRL-3 and in particular if the phosphorylation regulates the protein's catalytic activity.

I.1.3.C. Physiological roles of PRL-3

PRL-3 physiological functions are poorly investigated and unclear at the present. The generation of a knockout mouse has not provided clear insight about PRL-3's physiological roles. Mice without functional PRL-3 developed normally and did not present any apparent phenotype in the adult life. The only exception was a slight perturbation of the sex ratio, with lower number of male mice born (Zimmerman et al., 2013). These results are in contrast with the strong phenotype reported in mice lacking PRL-2, where reduced placenta development leads to severe fetal growth retardation (Dong et al., 2012). Notably, these remarkable differences between PRL-2/PRL-3 knockout mice may suggest that the functions of the two phosphatases are not overlapping *in vivo*.

I.1.3.D. PRL-3 and cancer metastasis

PRL-3 was originally identified as a protein that is highly overexpressed in all metastatic lesions derived from colorectal cancer (liver, lung, brain, and ovary). Notably, in this initial study the protein was neither detected in normal colorectal epithelium nor in the primary tumor, introducing the concept of a metastasis-associated phosphatase (Saha et al., 2001). In the past decade numerous studies have shown a tight correlation between elevated PRL-3 expression and the metastatic potential and poor prognosis outcome of multiple epithelial cancers, including gastric, breast, ovarian and lung cancers (Fig. I.3) (Al-Aidaroos and Zeng, 2010; Bessette et al., 2008; Guzińska-Ustymowicz and Pryczynicz, 2011; Rios et al., 2013; Stephens et al., 2005). Although it is generally accepted that PRL-3 could be an emerging prognostic marker for cancer metastasis, studies on PRL-3 knockout mice have recently opened the possibility that PRL-3 could also play a role in primary tumor formation. Indeed, PRL-3 knockout mice show a 50% reduction in colon tumors development after exposure to procarcinogenic and inflammatory agents (Zimmerman et al., 2013).

Nude mice-based experiments have extensively validated the causative role of PRL-3 in cancer metastasis showing that:

- PRL-3 expression promotes metastatic tumor spreading. Thus, *in vivo* injection of PRL-3-expressing B16 cells (mouse melanoma cells) into mice tail vein resulted in metastatic lung and liver lesions (Wu et al., 2004). Similar results were independently obtained by Zeng and colleagues, by showing that 100% of mice injected with PRL-3-expressing CHO cells (Chinese hamster ovary cells) had widespread lung tumors and, in some cases, liver metastasis (Zeng et al., 2003).
- PRL-3 expression triggers tumor angiogenesis. PRL-3-expressing CHO cells injected in nude mice not only promote the development of local tumors but also recruit host endothelial cells into the tumors to establish microvasculature (Zeng et al., 2003). As discussed previously, PRL-3 expression up-regulated VEGF levels in lung cancer cell lines. VEGF is a highly specific mitogen for endothelial cells, promoting the growth of blood vessels from pre-existing vasculature; thus it has been proposed that PRL-3 could facilitate angiogenesis by promoting VEGF expression. Moreover, a direct link between PRL-3 expression and microvessel density has been reported in human hepatocellular carcinoma (Zhao et al., 2008).

Cancer cell lines-based experiments further corroborated the data previously discussed. A tight correlation between elevated PRL-3 levels and the acquisition of a migratory and invasive cell phenotype has been reported in CHO and B16 cells stably expressing ectopic PRL-3. Furthermore, PRL-3 overexpression is also associated with a morphological transformation of B16 cells from epithelial-like shape to fibroblast-like shape. Interestingly, the overexpression of a catalytically inactive mutant (PRL-3 C104S) has never been associated with any of the mentioned phenotypes (Wu et al., 2004; Zeng et al., 2003). RNA interfering experiments conducted in cancer cell lines that endogenously express high PRL-3 levels support the aforementioned data. For example, downregulation of PRL-3 in human colon cancer DLD-1 cells strongly reduce their motility and hepatic colonization (Kato et al., 2004). Similar results were obtained by reducing the expression of PRL-3 in the highly metastatic melanoma cell line B16-BL6 (Qian et al., 2007). Taken together, these data emphasize the role of PRL-3 as major player in tumorigenic and metastatic processes.

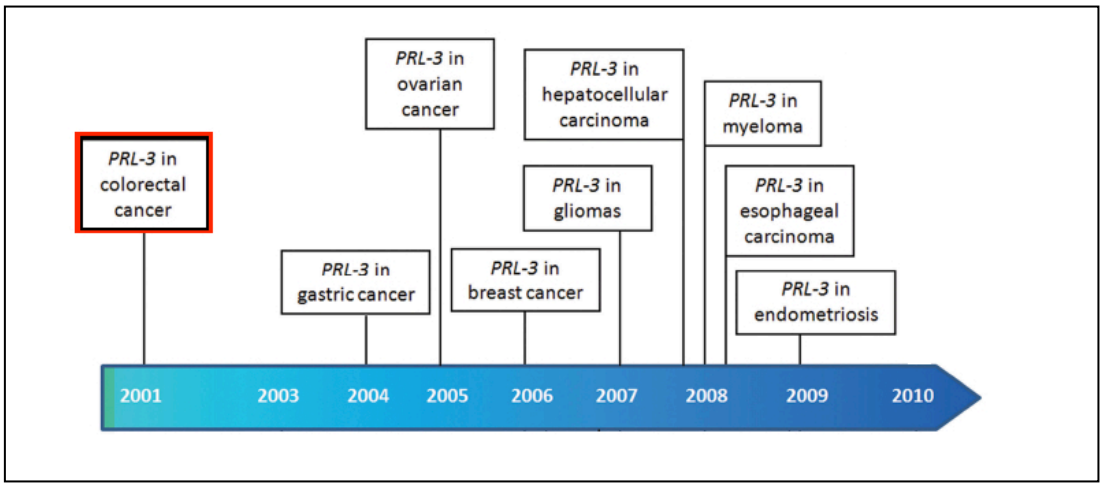

Figure I.3. Timeline of major discoveries in PRL-3 cancer biology. *During the last decade PRL-3 has been found as a protein highly overexpressed in multiple cancer types. The red box highlight the first study, published in 2001, about the role of PRL-3 in colorectal cancer metastasis. Adapted from Al-Aidaroos and Zeng (2010).*

I.1.3.E. Signaling pathways affected by PRL-3

The aberrant expression of PRL-3 has been connected with the alteration of intracellular signal transduction pathways related to cell survival, motility and invasion. A brief overview of the main pathways affected by PRL-3 overexpression is provided below.

I.1.3.E.1. PRL-3 regulates Rho GTPases

The small GTPases of the Rho family act as molecular switches, cycling between an active (GTP-bound) and an inactive (GDP-bound) conformation. GTP binding facilitates their interaction with many effectors molecules and in turn controls downstream signaling pathways. The best-characterized mammalian Rho GTPases involved in actin cytoskeleton dynamics are Rho (A, B, C isoforms), Rac and Cdc42 (Ridley, 2012; Sit and Manser, 2011). In colorectal cancer SW480 cells, overexpression of PRL-3 increases the fraction of GTP-bound Rho A and C, reduces the activity of Rac and has no effect on Cdc42 (Fiordalisi et al., 2006). On the other hand, studies conducted in CHO and DLD-1 reported contradictory results, showing that not only Rac but also RhoA is inhibited by PRL-3 overexpression (Wang et al., 2007). Although the authors propose that PRL-3- enhanced cell motility can be explained by its effect on Rho GTPase activity, at the moment there are still numerous open questions about how, at the molecular level, this happens.

I.1.3.E.2. PRL-3 regulates Arf GTPases

ADP-ribosylation factor (Arf) proteins are an additional family of small GTPases involved in actin cytoskeleton remodeling and vesicle trafficking. It has been reported that PRL-3 interacts with Arf1, a GTPase classically associated with the Golgi apparatus. Specifically, PRL-3 interacts with the active, GTP-boundArf1 and, promotes its activation. The interaction is mediated by the Golgi targeting MXXE motif (Fig. I.2) and seems to be necessary for the pro-migratory phenotype. The authors also propose that PRL-3 enhances cell motility in an Arf1-dependent manner by accelerating the recycling of the matrix receptor integrin alpha 5; however, the precise mechanism of Arf1 activation by PRL-3 is still missing (Krndija et al., 2012).

I.1.3.E.3. PRL-3 activates Src and PI3K, and promotes epithelial-mesenchymal transition (EMT)

PRL-3 overexpression triggers the activation of two classical oncogenes: the non-receptor protein tyrosine kinase Src and the phosphoinositide-3-kinase PI3K (Liang et al., 2007; Wang et al., 2007). Src activity is involved in a variety of cellular processes such as differentiation, motility and adhesion. It is well established that the aberrant activation of Src is implicated in the development and progression of many human tumors (Roskoski, 2004). The kinase activity is tightly controlled; fundamental is the intramolecular interaction between the phospho-Tyr 527 and the phosphotyrosine-binding domain SH2 that locks the kinase in an inactive conformation. The tyrosine protein kinase Csk (C-Src kinase) is the enzyme that catalyzes the phosphorylation of Src at Tyr-527 and thereby suppresses its activity (Thomas et al., 1991).

PI3K catalyzes the phosphorylation of the inositol ring of PtdIns at the position 3, mainly converting PtdIns(4,5)P_2 to PtdIns(3,4,5)P_3 (see paragraph I.2 for a detailed description of phosphoinositide molecules). PtdIns(3,4,5)P_3 is a key second messenger that acts as signaling hub in a wide range of cellular programs like cell survival, cell growth and cell migration. Therefore sustained PtdIns(3,4,5)P_3 signaling is strictly associated with tumorigenesis (Yuan and Cantley, 2008). To avoid persistent activation, a negative feedback loop ensures that PtdIns(3,4,5)P_3 is only transiently available at the plasma membrane. For this purpose the phosphatase PTEN catalyzes the dephosphorylation of PtdIns(3,4,5)P_3 into PtdIns(4,5)P_2, extinguishing the signal (Carracedo and Pandolfi, 2008). Intriguingly, PRL-3 overexpression triggers the

activation of these two oncogenes, promoting the degradation of their negative regulators. Indeed, it has been reported that elevated PRL-3 levels correlated with a substantial reduction in Csk and PTEN (Liang et al., 2007; Wang et al., 2007). As previously mentioned, PRL-3 itself seems to be a substrate of Src, thus a positive feedback loop may exist involving Src and PRL-3. As expected, PRL-3-mediated Src activation culminated in the persistent phosphorylation of downstream targets of Src such as ERK1/2. Interestingly, independent studies have also shown elevated ERK1/2 phosphorylation in PRL-3 overexpressing cells. However, the authors linked this observation with the reduction in integrin β1 phosphorylation (see paragraph I.1.3.F.) (Peng et al., 2009). Taking into account the drastic morphological and molecular changes needed for cell invasion and motility, it cannot be excluded that PRL-3 affects multiple input circuits that ensure a robust signaling. Additionally, it has been shown that PRL-3 promotes epithelial-mesenchymal transition (EMT) in a PI3K-dependent manner in DLD-1 human colorectal cancer cells (Wang et al., 2007). The EMT is an extremely complex process in which polarized epithelial cells are converted into migratory mesenchymal cells. Such long-lasting morphological and molecular changes typically occur during development. However, cancer metastasis could originate taking advantage of the same molecular machinery (Craene and Berx, 2013). Thus, PRL-3 overexpression is associated with the downregulation of epithelial markers such as E-cadherin, γ-catenin, and integrin β_3 (Wang et al., 2007). In agreement with these findings, it has been shown that PRL-3 silencing in SW480 cells correlates with the recovery of E-cadherin expression. Moreover, the authors prove a direct interaction between PRL-3 and CDH22 (cadherin 22), a member of the cadherin family (Liu et al., 2009). Finally, a significant negative correlation between PRL-3 and E-cadherin mRNA levels has been demonstrated in hepatocellular carcinoma tumor tissues (Zhao et al., 2008).

As expected, in DLD-1 cells PRL-3 also up-regulates mesenchymal markers such as fibronectin and Snail in a PI3K-dependent manner (Wang et al., 2007). Recently, it has been shown that in the region of the PRL-3 promoter three potential binding sites for the transcription factor Snail are present. This led the authors to suggest a key role of Snail in the regulation of PRL-3 expression in colorectal cancer, opening the possibility of an additional positive feedback loop that strengthens PRL-3 signaling (Zheng et al., 2011).

I.1.3.F. Potential substrates of PRL-3

Identification of PRL-3 substrates and correlation of these data with the phenotypes observed in PRL-3 overexpressig cells is probably, at the moment, one of the most challenging undertakings. Several substrates have been suggested for PRL-3, namely ezrin, integrin β1, keratin8, nucleolin, stathmin and elongation factor 2 (EF2) (Forte et al., 2008; Mizuuchi et al., 2009; Orsatti et al., 2009; Peng et al., 2006, 2009; Semba et al., 2010; Tian et al., 2012; Zheng et al., 2010). Ezrin and integrin β1 were shown to be directly dephosphorylated by PRL-3 and they will be discussed in detail. For the other, a correlation between PRL-3 overexpression and reduced phosphorylation has been shown. However, a formal prove that PRL-3 directly dephosphorylates these proteins is still missing. Hence, it is not possible to exclude that the reduced phosphorylation observed is an indirect effect.

- Ezrin is a member of the ERM (ezrin/radixin/moesin) family. ERM proteins work as molecular crosslinkers between the cell membrane and actin filaments, and are involved in a variety of cellular processes such as cell adhesion and cell polarity. Their activity is regulated by the state of phosphorylation of Tyr and Thr residues, as well as binding to the phosphoinositide PtdIns(4,5)P_2 (see paragraph I.2 for a detailed description of phosphoinositide molecules). Phosphorylation and PtdIns(4,5)P_2 binding are together necessary for full molecule opening and exposure of the actin binding sites (Neisch and Fehon, 2011). It has been shown *in vitro* and in cells that PRL-3 activity primarily affects the phosphorylation of ezrin at Thr567 (Forte et al., 2008). Thus, PRL-3 seems to counteract a crucial step necessary for Ezrin opening and activation. However, it cannot be excluded that these findings are cell type dependent, considering that in different experimental conditions the effect of PRL-3 on ezrin phosphorylation could not be confirmed (Mizuuchi et al., 2009).
- Integrins are a large family of transmembrane proteins that mediate cell-cell and cell-matrix interactions. Integrins are always found as heterodimers, containing two distinct chains, called the α (alpha) and β (beta) subunits. Structurally, each subunit consists of a large extracellular domain, a single transmembrane domain and a short cytoplasmic tail that, in the β subunits, can be subjected to phosphorylation (Shattil et al., 2010; Takada et al., 2007). PRL-3 seems to be an integrin-associated protein, more specifically with integrin α1 and β1 (Peng et al.,

2006, 2009; Tian et al., 2012). Moreover, PRL-3 is able to dephosphorylate *in vitro* and *in vivo* Tyr783 in the integrin β1 cytoplasmic tail (Tian et al., 2012). However, the biological significance of this activity still remains unclear.

In conclusion, although several protein substrates have been suggested, it is still not possible to describe a complete signaling cascade that could explain the pleiotropic phenotypes observed in PRL-3 overexpressing cells.

I.2. Phosphoinositides

I.2.1. The seven distinct phosphoinositide species

Phosphoinositides comprise a family of phosphorylated derivatives of the membrane lipid phosphatidylinositol (PtdIns). Reversible phosphorylation at the 3, 4, and/or 5 position(s) of the inositol ring generates seven chemically distinct but interconvertible phosphoinositide species (Fig. I.4) (Di-Paolo and De Camilli, 2006; Le-Roy and Wrana, 2005; Saarikangas et al., 2010; Shewan et al., 2011).

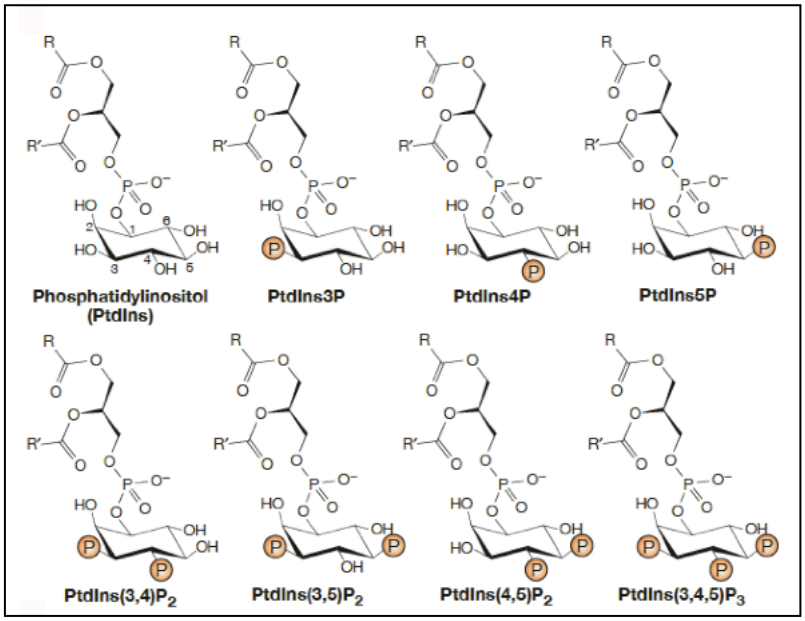

Figure I.4. Structurs of phosphatidylinositol and its phosphoinositide derivatives. *Phosphatidyinositol molecules comprise a fatty acid backbone which anchors the lipid moiety in the membrane, attached to a inositol ring head, which can be reversibly phosphorylated at the 3,4 and/or5 position(s) to generate up to seven distinct phosphoinositide species. R and R' are saturated or unsaturated acyl chains, respectively. The total carbon length of R and R' are in the range of 16-24. Adapted from Le Roy and Wrana (2005).*

All seven phosphoinositides are minor components of eukaryotic cell membranes. Despite their low abundance, phosphoinositides regulate fundamental biological processes ranging from membrane trafficking, cytoskeletal organization, to signal transduction acting as docking sites for effector molecules and/or precursor of secondary messenger (Balla, 2013; Di-Paolo and De Camilli, 2006; Saarikangas et al., 2010). The involvement of phosphoinositides in such a vast array of biological functions is related to a unique set of properties of these molecules:

a) Each of the seven phosphoinositides is a distinct cellular signal that is transduced by protein effectors able to recognize selectively the distinct phosphorylation sites (Fig. I.5) (Kutateladze, 2010).

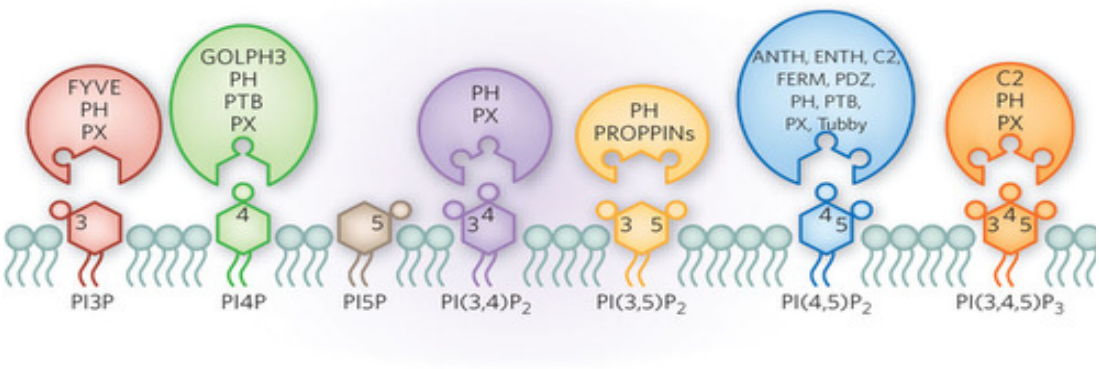

Figure I.5. Phosphoinositide-binding modules. *Summary of phosphoinositides binding domains and their binding specificity. Frequently, phosphoinositide binding proteins are multi-domain proteins that couple the lipid binding with conformational changes. These changes can for example modulate the protein enzymatic activity or expose a protein-protein interaction motif, leading subsequently to the activation or termination of signaling cascades. Notably, the use of fluorescently tagged phosphoinositide-binding domains has been a major breakthrough in understanding the phosphoinositide's subcellular distribution and in the visualization of dramatic changes in phosphoinositide levels in living cells. Adapted from Kutateladze (2010).*

b) Phosphoinositides can be rapidly and sequentially interconverted from one species to another by lipid kinases and phosphatases. These phosphoinositide-modifying enzymes fine-tune spatially and temporally phosphoinositide levels, maintaining cell homeostasis. Additionally, the cleavage of the inositol-phosphate head group by phosphoinositide-specific phospholipase C enzymes (PLCs) gives rise to metabolites that propagate and amplify signaling. Considering the broad spectrum of cellular processes regulated by phosphoinositides, abnormal phosphoinositide metabolism is associated with a wide range of human diseases including cancer, diabetes and autoimmune disorders (Balla, 2013; Bunney and Katan, 2010; Majerus and York, 2009).

c) Each of the seven phosphoinositides has its own distinctive subcellular localization, and this lipid signature code is not only fundamental for cellular membrane identity but also contributes to spatially restricted downstream signaling responses (Fig. I.6) (Kutateladze, 2010).

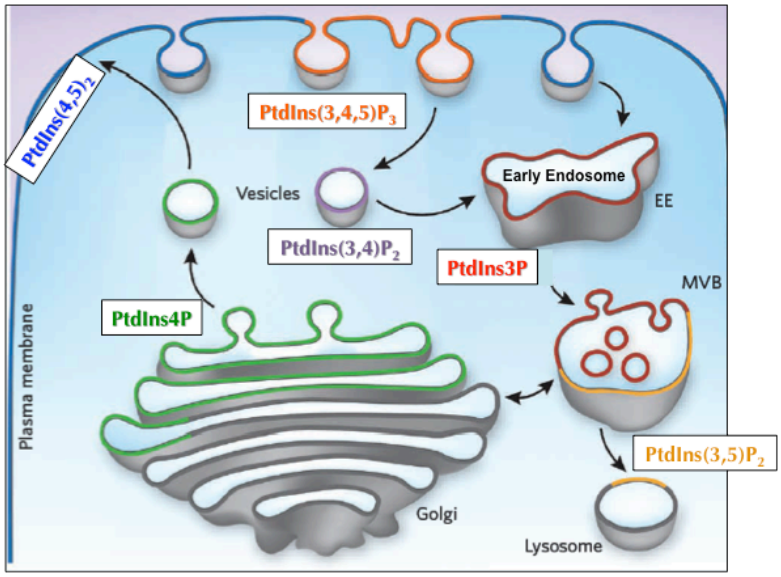

Figure I.6. Subcellular distribution of phosphoinositides. *Each of the seven phosphoinositides localizes to specific membrane compartments or organelles. PtdIns(4,5)P2 and PtdIns(3,4,5)P3 are primarily enriched at the plasma membrane. PtdIns(4,5)P2 is constitutively present and is one of the most abundant phosphoinositides whereas PtdIns(3,4,5)P3 is typically transient and is rapidly degraded following its synthesis. PtdIns(3,4)P2 and PtdIns(3)P are concentrated in the early endocytic pathway vesicles and in early endosomes (EE), respectively. PtdIns(3,5)P2 is mostly found in the multivescicular bodies (MVB) and lysosomes (late compartments of the endosomal pathway). PtdIns(4)P is enriched at the Golgi apparatus. The location of PtdIns(5)P remains poorly characterized. Adapted from Kutateladze (2010).*

I.2.2. Roles of PtdIns(4,5)P_2 at the plasma membrane

PtdIns(4,5)P_2 is a multipotent signaling molecule that participates in almost all events that occur at the plasma membrane (McLaughlin et al., 2002). It plays a central role in signal transduction as precursor of key second messengers, namely Inositol(1,4,5)-triphosphate (IP_3) and diacylglycerol (DAG) upon phospholipase cleavage, or PtdIns(3,4,5)P_3 during PI3K activation (Berridge and Irvine, 1987; Czech, 2000). On the other hand, PtdIns(4,5)P_2 directly regulates a plethora of cellular processes including exo- and endocytosis, ion channel mediated transport, cytokinesis, cell shape, motility, polarity and adhesion through fluctuations of its own levels as well as compartmentalization in plasma membrane microdomains (McLaughlin et al., 2002). PtdIns(4,5)P_2 directly regulates actin cytoskeleton dynamics affecting the function of several actin-associated proteins, often in cooperation with small GTPases. Typically,

PtdIns(4,5)P_2 predisposes the actin cytoskeleton to a “polymerization mode”. Indeed, PtdIns(4,5)P_2 inhibits actin-binding proteins that disassemble actin filaments, promotes nucleation of actin networks and enhances both actin filament cross linking and plasma membrane/actin cytoskeleton interactions (Lanier and Gertler, 2000; Saarikangas et al., 2010). One classical example of adaptor proteins that link the plasma membrane with the actin cytoskeleton in a PtdIns(4,5)P_2 –dependent manner are the proteins of the ERM family (Neisch and Fehon, 2011), already discussed in paragraph I.1.3.F.

I.2.3. Phosphoinositide phosphatases

Essential to elucidate biological and pathological roles of phosphoinositides is to characterize the enzymes involved in their synthesis, interconversion and degradation.

In mammals close to 50 genes encode for phosphoinositide kinases and phosphatases. These phosphoinositide-modifying enzymes allow cells to maintain phosphoinositide homeostasis as well as to respond rapidly and selectively to environmental changes (Balla, 2013).

The relevance of phosphoinositide phosphatases in cell homeostasis is highlighted by severe genetic disorders that result from mutations in genes encoding this class of enzymes. Additionally, many phosphoinositide phosphatases are referred to as oncogene or tumor suppressor, considering that somatic mutations in these enzymes are key events in cell transformation. Curiously, even if alterations in level or activity of phosphoinositide phosphatases often create striking phenotypes in animal models or cell culture, in most of the cases the underlying molecular mechanisms remain unknown (Majerus and York, 2009). Conventionally, phosphoinositide phosphatases can be classified on the basis of their catalytic mechanism of action or on the basis of their substrate specificity towards the phosphate in the 3, 4 or 5 positions. According to the first classification, historically, mammalian phosphoinositide phosphatases belong to two distinct superfamilies: the PTP superfamily (reviewed in paragraph I.1.2.) and the inositol polyphosphate 5-phosphatase (5-ptase) superfamily. The 5-ptases share the same mechanism of catalysis of apurinic/apyrimidinic base excision repair endonuclease. The catalysis has been shown to proceed without a phosphoenzyme intermediate, with direct transfer of the phosphate group to a nucleophilic water molecule (Ooms et al., 2009). In mammals, 10 distinct 5-ptases have been identified. These enzymes catalyze the removal of the phosphate in 5-

position from the inositol ring of PtdIns(4,5)P_2, PtdIns(3,4,5)P_3, and/or PtdIns(3,5)P_2. Some members of the family show additionally activity toward soluble inositol phosphates. Notably, 5-ptases are multidomain proteins in which subcellular targeting motifs such as the CAAX box have been identified (Ooms et al., 2009). 5-ptase type IV is one example of a C-terminally prenylated 5-ptase. The enzyme removes the 5-position phosphate from PtdIns(3,5)P_2, PtdIns(4,5)P_2 and PtdIns(3,4,5)P_3 and on the basis of kinetic data is considered to be the most potent PtdIns(3,4,5)P_3 phosphatase (Kisseleva et al., 2000). Interestingly, 5-ptase type IV knockout mice showed severe defects in primary cilia formation associated with multiorgan failure, opening the possibility of an additional role of phosphoinositides in ciliary functions (Jacoby et al., 2009). Although considerable effort has been directed toward characterizing phosphoinositide phosphatases *in vivo*, studies of phosphoinositides dynamics at the subcellular level are still challenging. Thus, most phosphoinositide phosphatases have only been characterized *in vitro* with respect to their substrates, and cell studies are often lacking. Thus far, the connection between the physiologic substrates of phosphoinositide phosphatases, signaling pathways and human diseases remains for most of the phosphatases elusive. We identified PRL-3 as a new PtdIns(4,5)P_2 phosphatase in our *in vitro* studies and this argument will be discussed in further detail in the result section (Chapter III). Additionally, we characterized the effects of PRL-3 over-expression on epithelial morphogensis (Chapter IV), thus the next paragraphs will give a brief overview on epithelial organization and cell polarity.

I.3. Epithelial organization and cell polarity

I.3.1. Structure of mammalian epithelial cells

Epithelial tissues are sheets of epithelial cells tightly packed together that provide a barrier between appropriate interfaces. Internal epithelial organs are typically constituted by two types of building block, cysts and tubules. Cysts are spherical single layers of epithelial cells that surround a central hollow lumen. Tubules are also a lumen-enclosing monolayer of polarized epithelial cells but are cylindrical instead of spherical. Epithelial organs such as lung or kidney are organized in a network of branching tubules that terminate in cysts (Brien et al., 2002). Each cell in mature cysts or tubules is polarized, showing three type of plasma membrane domains that are morphologically distinct: (i) a free, microvilli-rich apical membrane that faces the lumen, (ii) a lateral surface that contacts neighboring cells, and (iii) a basal membrane that adheres to the basement membrane, a specialized extracellular matrix (ECM) (Fig. I.7) (Brien et al., 2002; St Johnston and Ahringer, 2010). This clear apico-basal polarity is marked by the asymmetric distribution of both proteins and lipids across the plasma membrane. The apical domain, in contact with the fluid-filled central lumen, can contain specialized structures such as microvilli that increase the surface area and form the brush border. Under the apical membrane, a thick cortical belt of actin is linked to the plasma membrane through ERM family proteins. The lateral domain is characterized by the presence of junctional complexes that carry out barrier and adhesive functions needed to generate molecular asymmetry and mechanical stability, respectively (Brien et al., 2002; McCaffrey and Macara, 2009; Roignot et al., 2013). In vertebrates, the epithelial junctional complex comprises desmosomes, adherens junctions (AJs) and tight junctions (TJs). Desmosomes and adherens junctions carry out adhesive functions, tethering intermediate and actin cytoskeletal filaments to the plasma membrane. In both cases, members of the cadherin family bridge the adjacent plasma membranes of neighbouring cells via their homophilic interactions (Baum and Georgiou, 2011). Tight junctions work as barriers sealing the paracellular space and preventing diffusion of membrane components between the apical and the basolateral domain. TJs localize at the apico-lateral border and demarcate the boundary between the apical and the basolateral domain (see paragraph I.3.3.) (Matter and Balda, 2003). Finally, the basal membrane is depleted of intercellular adhesion molecules and enriched in integrin and non-integrin receptors

such as dystroglycan that anchor cells to the surrounding matrix, transducing basal cues to the cytoskeleton (Brien et al., 2002; Datta et al., 2011).

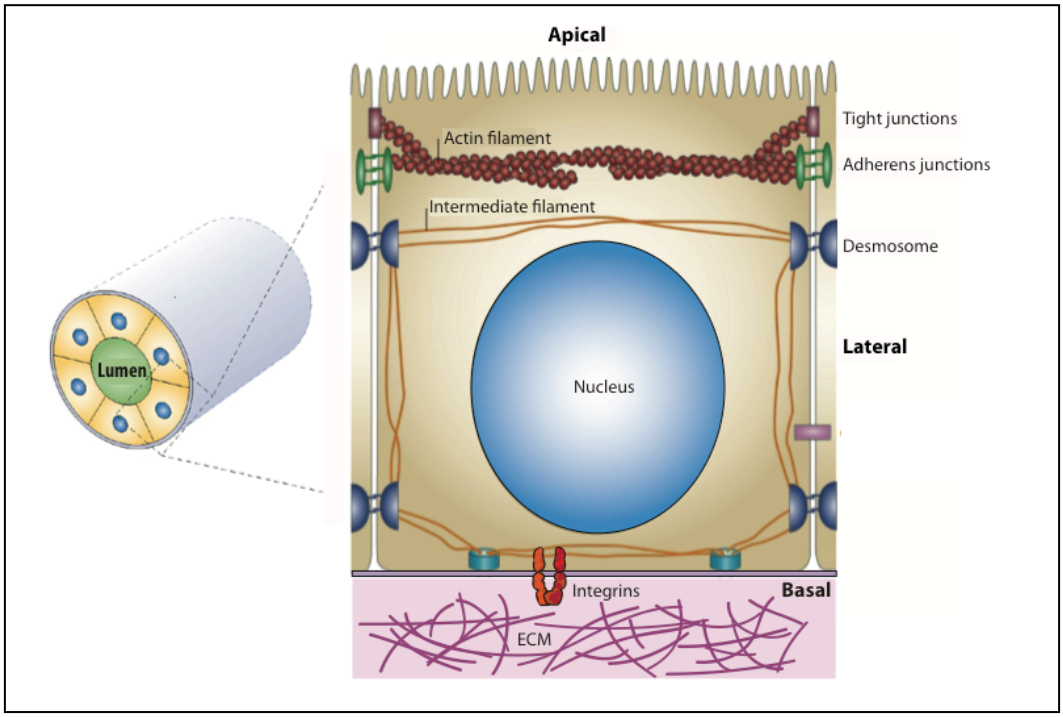

Figure I.7. Mammalian epithelial cell architecture. *Schematic representation of a polarized epithelial cell specialized in absorptive functions. Each cell presents three distinct plasma membrane domains: an apical membrane, directly in contact with the luminal space, a lateral membrane that adheres to the flanking cells and a basal membrane that anchors the cell to the extracellular matrix (ECM). Epithelial cells are joined to each other via the "apical junctional complex" that comprises: tight junctions (TJs), adherens junctions (AJs) and desmosome. Notably, TJs and AJs are linked to the actin cytoskeleton; desmosomes are linked to intermediate filaments. Adapted from Matter and Balda (2003).*

I.3.2. Phosphoinositides as polarity signals

Apico-basal polarization requires compartmentalization not only of proteins but also of lipids, particularly phosphoinositides. Phosphoinositides themselves, being asymmetrically distributed across the plasma membrane, are crucial determinants of apical and basolateral membrane identity (Shewan et al., 2011). Specifically, PtdIns(3,4,5)P_3 is restricted to the basolateral domain, being selectively excluded from the apical surface, whereas PtdIns(4,5)P_2 localizes all over the plasma membrane but is enriched at the apical surface (Gassama-Diagne et al., 2006; Martin-belmonte et al., 2007). The differential distribution of phosphoinositides on the plasma membrane is

fundamental for establishment and maintenance of polarity, recruiting asymmetrically lipid-binding proteins. It has been shown that lipid segregation proceeds in concert with junction assembly through the recruitment of PTEN at the apical border via direct interaction with the tight junction protein Par3. PTEN, converting PtdIns(3,4,5)P_3 to PtdIns(4,5)P_2, acts as a barrier to prevent PtdIns(3,4,5)P_3 diffusion in the apical domain (Comer and Parent, 2007; Datta et al., 2011; Martin-belmonte et al., 2007). The PtdIns(4,5)P_2 – dependent pathway, involved in apical domain specification, will be discussed in detail in the paragraph I.3.6.

I.3.3. Structure and composition of epithelial tight junctions

Tight junctions localize at the lateral-apical border of epithelial cells and function as a barrier restricting protein and lipid movements between the apical and basolateral compartments and selectively sealing the space between neighboring cells (Matter and Balda, 2003). Epithelial TJs are formed by evolutionary conserved multiprotein complexes. It is possible to distinguish two major groups of junctional proteins: the transmembrane proteins and the cytoplasmic "plaque". Transmembrane proteins such as occludin, claudin and JAMs (junctional adhesion molecules) mediate cell-cell adhesion and constituite a selective paracellular diffusion barrier. The cytoplasmic plaque contains functionally distinct complexes that include adaptors, regulatory and signaling proteins. Adaptors are able to bind directly the TJ transmembrane components and, in turn, recruit regulatory proteins such as kinases, phosphatases and GTPases at the TJ site. Adaptors are usually multidomain proteins characterized by several protein-protein interaction modules such as the PDZ domain. Among the adaptors, the zona occludens (ZO) proteins are involved in the clustering of transmembrane proteins, binding the cytoplasmic tail of claudin and occludin via their PDZ domains. In addition, several components of the cytoplasmic plaque and the transmembrane protein occludin contact the actin cytoskeleton, functioning as plasma membrane-actin cytoskeleton linkers (Paris et al., 2008; Schulzke and Fromm, 2009; Shin et al., 2006).

I.3.4. The PAR-aPKC polarity complex

Essential for epithelial cells polarization is the coupling of the PAR-aPKC polarity complex to junctional structures. The Par3-Par6-aPKC complex (where Par is for "partitioning defective" and aPKC is for " atypical protein kinase C) are a set of

evolutionary conserved proteins involved in cell polarity in various biological contexts (St Johnston and Ahringer, 2010). Both Par3 and Par6 are PDZ domain-containing scaffold proteins that work as adaptors at the TJ site; aPKC isoforms (PKCζ and PKCι in human) are serine/threonine protein kinases, which share a calcium- and diacylglycerol- independent mechanism of activation. Par3, Par6 and aPKC form a physical complex by multiple direct interactions. Notably, the complex does not assemble in a constitutive manner but is subjected to multiple levels of regulation (Fig. I.8). Indeed, Par3 is primarily recruited to the primordial adhesion sites through the interaction with adhesion complex proteins and JAM proteins, whereas Par6/aPKC recruitment relies on Cdc42 activation. More specifically, GTP-bound Cdc42 associates with the Par6/aPKC complex by direct binding to Par6 and leads, in turn, to the activation of aPKC. Subsequently, the active Par6-aPKC complex is recruited at the TJ site through multiple interactions with the scaffold Par3. This model suggests a simple mechanism of specific aPKC activation within a cell in which the kinase activity is timely regulated subsequent to Cdc42 activation. Thus, the complex, asymmetrically localized, promotes TJ maturation and thereby contributes to the separation of the apical and basolateral domain (Aranda et al., 2008; Suzuki and Ohno, 2006). Additionally, Par3 holds at the TJ site the RAC exchange factor TIAM1, necessary for RAC-mediated assembly of the actin ring at the cell cortex, and the lipid phosphatase PTEN, necessary to induce phosphoinositides asymmetry at the plasma membrane (Chen and Macara, 2005; Feng et al., 2008). Notably, in fully polarized epithelial cells, Par3 does not strictly colocalize with Par6 and aPKC. Indeed, Par6 and aPKC are restricted to the apical domain whereas Par3 maintains TJ localization (Martin-belmonte et al., 2007).

I.3.5. Three-dimensional (3D) epithelial cultures: a tool for studying epithelial architecture

In vitro studies of epithelial cells cultured on plastic or glass bottom dishes (two-dimensional (2D) cultures) have revaled important mechanisms and molecular pathways required for cell polarization. However, 2D cultures might not successfully recapitulate the physiological characteristics distinctive of epithelial cells in vivo.

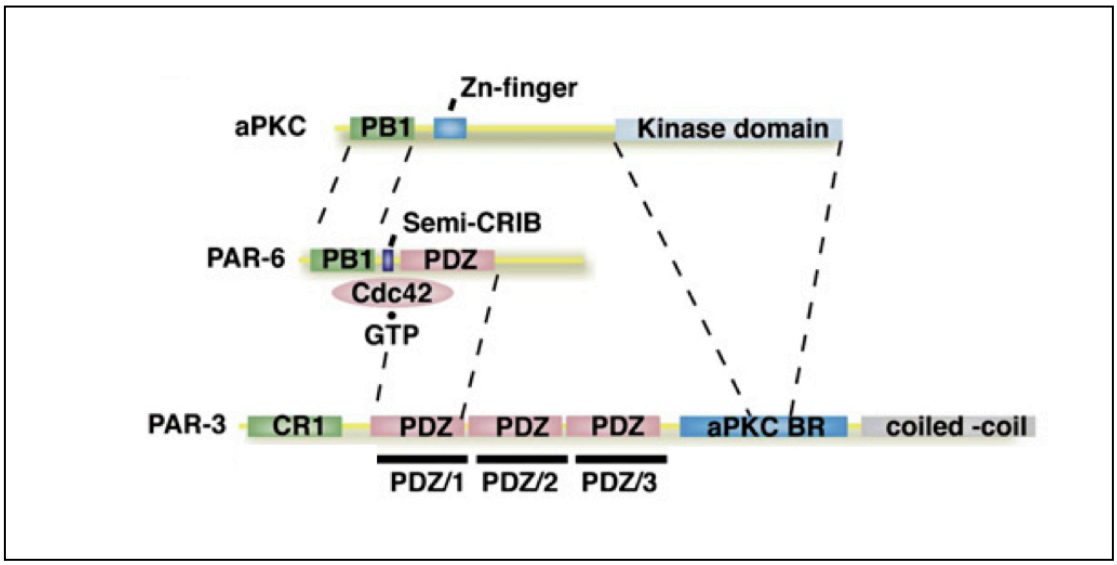

Figure I.8. Domain architecture of the Par3/Par6/aPKC polarity complex. *Par6 and aPKC are constitutively associated through their N-terminal PB1 (Phox and Bem1p 1) domains and this conformation inhibits the basal activity of aPKC. Par6 contains, in addition to the PB1 domain, a semi-CRIB (Cdc42/Rac interactive binding) motif and a single PDZ (PSD95/Dlg/ZO-1) domain. Upon Cdc42 activation, GTP-bound Cdc42 is able to associate with Par6, binding simultaneously the semi-CRIB motif and the contiguous PDZ domain. The binding of Cdc42 to Par6 induces a conformational change that allows the activation of the associated aPKC (Lin et al., 2000). Par3 is characterized by an amino-terminal conserved region 1(CR1) domain responsible for Par3 self-oligomerization (Mizuno et al., 2003), three central PDZ domains that mediate protein-protein or protein-lipid interactions and the C-terminal region containing the aPKC-binding motif. It has been shown that Par3 can associate with Par6 through a PDZ-PDZ interaction (first PDZ domain of Par3), as well as with aPKC, binding directly its kinase domain. The second PDZ domain of Par3 binds with high affinity phosphoinositides and this interaction is essential for Par3 plasma membrane localization (Wu et al., 2007). Finally, the third PDZ domain of Par3 binds the lipid phosphatase PTEN (Feng et al., 2008). Interestingly, Par3 itself is a substrate of aPKC and its phosphoryalation lowers the affinity between Par3 and Par6/aPKC (Nagai-tamai et al., 2002). In the figure, domain interactions are indicated by dashed lines. Adapted from Nakayama et al. (2008)*

Indeed, epithelial cells grown on plastic substrates show a considerably different morphology as compared to the epithelium in vivo, becoming partially depolarized and rather flat. Responsible for such different morphology is the lack of a three-dimensional (3D) microenvironment and therefore the signaling pathways generated by cell-matrix and cell-cell adhesion. Thus, in the last two decades considerable efforts have been made to develop cell culture conditions more representative of an "in-vivo-like" environment. The best results have been obtained with the growth of epithelial cells in 3D gels of ECM such as the Matrigel (solubilized basement membrane preparation extracted from the Engelbreth-Holm-Swarm (EHS) mouse

sarcoma). Selected epithelial cells, both from primary cultures and established lines, are able to form complex epithelial structures that share the same key features of in vivo glandular epithelial organs when grown in 3D cultures (Zegers et al., 2003). Two widely used cell lines are the MDCK, canine kidney epithelial cells and MCF10A human breast cells. Both cell lines, cultured in presence of the 3D matrix, can form spheroid structures, variably named cysts or acini according to the epithelial cell origin (Debnath and Brugge, 2005). More specifically, MDCK cells in 3D cultures form cyst-like spherical structures in which a single layer of polarized epithelial cells encloses a central hollow lumen. Each cell in the cyst shows a clear apicobasal polarization with its apical surface facing the central fluid-filled lumen, its basal membrane in contact with the ECM and mature tight junctions delimiting the lateral/apical border (Schlüter and Margolis, 2009). Moreover, 3D epithelial culture systems not only permit to mimic epithelial cell architecture but also to apply cellular and molecular biology tools (i.e., cDNA overexpression, RNA interference, imaging). Thus, 3D cell cultures were shown to be a powerful system to decipher the molecular and cellular aspects of epithelial morphogenesis, such as the molecular pathways regulating lumen establishment and maintenance, as well as to investigate the mechanism associated with epithelial tumor initiation and progression (Brien et al., 2002; Debnath and Brugge, 2005). These arguments will be discussed in detail in the following sections.

I.3.6. *De Novo* lumen generation

During development, tubular structures can originate through remarkably different mechanisms. Tubules can arise by mechanical deformation of epithelial sheets, or they can originate by conversion of poorly adherent mesenchymal cells into polarized, tightly connected epithelial cells (mesenchymal-epithelial transition). In the first case, existing epithelial sheets rearrange in the course of major morphogenetic movements to give rise to hollow tubes. In the second case, groups of cells rapidly polarize and generate a central lumen *de novo* (Lubarsky and Krasnow, 2003). Two mechanisms of *de novo* lumen generation have been predominantly observed: cavitation and hollowing (Fig. I.9) (Bryant and Mostov, 2008; Datta et al., 2011). During cavitation, the lumen is formed by selective apoptosis of the inner cell population that is not in contact with the ECM, whereas the outer layer of cells, connected to the matrix, progressively polarizes. This process has been described, for example, in 3D culture

of MCF-10A during acinar morphogenesis, and *in vivo* during mammary gland development (Debnath et al., 2002; Humphreys et al., 1996; Mailleux et al., 2007). In the hollowing mechanism instead, polarization is generated by membrane domain separation coupled to polarized exocytosis. Thus, during hollowing, cells acquire apical-basal polarity *de novo*, assemble cell-cell junctions and form initially a small lumen in the center of the system between closely apposed cells that subsequently expands by fluid and ion efflux. This mechanism has been observed in 3D culture of MDCK during cystogenesis as well as *in vivo* during zebrafish gut development (Apodaca et al., 2012; Bagnat et al., 2007; Bryant and Mostov, 2008; Datta et al., 2011). The molecular pathways behind the hollowing mechanism will be described in the next paragraph.

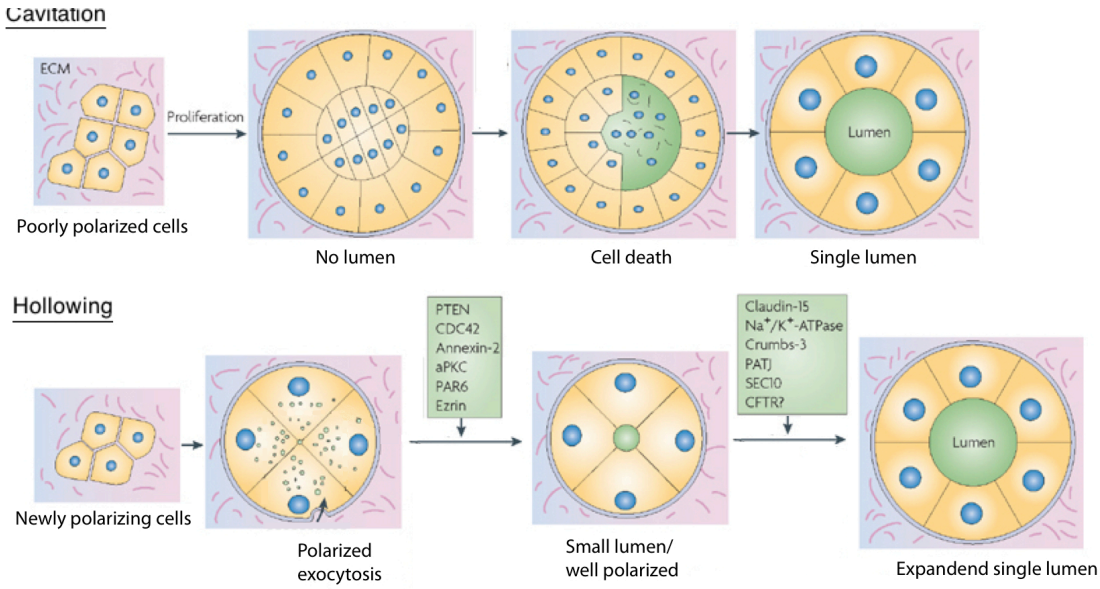

Figure I.9. **Mechanisms of *de novo* lumen formation.** *Two distinct mechanisms of de novo lumen formation, namely cavitation and hollowing, have been predominantly observed when cysts or tubules originate from poorly polarized cell aggregates. During cavitation, de novo lumen formation requires survival and polarization of the ECM-contacting cells in the periphery as well as selective apoptosis of the inner cells mass. During hollowing, cells precociously establish the axis of polarity. This process requires ECM-ECM receptors interactions, intracellular vesicles delivery of apical membrane determinant to the center of the system as well as phosphoinositide segregation in order to establish membrane identity. Once a rudimentary lumen is formed, tight junctions, pump proteins and possibly ezrin promote lumen expansion. Adapted from Bryant and Mostov (2008).*

I.3.7. The hollowing mechanism: molecular regulation of lumen morphogensis

When tubular epithelia are formed *de novo* from non-polarized cells, combinatorial inputs provide the molecular cues necessary to establish apicobasal polarization and thus the spatial coordinates for determining the direction of lumenogenesis.

The initial cue derives from protein of the basal lamina (specialized ECM), in particular laminins and collagen IV that provide one axis from which to orient lumen position. Indeed lumens originate in most cases perpendicularly to the ECM-contacting membrane, with the exception of hepatocytes where lumens originate laterally between cells (Cohen et al., 2004; Datta et al., 2011; Treyer and Müsch, 2013). It has been demonstrated that integrin β1 plays a critical role in mediating cell-ECM interactions and thus to correctly orient polarity. In detail, in 3D culture of MDCK cells it has been shown that the pathway laminin-integrin β1-Rac1 controls apicobasal polarization by influencing cytoskeletal tension (O'Brien et al., 2001; Yu et al., 2005). The second spatial cues come from cell-cell interactions through the formation of intercellular junctions (Datta et al., 2011). Cell-cell contact occurs via a multitude of adhesion molecules, including cadherins (epithelial junctional complexes were already discussed in paragraph I.3.1 and I.3.3.). It has been observed that the process of polarization in MDCK cysts starts in a very early stage, immediately after the first cytokinesis (Schlu et al., 2009). Once newly polarizing cells establish the axis of polarity, recognizing the ECM and assembling primordial junctions, luminal space can be generated. In MDCK cysts, one of the earliest intermediate in luminogenesis described is the specification of the "apical membrane initiation site" (AMIS) (Apodaca, 2010; Bryant et al., 2010). The AMIS is a specialized membrane domain at the zone of cell-cell contact, in the core region of the nascent cyst, in which key apical determinants such as polarity and trafficking proteins are transiently enriched. This region is established before a tight junction-demarcated lumen can be observed and is the site where the lumen will subsequently open. Therefore, selective delivery of vesicles containing apical determinants to a discrete common landmark (the AMIS) is the critical step that specifies lumen position. This process, named polarized exocytosis, is governed by the small GTPases of the Rab family, which regulate cargo selection, vesicle maturation and vesicle tethering with target membranes (Apodaca, 2010; Bryant et al., 2010). Fundamental for polarized traffic is also the role of the

cytoskeleton, in particular the directional transport along microtubules that is directed by several proteins of the kinesin family. For the transport of apical cargo the kinesin Kifc3, Kif5B and Kif17 were demonstrated to be primarily involved (Jaulin and Kreitzer, 2010; Jaulin et al., 2007; Noda et al., 2001). Finally, vesicles fusion is mediated by t-SNAREs proteins, including syntaxin-1,-2 and -3 (Sharma et al., 2006; Torkko et al., 2008). Studies on 3D culture of MDCK cells have revealed that the transition between unpolarized epithelia to cysts starts precociously, right after the first cytokinesis, at the two-cell stage (Schlu et al., 2009). At this stage, several apical signaling molecules are still not properly compartmentalized, showing a diffuse staining all over the plasma membrane, or localizing mainly at the ECM-contacting plasma membrane. Apico-basal polarization is rapidly established through transcytosis of apical determinants from the basolateral membrane to the forming luminal surface. This directional transport relies on the Rab11a-Rabin8α-Rab8a cascade (Fig. I.10). Indeed, apical determinants are initially internalized from the basolateral membrane into Rab11a positive vesicles to which Rab8a is recruited through the Rab guanine nucleotide exchange factor (GEF) Rabin8. This Rab cascade is responsible for vesicle delivery, probably by regulating motor proteins such as myosin-5B (Apodaca et al., 2012; Bryant et al., 2010). Subsequently, the hetero-octameric exocyst complex mediates the docking and tethering of apical cargo to the target membrane to create the AMIS. Notably, exocyst subunits show a non-overlapping subcellular distribution during polarized exocytosis, with Sec15a recruited to the Rab11a-positive vesicles whereas Sec10 and Sec8 are localized on the target membrane, underlying the lumen initiation site. Therefore, the interaction between the vesicular Sec15a and the membrane localized Sec10 may promote the accurate docking of apical cargo to the AMIS (Bryant et al., 2010; He and Guo, 2009). Finally, in MDCK cystogenesis, the exocyst complex is also important for the recruitment of the Par3-aPKC complex to the AMIS, through the direct binding of Sec8 to Par3 (Apodaca, 2010; Bryant et al., 2010; Zuo et al., 2009). Moreover, the Cdc42-GEF Tuba, responsible for Cdc42 activation, is also recruited on apical vesicles in an active Rab8–dependent manner. Thus, polarized trafficking contributes to this initial step of lumenogenesis by promoting compartmentalization of the Par3-aPKC complex as well as by activation of Cdc42 specifically at the apical membrane (Apodaca, 2010; Bryant et al., 2010). In conclusion, it has been shown that during the

early phase of lumenogensis, the robust crosstalk between the trafficking and the polarity machinery is fundamental to establish and maintain the apical domain.

Once the AMIS has been established, lumenogenesis proceeds with lumen maturation. This transition is characterized by the relocalization of Par3 and the plasma membrane-associated exocysts subunits Sec8 and Sec10 to the tight junction regions (Bryant et al., 2010).

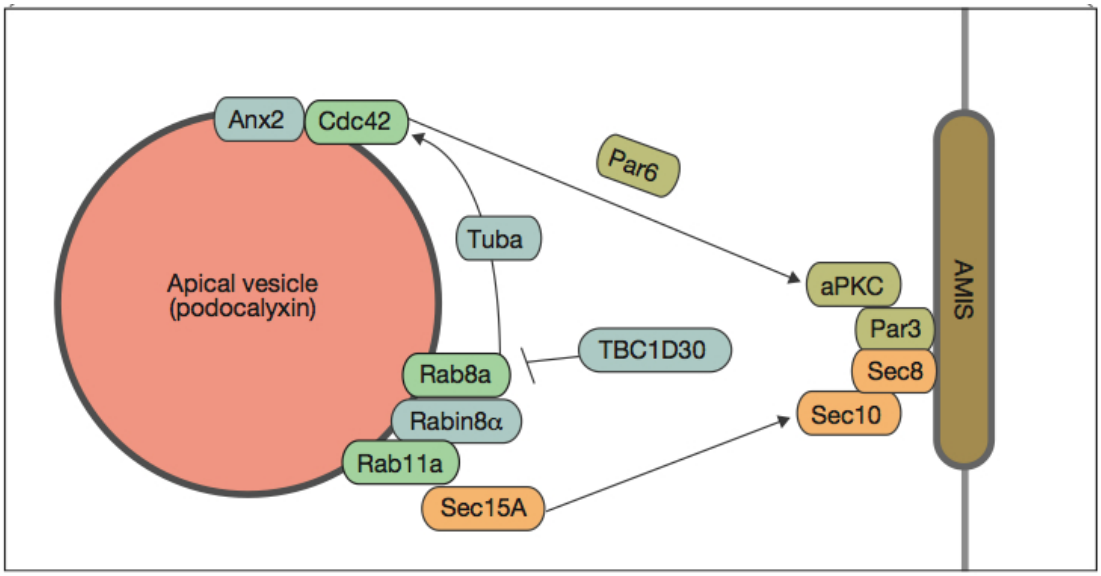

Figure I.10. **Molecular machinery required for de novo lumen formation.** *Apical determinants like the sialoglycoprotein podocalyxin, are rapidly internalized from the ECM-contacting plasma membrane into Rab11a positive vesicles. Polarized trafficking of apical cargo requires the recruitment and activation of Rab8, through the GEF Rabin8α, to the apical vesicles. Vesicle exocytosis is promoted by the Rab-dependent recruitment of the exocyst complex subunit Sec15A, which will drive the selective docking of apical cargo to the AMIS, where the other exocyst subunits Sec8 and Sec10 are already localized. Trafficking and polarity machinery are robustly linked together at multiple levels. Indeed, the exocyst subunit Sec8 restricts the localization of the Par3-aPKC complex to the AMIS; moreover, the Rab8-dependent recruitment of the Cdc42-GEF Tuba to the apical vesicles promotes Cdc42 activation, leading, in conclusion, to the specific delivery of active Cdc42 to the AMIS. Adapted from Bryant et al. (2010).*

As previously mentioned, apico-basal polarization relies on the asymmetric distribution of both proteins and lipids. In MDCK cysts, the compartmentalization of phosphoinositides is a crucial step to generate membrane identity. Exclusion of PtdIns(3,4,5)P_3 from the apical surface is governed by the lipid phosphatase PTEN, which metabolizes PtdIns(3,4,5)P_3 into PtdIns(4,5)P_2 and may also participate in the PtdIns(4,5)P_2-enrichment observed at the luminal surface (Martin-belmonte et al.,

2007). Strikingly, during cysts development, PTEN localizes at the tight junction border through a direct binding with Par3, which partially explains how basolateral/apical phosphoinositide asymmetry has been generated (Feng et al., 2008; Martin-belmonte et al., 2007). Although it is likely that the PtdIns(4,5)P_2/ PtdIns(3,4,5)P_3 differential distribution reinforces cell polarization by selective recruitment of key effecting proteins on separate membrane domains, the identity of these targets is still unknown.

Notably, it has been reported that the PtdIns(4,5)P_2-binding protein Anx2 (AnnexinA2) in the early stage of luminogenesis localizes on Rab11a positive vesicles, where it promotes the recruitment of Cdc42 (Bryant et al., 2010). However, whether PtdIns(4,5)P_2 is directly enriched at the AMIS, taking advantage of the fusion of vesicles, has not yet been demonstrated. Finally, the last step of de novo lumen formation is the physical opening of the lumen. This stage seems to be governed by apical delivery and activation of pumps and channels as well as by proteins characterized by anti-adhesive properties (Bryant and Mostov, 2008). Generally, proteins with antiadhesive properties, as for example the apical determinant podocalyxin, carry in their extracellular domains highly negatively charged groups, as for example glycosyl and/or sialyl moieties (Meder et al., 2005). Thus, at the moment, it is suggested that the electrostatic repulsion from opposing plasma membrane is the initial step that generates extracellular space necessary for subsequent lumen expansion.

I.3.8. Reconstruction of tumor phenotypes in 3D culture

In the above paragraph several key molecular regulators governing de novo formation of the lumen have been described. Notably, understanding the molecular mechanisms beyond lumen formation and maintenance is not only crucial for our comprehension of these morphogenic processes during development but also to shed light into the molecular alterations connected with luminal networks dysfunction in common human diseases. In particular, loss of polarity and luminal filling are considered key steps during glandular epithelial organ tumorigenesis, such as in the ductal carcinoma in situ (pre-invasive breast cancer) (Burstein et al., 2004). 3D epithelial cell culture systems were shown to be precious cell models to investigate the role of cancer genes and pathways involved in epithelial architecture disruption during tumorigenesis (Debnath and Brugge, 2005). One possible strategy is to mimic tumor phenotypes by

manipulating the expression of genes using molecular biology tools (i.e. RNA interference, cDNA overexpression). In general, studies on 3D culture have permitted to model several events associated with epithelial transformation, including loss of cell adhesion and polarity, filling of the luminal space, escape from apoptosis and invasive behavior (Debnath and Brugge, 2005). For example, in a series of elegant experiments using 3D culture of non-transformed human mammary epithelial cells (MCF10A), C. T. Leung and J. S. Brugge have dissected the process by which sporadic oncogenic mutations could initiate clonal cancer progression in the early stages of human breast tumorigenesis. More specifically, the authors have evaluated the effects of a single oncogene-expressing cell in the context of a tightly regulated epithelial architecture. Notably, overexpression of classical oncogenes, such as the transcription factor Myc or the constitutively active kinase AKT, is not able to drive clonal outgrowth (Fig. I.11). These data indicate that within acinar structures oncogenic mutations could remain quiescent, highlighting the suppressive influence of an organized epithelial environment on initial neoplastic stages. By contrast, overexpression of ERBB2, a tyrosine kinase receptor classically found amplified in breast tumors, is sufficient to drive cell translocation in the luminal space (lumen filling) and clonal outgrowth (Fig. I.11). Moreover, the forced translocation of quiescent, oncogene-expressing cells to the luminal space correlates with their survival and expansion, lacking the suppressive effect of the neighboring cells. In conclusion, the authors propose a model in which cell translocation to the luminal space could be the trigger that initiates neoplastic progression (Leung and Brugge, 2012).

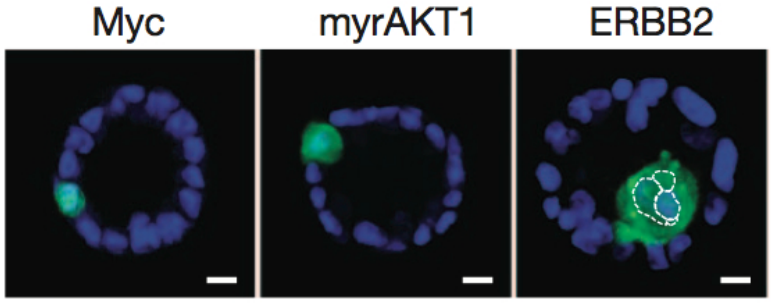

Figure I.11. **Single oncogene-expressing cell in mammary acinar culture.** *Single cells overexpressing the oncogenic transcription factor Myc or the myristoylated (constitutively active) form of AKT1 kinase remain quiescent in the 3D architecture of mammary acini. In contrast, overexpression of the tyrosine kinase receptor ERBB2 is associated with lumen filling, with cells actively protruding inside the luminal space. Reprinted by permission from Macmillan Publishers Ltd: Leung and Brugge,*

copyright 2012, Nature Publishing Group.

I.3.9. Functions of the exocyst complex beyond cell polarity

As already described in the context of lumenogenesis, the polarized trafficking of apical determinants is a crucial step in lumen specification that strictly requires the exocyst complex. Besides its function in cell polarity, studies in other systems indicate that the exocyst tethering complex might have additional roles. Indeed, the complex regulates the interaction of vesicles with their target plasma membrane and controls different aspects of cell physiology, including abscission (Gromley et al., 2005; Neto and Gould, 2011). Abscission is the final stage of cyokinesis when the plasma membrane of the two daughter cells is physically divided and occurs, as lumenogenesis, through targeting and fusion of exocyst vesicles with the intracellular-bridge plasma membrane (Neto and Gould, 2011). Indeed, several subunits of the exocyst complex, including Sec8, are localized at the ring-like structure, named midbody, that connects the two daughter cells during abscission (Chen et al., 2013; Gromley et al., 2005). Considering that in MDCK cells cyst lumenogenesis starts right after the first cell division, it is attractive to speculate that the exocyst complex might work as the first landmark for the formation of specialized membrane domains. This argument will be examined in more detail in the result (Chapter IV) and discussion (Chapter V) sections.

Chapter II: Objectives of the research

PRL-3 is a dual specificity phosphatase suspected to play a causative role in the development of cancer metastasis when aberrantly overexpressed. To date, the molecular basis of PRL-3 functions and its putative substrate(s) remain elusive, making it impossible to dissect the mechanism by which PRL-3 overexpression promotes cellular metastasis. Moreover, cell culture studies have revealed that the aberrant expression of PRL-3 results in a wide range of pleiotropic effects, leading to the activation of a multitude of cellular oncogenic pathways. At the start of my research project a phosphopeptide library was screened to identify novel candidate PRL-3 substrates. This analysis showed no detectable activity of PRL-3 against any of the phosphopeptides. On the contrary, preliminary results were suggesting catalytic activity toward phosphoinositides. Therefore, the main goal of my thesis was to gain more insight into PRL-3 lipid phosphatase activity. Moreover, considering the pleiotropic effects of PRL-3 overexpression in standard cell culture conditions, I wanted to explore the impact of PRL-3 overexpression in an organotypic 3D cell culture model. The underlying idea was to use this system to shed light into the mechanism(s) by which PRL-3 promotes metastasis of epithelium-derived cancers in a context were PRL-3 overexpression is the dominant oncogenic lesion.

In chapter III, entitled *"The Metastasis-Promoting Phosphatase PRL-3 Shows Activity toward Phosphoinositides"* PRL-3 catalytic activity against phosphoinositides was studied. For this purpose, the wild-type (WT) protein and several variants carrying mutations in key catalytic residues were tested in vitro using two complementary biochemical assays for substrate specificity and activity toward phosphoinositides. The data were additionally supported by molecular docking studies, analysis of the structural stability of the protein variants and migration assays.

In chapter IV, entitled *"The Metastasis-Promoting Phosphatase PRL-3 affects epithelial cell polarization by altering post-mitotic midbody fate"* the effect of PRL-3 aberrant overexpression was examined in the context of an organotypic 3D cell culture model. Next, the observed phenotypes were extensively characterized by imaging and biochemistry techniques. Finally, analyzing the PRL-3-mediated phenotype, new insights into the process of lumenogenesis were made.

Chapter III: The Metastasis-Promoting Phosphatase PRL-3 Shows Activity toward Phosphoinositides

Reprinted with permission from:

Victoria McParland, * **Giulia Varsano**, * Xun Li, Janet Thornton, Jancy Baby, Ajay Aravind, Christoph Meyer, Karolina Pavic, Pablo Rios, and Maja Köhn. (2011).

Biochemistry 50, 7579–7590.

Personal contribution:

Fig. III.6, III.7, III.9, III.10 and III.11

* Victoria McParland and Giulia Varsano contributed equally to this work.

III.1. Abstract

Phosphatase of regenerating liver 3 (PRL-3) is suggested as a biomarker and therapeutic target in several cancers. It has a well-established causative role in cancer metastasis. However, little is known about its natural substrates, pathways, and biological functions, and only a few protein substrates have been suggested so far. To improve our understanding of the substrate specificity and molecular determinants of PRL-3 activity, the wild-type (WT) protein, two supposedly catalytically inactive mutants D72A and C104S, and the reported hyperactive mutant A111S were tested in vitro for substrate specificity and activity toward phosphopeptides and phosphoinositides (PIPs), their structural stability, and their ability to promote cell migration using stable HEK293 cell lines. We discovered that WT PRL-3 does not dephosphorylate the tested phosphopeptides in vitro. However, as shown by two complementary biochemical assays, PRL-3 is active toward the phosphoinositide PI(4,5)P_2. Our experimental results substantiated by molecular docking studies suggest that PRL-3 is a phosphatidylinositol 5-phosphatase. The C104S variant was shown to be not only catalytically inactive but also structurally destabilized and unable to promote cell migration, whereas WT PRL-3 promotes cell migration. The D72A mutant is structurally stable and does not dephosphorylate the unnatural substrate 3- O-methylfluorescein phosphate (OMFP). However, we observed residual in vitro activity of D72A against PI(4,5)P_2, and in accordance with this, it exhibits the same cellular phenotype as WT PRL-3. Our analysis of the A111S variant shows that the hyperactivity toward the unnatural OMFP substrate is not apparent in dephosphorylation assays with phosphoinositides: the mutant is completely inactive against PIPs. We observed significant structural destabilization of this variant. The cellular phenotype of this mutant equals that of the catalytically inactive C104S mutant. These results provide a possible explanation for the absence of the conserved Ser of the PTP catalytic motif in the PRL family. The correlation of the phosphatase activity toward PI(4,5)P_2 with the observed phenotypes for WT PRL-3 and the mutants suggests a link between the PI(4,5)P_2 dephosphorylation by PRL-3 and its role in cell migration.

III.2. Introduction

Dual-specificity phosphatases (DSPs) belong to the superfamily of protein tyrosine phosphatases (PTPs). Classical PTPs remove a phosphate from tyrosine residues of

proteins, whereas DSPs exhibit activity toward a variety of different substrates such as phosphoserine, -threonine, and -tyrosine but also phosphatidylinositol phosphates (PIPs). The DSP PRL-3 is a cancer biomarker and promising therapeutic target.[1,2] PRL-3 is involved in cell growth, proliferation, and invasion,[1−4] and it is consistently overexpressed in colorectal cancer metastases.[5] It has also been shown to play a causative role in other cancer types and to correlate with increased metastatic potential and poorer prognoses.[1,2] In normal tissue, it is expressed at basal levels in skeletal muscle and the heart.[1] It contains a C-terminal CAAX box (where C is cysteine, A an aliphatic amino acid, and X any amino acid), which is farnesylated in vivo and localizes PRL-3 to inner membranes, particularly the plasma membrane and early endosome.[1] This is a unique feature among PTPs; however, it is a common feature among inositol phosphatases.[6] One of the DSPs structurally most similar to PRL-3 is PTEN,[7] and the sequence homology between the two (Figure III.1) has already been recognized in early molecular cloning studies.[8] PTEN is a DSP with activity toward 3-phosphorylated PIPs, particularly $PI(3,4,5)P_3$.[9] Studies in cell lines that stably express ectopic PRL-3 prove a direct correlation between elevated PRL- 3 levels and the acquisition of a migratory and invasive phenotype.[1,2] However, until now, the underlying biochemical mechanisms are still widely unknown.[1,2] So far, only a limited number of proteins have been suggested as natural substrates: Ezrin,[10,11] Keratin 8,[12] Integrinβ1,[13,14] and Stathmin.[15] Integrinα1 has been described as a direct interaction partner of PRL-3.[13] PRL-3 has been reported to regulate Rho family GTPases[16,17] and to be involved in downregulating Csk (C- terminal Src kinase) leading to Src kinase activation[18] via eIF2 using a general mechanism of inhibition of protein translation.[19] PRL-3 activity in cancer has also been linked to the PTEN-PI3K pathway potentially as an upstream posttranscriptional negative regulator of PTEN translation to promote epithelial-mesenchymal transition (EMT).[16] In addition, PRL-3 has been shown to promote EMT by direct regulation of Cadherin.[20] Unfortunately, the suggested substrates have so far not been placed into direct context with the pathways affected by PRL-3. Because PRL-3's natural substrates remain unclear and the enzyme so far could not be placed conclusively into any signaling pathway, we sought to map PRL-3's substrate specificity in vitro and to investigate the structure−activity relationship of PRL-3 toward potential substrates by investigating key PRL-3 variants. Thereby, we analyzed wild-type (WT) PRL-3 and three PRL-3

variants known to affect the catalytic activity of the enzyme: C104S, D72A, and A111S (Figure III.1).

First, the phosphatase activity of these variants was compared using OMFP as a substrate,[21] and far-UV circular dichroism (CD) spectra were acquired, including melting temperatures, to analyze the secondary structure of the variants.[22] The PRL-3 variants were then further characterized with respect to their phosphatase activity toward phosphopeptides and phosphoinositides. The chosen peptides were designed on the basis of proteins reported to be potential natural substrates. PRL-3 did not show any significant activity toward the phosphopeptides. Phosphoinositide activity for PRL-3 has not yet been reported.[23] We discovered that PRL-3 dephosphorylates $PI(4,5)P_2$ and, to a lesser extent, $PI(3,4,5)P_3$ in vitro. Our data, including dephosphorylation assays and molecular modeling, suggest that PRL-3 is a phosphatidylinositol 5- phosphatase. Subsequently, the cellular phenotype of WT PRL- 3 and the variants with respect to promoting cell migration in a wound healing assay was investigated using stably transfected HEK293 cell lines. The cellular phenotype that we observed correlates well with the structure−activity analysis of all variants and the WT protein. Thus, we can suggest that PRL-3's role in cell migration can be related to its ability to dephosphorylate $PI(4,5)P_2$ or $PI(3,4,5)P_3$.

Figure III.1. Sequence and structural alignment of PRL-3 with PTEN.[21] *The mutated residues in PRL-3 used in this study are colored purple (D72, C104, and A111). Catalytic residues are underlined. Secondary structures are labeled according to PDB entries 1V3A and 1D5R (α-helix, red band; β-sheet, green arrow).*

III.3. Materials and methods

III.3.1. Materials

Fmoc-protected amino acids HBTU, HOBt, and Rink amide resin were purchased from Calbiochem. DMF, piperidine, and DCM were purchased from VWR. Glutathione *S*-transferase (GSTrap FF, 1 mL) and NiNTA purification columns were purchased from Amersham Biosciences/GE Life Science. Protease inhibitor cocktail tablets were purchased from Roche. The EnzChek phosphatase assay kit was purchased from Molecular Probes. All soluble di-C8-D-myophosphatidylinositol phosphates were purchased from Echelon Biosciences. All other reagents were purchased from Sigma-Aldrich.

III.3.2. Bacterial Strains and Plasmid Vectors

Plasmid vector pET15b was used to overexpress recombinant human WT and mutant PRL-3 forms as His-tagged fusion proteins, and vector T7-7 was used to overexpress human His-tagged PTP1B. Human PTEN and human type IV 5-phosphatase (5-ptase) were overexpressed as GST-tagged fusion proteins using pGEX-4T-1 and pBADM-30, respectively, as vectors. All recombinant proteins were transformed into *Escherichia coli* strain BL21 DE3 using standard methods that have been previously described.[24] Bacterial cultures were grown at 37 °C with shaking, and protein expression was induced with 0.1 mM IPTG for PRL-3 variants and PTEN and 0.2% arabinose for 5-ptase. Proteins were induced for 3 h at 37 °C.

III.3.3. Construction of Mutant PRL-3 Proteins

A111S PRL-3, C104S PRL-3, and D72A PRL-3 proteins were constructed using single-step polymerase chain reaction using complementary primers encoding the codon change. Primers 5′ ggcctgggccggtctccagtccttg 3′ and 5′ caaggactggagaccggcccaggcc 3 ′ were used to construct A111S . Primers 5 ′ cgtttgacgctggggcgcc 3′ and 5′ ggcgccccagcgtcaaacg 3′ were used to construct D72A. Primers 5′ ctgtgcactccgtggcggg 3′ and 5′ cccgccacggagtgcacag 3′ were used to construct C104S. Mutant constructs were confirmed by DNA sequencing.

III.3.4. Expression and Purification of Recombinant Proteins

BL21 DE3 cells expressing the recombinant WT and mutant forms of PRL-3 were lysed by sonication in buffer A [50 mM Tris-HCl (pH 7.4) containing 500 mM NaCl,

20 mM imidazole, 1 mM dithiothreitol (DTT), and 0.5 mM protease inhibitor cocktail]. The proteins were purified using a FPLC Histrap HP 1 mL column using an elution gradient from 20 to 500 mM imidazole in buffer A. The purified PRL-3 proteins were dialyzed against 50 mM Tris-HCl (pH 7.4), 150 mM NaCl, 5 mM DTT, and 10% glycerol. BL21 DE3 cells expressing the recombinant His-PTP1B were lysed by sonication in lysis buffer [20 mM Tris-HCl (pH 8.0) containing 150 mM NaCl, 10 mM imidazole, 1 mM DTT, and 0.5 mM phenylmethanesulfonyl fluoride (PMSF)]. The protein was purified using a FPLC Histrap HP 1 mL column using an elution gradient from 10 to 500 mM imidazole in buffer A. BL21 DE3 cells expressing recombinant GST−PTEN fusion protein were lysed in 50 mM Tris-HCl (pH 8.0), 250 mM NaCl, and 0.5 mM protease inhibitor cocktail. The cell lysate was applied to a FPLC GSTrap FF 1 mL column; the column was washed with 50 mM Tris-HCl (pH 8.0) and 50 mM NaCl, and then the GST−PTEN fusion protein was eluted with 50 mM Tris-HCl (pH 8.0), 50 mM NaCl, and 10 mM glutathione. Purified GST−PTEN fusion protein was dialyzed against 50 mM Tris-HCl (pH 8.0), 150 mM NaCl, and 1 mM DTT. BL21 DE3 cells overexpressing the pBADM-30-GST-5-ptase were lysed in 50 mM sodium phosphate (pH 6.8), 200 mM NaCl, 2 mM DTT, 0.1 mg/mL lysozyme, and 0.5 mM protease inhibitor cocktail, using a French press, with four passes. The cell lysate was applied to a FPLC GSTrap FF 1 mL column, and the column was washed with 50 mM sodium phosphate (pH 6.8), 50 mM NaCl, 2 mM DTT, and 0.5 mM protease inhibitor cocktail. Then the GST−5-ptase fusion protein was eluted with 50 mM sodium phosphate (pH 6.8), 50 mM NaCl, 2 mM DTT, and 10 mM glutathione. The integrity of all proteins was confirmed by molecular weight determination by electrospray ionization mass spectroscopy (ESI-MS).

III.3.5. Peptide Synthesis

Peptides were synthesized on solid phase Rink amide resin by standard coupling and Fmoc protection strategies using an automated MultiSynTech peptide synthesizer. Peptides were isolated after cleavage from resin and deprotection using 95 vol % trifluoroacetic acid and 5 vol % triisopropylsilane. The peptides were ether-precipitated and purified to homogeneity (>90% purity) using high-performance liquid chromatography, and identities were confirmed by ESI-MS.

III.3.6. Far-UV Circular Dichroism (CD)

WT PRL-3 and mutant variants were dialyzed into 20 mM Tris-HCl (pH 7.4), 50 mM NaCl, and 1 mM DTT. Protein concentrations after dialysis were determined by absorption at 280 nm using a NanoDrop spectrophotometer. The concentrations used in the CD measurements were 0.48 mg/mL for WT PRL-3, 0.43 mg/ mL for the D72A mutant, 0.64 mg/mL for the A111S mutant, and 0.6 mg/mL for the C104S mutant. Far-UV CD spectra were recorded using a Jasco J-715 spectropolarimeter. The spectropolarimeter was purged with N_2 for 15 min prior to measurement. CD was measured over the far-UV range (195− 250 nm) at 20 °C using a path length of 0.1 cm. The scan speed was set to 10 nm/min with a wavelength interval of 1 nm. Four or five scans were acquired and automatically averaged. The far-UV signal over the entire range was initially measured using a buffer sample in the absence of enzyme to determine the baseline for subsequent CD spectra. Far-UV CD spectra were acquired for WT PRL-3 and for the variants in duplicate. The spectra were then averaged and buffer subtracted as well as normalized to a protein concentration of 1 mg/mL. The thermal stability of the PRL-3 proteins was also compared by monitoring the CD signal at 223 nm as a function of temperature over a range of 20−85 °C with intervals of 0.2 °C. The sample was cooled in the spectropolarimeter, and observation of the CD signal upon cooling showed that the thermal denaturation of WT PRL-3 and the variants was irreversible. Therefore, thermodynamic parameters could not be quantitatively determined from the CD data. The midpoint of the thermal denaturation curve was estimated and used as a qualitative comparison of the stability of the different proteins.

III.3.7. Phosphatase Activity Assays

A standard enzymatic activity assay was conducted using 3-*O*-methylfluorescein phosphate (OMFP) as a substrate. The assay was conducted at 37 °C in 40 mM Tris-HCl (pH 6.2), 150 mM NaCl, and 4 mM DTT. WT PRL-3 and mutant variants were assayed at 6 μM. OMFP was used at 600 μM in all reactions. The assay was conducted in 96-well plate format and monitored by absorbance at 450 nm over time. The release of phosphate from candidate peptide and lipid substrates was monitored using a commercially available phosphatase assay kit, EnzChek, according to the manufacturer's instructions. WT PRL-3 and mutant variants [2 μM, 4.5 μM (for phosphopeptide activity assays), or 6 μM (for PIP activity assays)] were incubated

with 50 mM Tris-HCl (pH 7.5), 150 mM NaCl, 1 mM $MgCl_2$, and 4 mM DTT in 96-well plates with either 100 μM phosphopeptide or 100 μM phosphoinositide substrates. The assay was conducted at 37 °C with shaking in a Tecan Safire TM plate reader. The release of phosphate from the candidate substrates was continually monitored by measuring absorbance at 360 nm. For the controls, 52 nM PTP1B was incubated with 50 μM phosphopeptide substrate, and 0.9 μM PTEN and 5.8 μM 5-ptase were incubated with 100 μM phosphoinositide in the same buffer used for the PRL-3 measurements. Assays conducted in the absence of enzyme were included in the 96-well plate setup in triplicate for all the substrates analyzed. The measurements in the absence of enzyme were averaged and subtracted from the data to account for nonspecific hydrolysis of the substrates and for background absorption. The data were normalized toward the signal of $PI(3,4,5)P_3$ in the no enzyme control to account for potential difference due to the use of multiple plates. In all phosphatase assays, the measurements were taken in triplicate and the standard deviation of the measurements is represented as error bars. Data were plotted using SigmaPlot11.

Dephosphorylation assays of fluorescently labeled PIPs (Echelon Biosciences) were conducted using recombinant PRL-3 (4.5 or 9 μg) in 20 μL of reaction buffer containing 50 mM MES (pH 6.5) and 1 mM TCEP [tris(2-carboxyethyl)-phosphine] with 1.0 μg of fluorescent di-C6-NBD6 or fluorescent di-C6-BODIPY phosphoinositide substrates for 1 h at 37 °C. Phosphatase assays using recombinant PTEN were conducted in 20 μL of reaction buffer containing 50 mM ammonium carbonate (pH 8.0) in the presence of 1 mM TCEP. Phosphatase assays using recombinant 5-ptase were conducted in 20 μL of reaction buffer containing 50 mM Tris-HCl (pH 7.5), 50 mM NaCl, and 3 mM $MgCl_2$. Phosphatase reactions were terminated by addition of 100 μL of acetone and then mixtures evaporated to dryness in a Speed-Vac evaporator. The dried reaction products were resuspended in 20 μL of a methanol/chloroform mixture (1/1) and spotted onto a glass-backed TLC plate (HPTLC Silica gel 60, 10 cm × 10 cm, Merck).[25] The TLC plate was developed in a chloroform/ acetone/methanol/glacial acetic acid/water solvent system (80/30/26/24/14) as described previously and air-dried.[25] Fluorescent lipids were visualized using a model FLA 7000 Fuji Bio-Imaging System.

Phosphatase assays using immunoprecipitated FLAG-tagged PRL-3 wild-type, C104S, D72A, or A111S proteins were conducted by incubating resin-bound proteins for 1 h at 37 °C in 30 μL of reaction buffer (above) containing 1 μg of di-C6-NBD6-

phosphatidylinositol 4,5-diphosphate. The samples were then centrifuged for 30 s to pellet the beads, and 20 μL of supernatant was removed. Acetone (100 μL) was added to each supernatant, and the samples were dried and analyzed as described above.

III.3.8. Molecular Modeling

The PRL-3 structure in the "closed" active conformation was obtained via homology modeling using the crystal structure of PRL-1 (C104S) in complex with a sulfate ion (PDB entry 1XM2)[26] as a template. Homologue proteins of human PRL-3 were identified from UniProt,[27] and ClustalW2[28] was used for multiple-sequence alignment. The alignment result between PRL-3 (Q75365) and PDB entry 1XM2 coincides with those in previous studies.[26,29] MODELER (Release 9v8)[30] was then used for homology modeling. The sulfate ion was kept in the active site during model generation. Eleven models were generated, and the best model was selected by three criteria: "normalized DOPE score" (MODELER), "dfire_energy" (DFire),[31] and "model quality score" (ModFOLD).[32] This model was further refined by MD simulation using NAMD (version 2.7b4)[33] with an Amber force field. The charges and force field parameters of the sulfate ion were obtained using the Antechamber[34] module in AMBER-Tools (version 1.4), where the charge models were calculated via the AM1-BCC method. Atoms on PRL-3 were assigned the parameters of the ff03 force field. The PRL-3−sulfate complex was soaked in a box of TIP3P[35] water molecules with a margin of 10 Å along each dimension. Chloride ions were added to neutralize the whole system. The system was first minimized with restraints of 5.0 kcal/mol on protein and sulfate ion for 5000 steps. The time step size was set to 2 fs. Then, the system was further minimized without constraints for 15000 steps. After that, a 62 ps simulation was used to gradually increase the temperature of the system from 0 to 310 K. A subsequent 500 ps simulation was performed to equilibrium under a constant temperature of 310 K and a constant pressure of 1 atm. The nonbonded cutoff distance was set to 12 Å. During the entire MD simulation, Cys-104 was treated as the deprotonated form while Asp-72 was treated as the protonated form. The last snapshot of the MD simulation was selected as the final PRL-3 model.

The three-dimensional (3D) structural model of diC8-PI(4,5)P_2 (the deprotonated form) was built on the basis of PI(3)P, which was extracted from PDB entry 1ZSQ.[36] It was further optimized via OpenBabel (version 2.2.3)[37] using the MMFF94 force field. GOLD (version 5.0.1, CCDC Software)[38] was then used in molecular docking

of diC8-PI(4,5)P_2 to the PRL-3 model. GoldScore was selected as fitness function and automatic (ligand-dependent) genetic algorithm parameter settings were used with the search efficiency set to 100%. The active site residues Arg-6, Asp-72, Val-105, Leu-108, Arg-110, and Arg-138 were treated as flexible during docking. For the constrained docking study, the 4- or 5-phosphate group of diC8-PI(4,5)P_2 was constrained to point into the catalytic site during docking by setting the constraints for the H−O distance between Asp-72 COOH and O-PO3-diC8-PI(4,5)P_2 (1.6−2.0 Å) and the S−P distance between Cys-104 S and P-O4-diC8-PI(4,5)P_2 (3.0−3.8 Å).

III.3.9. Generation of Cell Lines Stably Expressing PRL-3 Variants

The Flp-In 293 T-Rex (tetracycline-regulated system) cell line (Invitrogen) was used to create isogenic cell lines stably expressing wild-type and mutant PRL-3 proteins with N-terminal FLAG epitope tags. Cells were grown in Dulbecco's modified Eagle's medium (DMEM) supplemented with 1% glutamine, 1% penicillin/streptomycin, 10% fetal bovine serum (FBS) (Invitrogen), 15 μg/mL of blasticidin, and 100 μg/mL hygromicin. The expression of the PRL-3 proteins was induced by addition of 1 μg/mL tetracycline to the growth medium.

III.3.10. Western Blot

Cell lysates were subjected to sodium dodecyl sulfate−polyacrylamide gel electrophoresis (SDS− PAGE) and immunoblot analysis with antibodies against FLAG (Sigma) and β-actin (Sigma).

III.3.11. Indirect Immunofluorescence

To visualize FLAG-tagged PRL-3, HEK293 cells stably expressing either WT PRL-3 or mutants were seeded onto LabTek eight-well chamber slides (NUNC) precoated with polylysine. Cells were fixed with 4% paraformaldehyde for 15 min at room temperature, permeabilized with 0.1% Triton X-100 and phosphate-buffered saline for 10 min, and blocked with 1% bovine serum albumin for 1 h. The anti-FLAG antibody was then added to the cells, followed by the Alexa Fluor 488 goat anti-mouse IgG secondary antibody (Invitrogen). After being washed with phosphate-buffered saline, cells were incubated with Hoechst 33342 (2 μg/mL) for 5 min and imaged using a Leica SP2 sirius confocal microscope system.

III.3.12. Wound Healing Motility Assays

Cell migration assays were conducted using μ-Dish 35 mm Culture Inserts (Ibidi) according to the manufacturer's protocols. In brief, cells stably expressing either PRL-3 wild-type, mutants, or an empty vector were seeded into each well of the culture inserts in the presence of tetracycline and incubated at 37 °C in a humidified atmosphere with 5% CO_2. On the day of experimentation, the culture inserts were gently removed by using sterile tweezers, and the dish was filled with fresh DMEM supplemented with 5% FBS. Photos of the wound were taken under a Zeiss Cellobserver HS microscope (10× magnitude).

III.3.13. Immunoprecipitation of PRL-3 Proteins

Cells stably expressing PRL-3 proteins were grown in the presence of tetracycline. Cells were lysed on ice in a buffer containing 50 mM Tris-HCl (pH 7.4), 150 mM NaCl, 1 mM EDTA, and Complete Protease Inhibitor (Roche) by being passed through 26-gauge needles 10 times. Lysates were cleared by centrifugation (10 min at 18000*g* and 4 °C), and the supernatants were incubated on a rocker for 2 h at 4 °C with 40 μL of anti-FLAG M2-agarose affinity resin (Sigma). Samples were washed three times with lysis buffer followed by an additional wash with the phosphatase reaction buffer (see above).

III.4. Results and discussion

III.4.1. Characterization of the PRL-3 Variants

To characterize the in vitro phosphatase activity of PRL-3, we analyzed wild-type (WT) PRL-3 and three key variants, C104S, D72A, and A111S PRL-3. Mutation of the essential active site Cys 104 to Ser inactivates PRL-3 phosphatase activity.[10] In the D72A mutant, the activity of PRL-3 is also affected by the disruption of the acidic loop that is required for hydrolysis of a substrate once it is bound to the active site, and the mutant has been reported to be catalytically inactive, at least toward OMFP.[21] With regard to the A111S mutant, an active site Ser residue is a conserved feature among many DSPs and is implicated in the catalytic mechanism. Such a Ser is not featured in the PRL family of DSPs, possibly explaining the much weaker in vitro activity of PRLs relative to those of other DSPs. The variant of PRL-3 in which Ala 111 has been substituted with Ser has been reported to be hyperactive toward OMFP.[21] The phosphatase activity of the proteins was initially compared using

OMFP as a substrate[21] (Figure III.2). Consistent with a previous report,[21] WT PRL-3 exhibits very weak activity toward OMFP, D72A PRL-3 shows no significant dephosphorylation of OMFP, and the A111S mutant exhibits considerably higher activity than WT PRL-3. Mutation of the essential active site Cys 104 to Ser inactivates PRL-3 phosphatase activity.

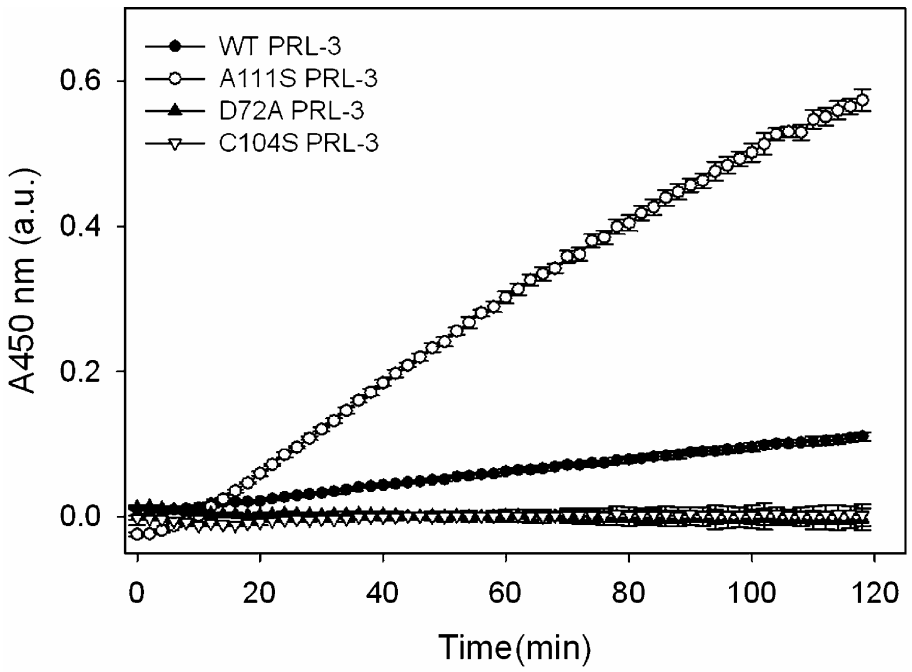

Figure III.2. *Hydrolysis of OMFP (600 μM) by wild-type PRL-3 and mutant forms of PRL-3: A111S, D72A, and C104S (6 μM each). Measurements were taken in triplicate, and the standard deviation of the measurements is represented as error bars.*

To further characterize WT PRL-3 and its variants, far-UV circular dichroism (CD) spectra were acquired.[22] The CD measurements show significant structural changes for the A111S and C104S mutants compared to WT PRL-3, whereas D72A exhibited much less structural perturbation (Figure III.3A). The CD signal was then monitored at increasing temperatures to compare the thermal stability of the PRL-3 variants. The apparent melting temperatures of C104S (52 ± 2 °C) and A111S (51 ± 2 °C) are significantly lower than that of WT PRL-3 (62 ± 2 °C), while the melting temperature of D72A appears to be higher [>65 °C (Figure III.3B−E)]. These results suggest that the mutations within the catalytic region of PRL-3, i.e., the A111S and C104S mutations, have a more significant impact on the structural stability of PRL-3 than a mutation in a distant region (D72A). In both destabilized variants, a hydrophilic

residue is introduced into the hydrophobic p-loop of PRL-3.[39] This could also contribute to the structural destabilization.

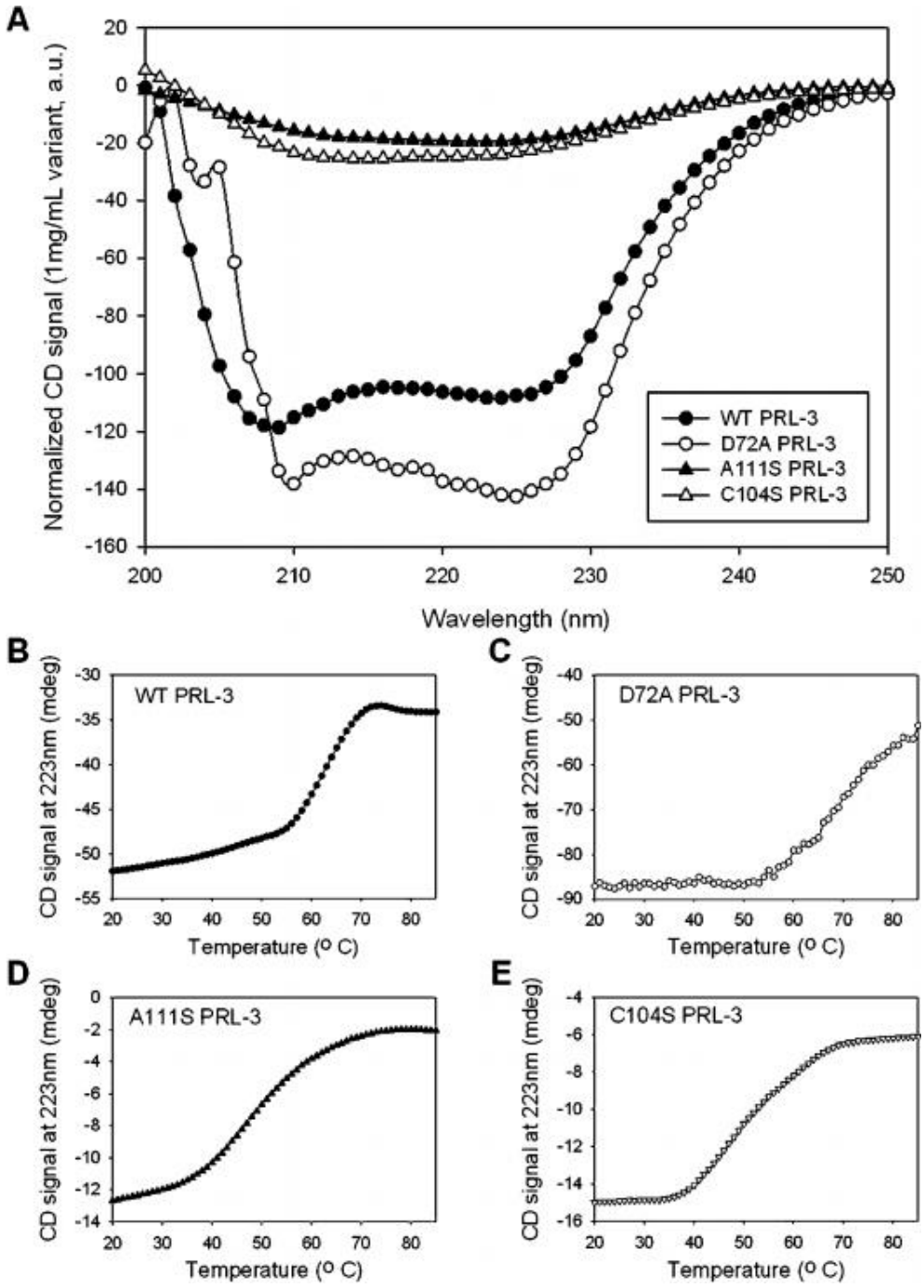

Figure III.3. Secondary structure analysis of the PRL-3 variants by far-UV CD. *(A) Far-UV CD spectra of WT PRL-3 as well as the D72A, C104S, and A111S mutants. (B−E) Thermal stability curves of WT PRL-3 (B), D72A PRL-3 (C), A111S PRL-3 (D), and C104S PRL-3 (E). For experimental details, see Materials and Methods*

III.4.2. Determination of the Catalytic Activity and Specificity of WT PRL-3 and Its Variants

The phosphatase activity of WT PRL-3 and A111S PRL-3 toward phosphorylated peptide substrates was then analyzed. The A111S mutant was used because of its enhanced activity toward OMFP and thus potential higher sensitivity. The phosphatase concentrations were chosen to be in the low micromolar range, and thus quite high, because of the reported low activity of PRL-3 toward peptides and OMFP in vitro,[21] and for the same reason, a high peptide concentration was selected (100 μM). A commercially available dephosphorylation assay (EnzChek) was used to monitor the release of phosphate continuously over time (Figure III.4, data at 30 min). The peptide substrates [peptides 1−6 (Table 1)] were designed on the basis of proteins reported to be affected by PRL-3 and thus potentially interact with PRL-3 in vivo.[7,10,11,13,14,16−18] Three more peptides [peptides 7−9 (Table 1)] were included to increase the variety of amino acid properties and peptide length.

Table 1. Sequence Features and Origins of the Phosphorylated Peptides Used as Substrates for in Vitro Dephosphorylation Assays

entry	sequence[a]	protein origin	phospho site
1	biotin-GENPIpYKSAV-NH_2	Integrinβ1	Y783[b]
2	Ac-GENPIpYKSAV-NH_2	Integrinβ1	Y783[b]
3	biotin-VVNPKpYEGK-NH_2	Integrinβ1	Y795[b]
4	biotin-QGRDKYKpTLRQIRQG-NH_2	Ezrin	T567[c]
5	biotin-ASSSTSVpTPDVSDNEPDHY-NH_2	PTEN	T366[b]
6	Ac-IpSPPPTANL-NH_2	FAK1	S910[b]
7	Ac-IQAAApSTP-NH_2	GSK3β	S389[b]
8	Ac-DpYpYR-NH_2	IR	Y1189, Y1190[b]
9	Ac-DKEpYpYKVKEPGES-NH_2	JAK2	Y1007, Y1008[b]

[a]NH_2 is the C-terminal amide; Ac is the N-terminal acetyl group, and biotin denotes N-terminal biotinylation. [b]UniProt data. [c]From refs 10 and 11

Neither WT PRL-3 nor A111S PRL-3 dephosphorylates any of our peptide substrates significantly (Figure III.4). As a positive control, dephosphorylation of

peptides by the Tyr-specific phosphatase PTP1B[40] was monitored in parallel with PRL-3. PTP1B shows a high degree of phosphatase activity toward phosphotyrosine peptides. Because of the potential further application of the peptides, they were either biotinylated or acetylated. Comparison between peptides 1 and 2 shows that the addition of either group has no effect on PRL-3 phosphatase activity. The lack of in vitro activity of PRL-3 toward phosphopeptides could indicate that PRL-3 needs a cofactor or post-translational modification to be able to dephosphorylate proteins, or that it requires the entire protein for recognition as a substrate. On the other hand, other DSPs such as CDC25 and MKP3 have also been reported to have weak activity toward peptides derived from protein substrates;[41,42] thus, the lack of in vitro activity is not necessarily unusual.

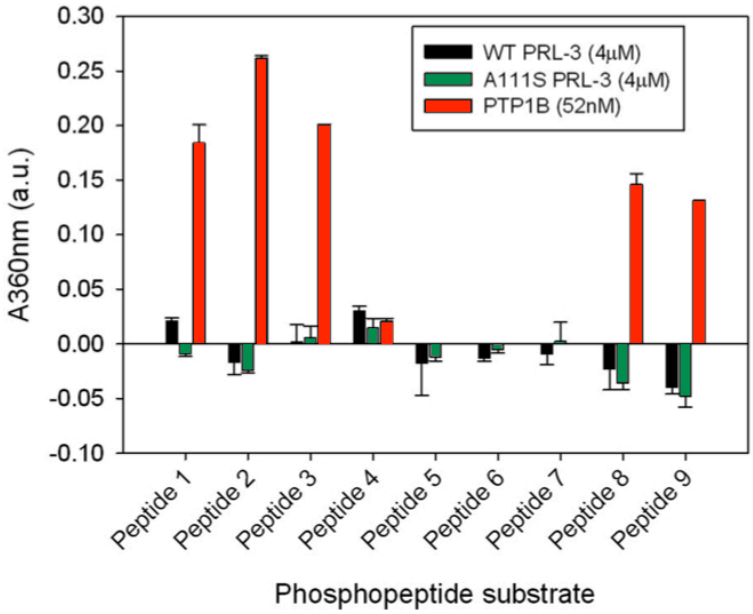

Figure III.4. *Dephosphorylation of phosphopeptides by WT PRL-3 (4 μM, black), A111S PRL-3 (4 μM, light gray), and PTP1B (52 nM, dark gray). Phosphopeptides were assayed at 100 μM for PRL-3 variants and at 50 μM for PTP1B. Phosphate release was measured in triplicate using the EnzChek assay (see Materials and Methods). The averaged data are shown, and the standard deviation is represented as error bars. Absorption intensities of <0.05 au are considered to be not significant because of combined spectral and manual error.*

PRL-3 is structurally similar with the lipid phosphatase PTEN (Figure III.1), and it carries a C-terminal CAAX box, which not only is featured in known lipid phosphatases but also localizes PRL-3 to the cellular compartments rich in phosphoinositides (PIPs). In addition, certain PIPs such as PI(3,4,5)P_3 and PI(3,4)P_2

and also depletion of $PI(4,5)P_2$ have been described as being involved in promoting cell motility, and these roles have been shown to be important in cancer.[43] Thus, further investigations were conducted using PIPs as lipid substrates. The release of phosphate from soluble PIP substrates carrying dioctanoyl (diC8) lipid chains by WT, C104S, D72A, and A111S PRL-3 as well as PTEN and type IV 5-phosphatase (5-ptase) was continuously measured over 2 h using the EnzChek assay. 5-ptase does not belong to the PTP superfamily and uses a catalytic mechanism different from that of PTPs; however, it has been reported to dephosphorylate $PI(4,5)P_2$ and $PI(3,4,5)P_3$ [44] and was therefore used here as a second control. The signal intensity after dephosphorylation for 30 min was used to compare the substrate preferences of each individual enzyme against the whole range of phosphoinositides. The resulting substrate preference profiles are shown in Figure III.5A.

As expected, PTEN dephosphorylates $PI(3,4,5)P_3$ and shows no significant activity toward the other PIPs (Figure III.5A). Also as expected, 5-ptase removes phosphate preferentially from $PI(4,5)P_2$ and $PI(3,4,5)P_3$, demonstrating the robustness of the assay. WT PRL-3 exhibits lipid phosphatase activity toward $PI(4,5)P_2$ and, to a lesser extent, toward $PI(3,4,5)P_3$, with no significant activity measured against the other PIP substrates. D72A PRL-3 shows weakened lipid phosphatase activity but with the same substrate preferences as WT PRL3. The C104S and, surprisingly, A111S variants exhibit no lipid phosphatase activity toward any of the measured phosphoinositide substrates.

By comparison of the substrate preference profiles of all the phosphatases assayed here (Figure III.5A), it is clear that WT PRL-3 and the less active D72A variant show substrate preferences very similar to those of 5-ptase, rather than those of PTEN. Although the substrate preferences of PRL-3 match those of the 5-ptase and partially match those of PTEN, there are significant differences in the kinetics of dephosphorylation for each of these enzymes. Dephosphorylation of $PI(3,4,5)P_3$ by PRL-3 compared to that by PTEN and 5-ptase is shown in Figure III.5B. In spite of the lower concentration used in our assay, PTEN is more active than PRL-3 toward $PI(3,4,5)P_3$. The 5-ptase, assayed here at high concentrations like those of PRL-3, also has faster activity against $PI(3,4,5)P_3$ than PRL-3. The dephosphorylation of $PI(4,5)P_2$ by PRL-3 and 5-ptase is compared in Figure III.5C. These kinetic traces clearly show that 5-ptase demonstrates faster reaction kinetics toward $PI(4,5)P_2$ than PRL-3.

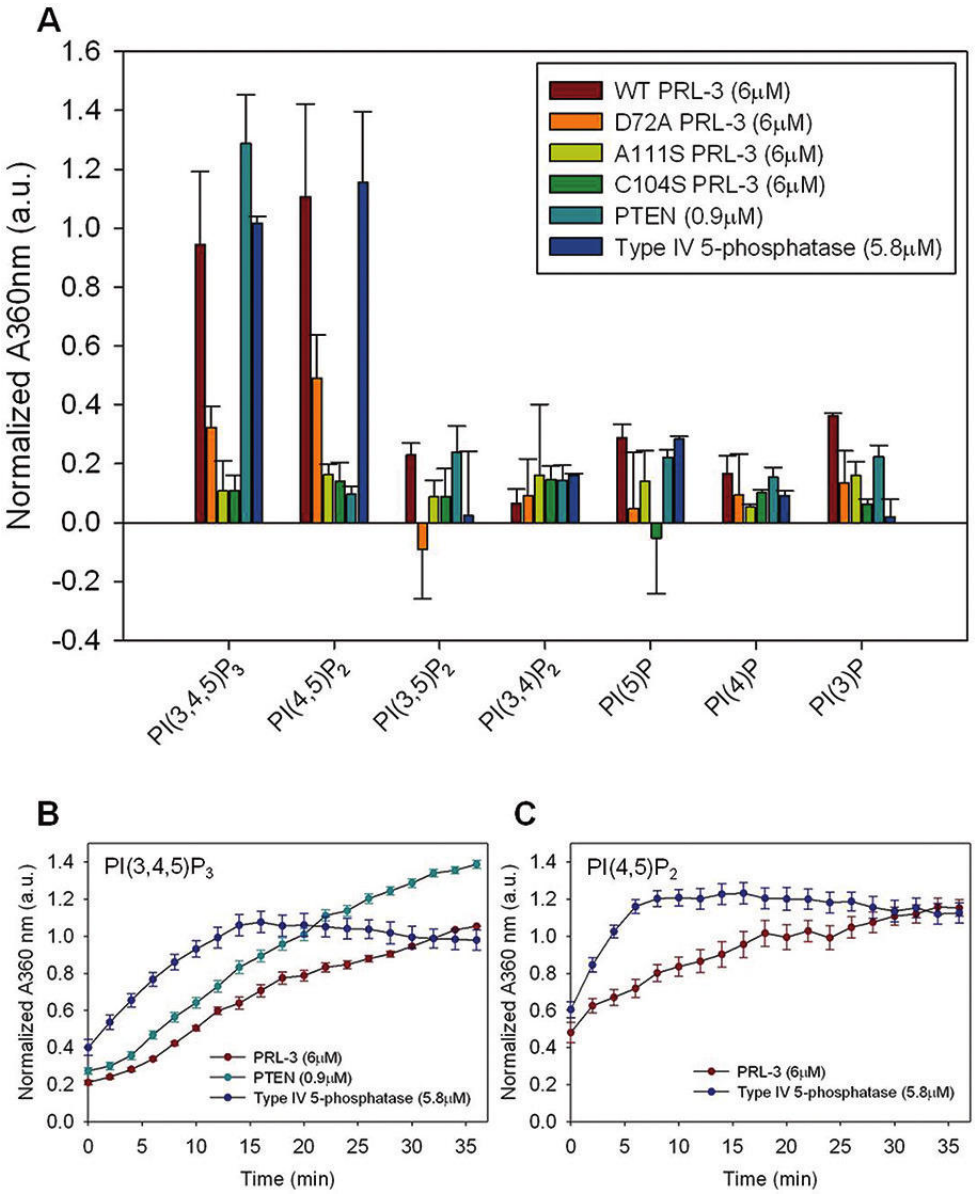

Figure III.5. Dephosphorylation of PIPs by WT PRL-3 and its variants (6 μM), PTEN (0.9 μM), and type IV 5-phosphatase (5.8 μM). The full range of phosphoinositide substrates was analyzed at 100 μM. *(A) The absorption at 360 nm after dephosphorylation of each substrate for 30 min shows the substrate preference profiles for each enzyme. (B and C) Kinetic traces of dephosphorylation of (B) PI(3,4,5)P_3 by WT PRL-3, PTEN, and type IV 5-phosphatase and (C) PI(4,5)P_2 by WT PRL-3 and type IV 5-phosphatase. Measurements were taken in triplicate and individually corrected for background by subtracting the absorbance from a corresponding PIP sample incubated in the absence of enzyme. The background-corrected absorbance was then normalized to the signal of the PI(3,4,5)P_3 control without enzyme and averaged. The standard deviation of the averaged normalized data is represented as error bars. Absorption intensities below 0.30 au (resulting from normalization of the original value of 0.05 au and averaging) are considered to be not significant because of the combined spectral and manual error.*

The D72A and A111S PRL-3 variants show discrepancies between their activities toward OMFP and toward PIPs. The D72A variant has no activity against OMFP but does have attenuated wild-type-like activity toward the PIP substrates (Figures III.2 and III.5A). This could be simply due to enhanced sensitivity to the PIPs as potential natural substrates compared to the unnatural OMFP substrate, or because of the apparent overall structural stabilization of the mutant as indicated by our CD studies. In addition, D to A mutant PTPs have been reported to be able to sustain some catalytic activity, presuming another residue in the protein can substitute the missing general acid required for the catalytic mechanism.[45] Within the active site of PTPs, there is a conserved Ser/Thr that could fulfill this role.[45] However, there is no such equivalent residue in the active site of PRL-3 (A111), indicating that the general acid property needs to be provided by another residue within the protein or from the substrate itself. The highly negatively charged PIPs as substrates for PRL-3 could quite feasibly compensate for the loss of acid in the mechanism of dephosphorylation by the D72A mutant. The A111S PRL-3 variant has been shown to be a hyperactive form of the protein toward OMFP[21] (Figure III.2), yet this mutant does not dephosphorylate any PIP substrates in our in vitro assays (Figure III.5A). Given that our CD studies show perturbations in the structure of A111S PRL-3 relative to that of the wild-type protein, this Ala residue could play an important role in maintaining the integrity of the active site. However, on the basis of our current data, we cannot determine unequivocally whether the inactivity of A111S PRL-3 and the activity of D72A PRL-3 toward PIP substrates are due to structural changes relative to the WT protein or differences in the enzymatic mechanism. For C104S PRL-3, the lipid phosphatase activity is consistent with the OMFP activity assays, which demonstrates that replacing Cys 104 with Ser completely inactivates the phosphatase.

To further validate our findings, we repeated the dephosphorylation assay with PI(4,5)P_2 and PI(3,4,5)P_3 using PIP derivatives that are fluorescently labeled in one lipid chain. The dephosphorylation of the substrates was analyzed by thin layer chromatography (Figure III6). As seen in Figure III6A, PI(4,5)P_2 is dephosphorylated by PRL-3 and 5- ptase but not PTEN, confirming the results of the previous assay. Dephosphorylation of PI(3,4,5)P_3 by WT PRL-3 was not seen in this assay; it was, however, dephosphorylated by PTEN and 5-ptase, showing the robustness of this assay (Figure III6B).

It is unclear why PRL-3 lacks PI(3,4,5)P_3 phosphatase activity in this assay. We can

speculate that the different result could be due to the presence of a different lipid chain in the fluorescent PIP; however, this was not represented in the $PI(4,5)P_2$ data. Also, the weak in vitro activity of PRL-3 could contribute to this result. Despite such discrepancies, we have definitively confirmed PRL-3 phosphatase activity toward $PI(4,5)P_2$, and thus, PRL-3 could be the first phosphatase in the PTP superfamily to dephosphorylate this PIP.

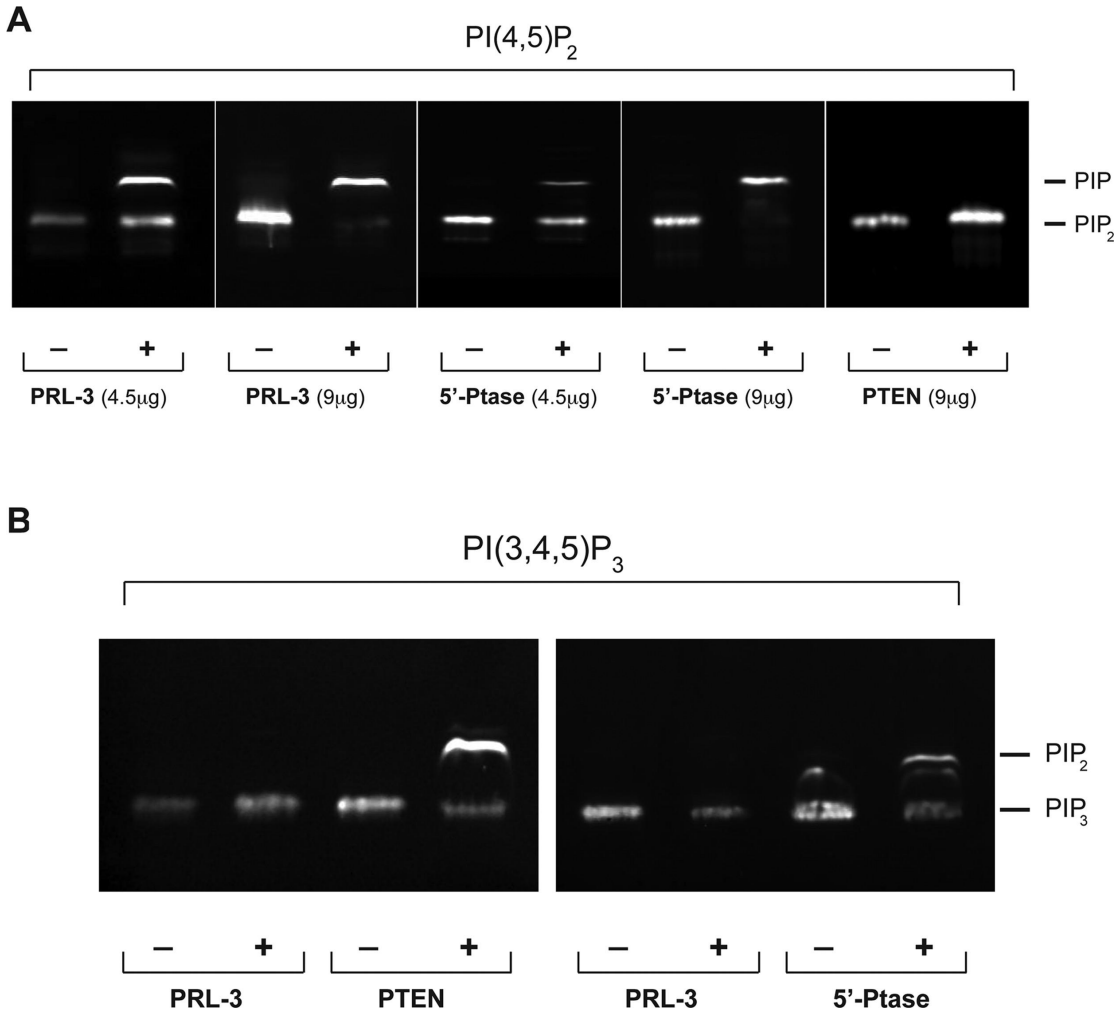

Figure III.6. Dephosphorylation of fluorescently labeled $PI(4,5)P_2$ (A) and $PI(3,4,5)P_3$ (B) by WT PRL-3, 5-ptase, and PTEN. *Phosphatase assays containing 1.0 μg of fluorescent phosphoinositide substrate were conducted for 1 h at 37 °C with buffer (−) or with different concentrations of recombinant proteins (as indicated), processed as described in Materials and Methods, and analyzed by TLC. $PI(3,4,5)P_3$ dephosphorylation assays were performed under the same conditions using 9 μg of recombinant protein. Shown is a representative result of three experiments.*

We then analyzed the product of $PI(4,5)P_2$ dephosphorylation by PRL-3 by comparing the product to the mono-phosphorylated PIPs to determine which phosphate on the ring is released by PRL-3. Figure III.7 shows the fluorescence read-out of the dephosphorylation of $PI(4,5)P_2$, PI(4)P, and PI(5)P by PRL-3. The monophosphorylated PIPs run quite close. PI(4)P runs closer to the product of the $PI(4,5)P_2$ dephosphorylation by PRL-3, whereas there is a clear gap between the product and PI(5)P. This result provides support for PRL-3 being a phosphatidylinositol 5-phosphatase.

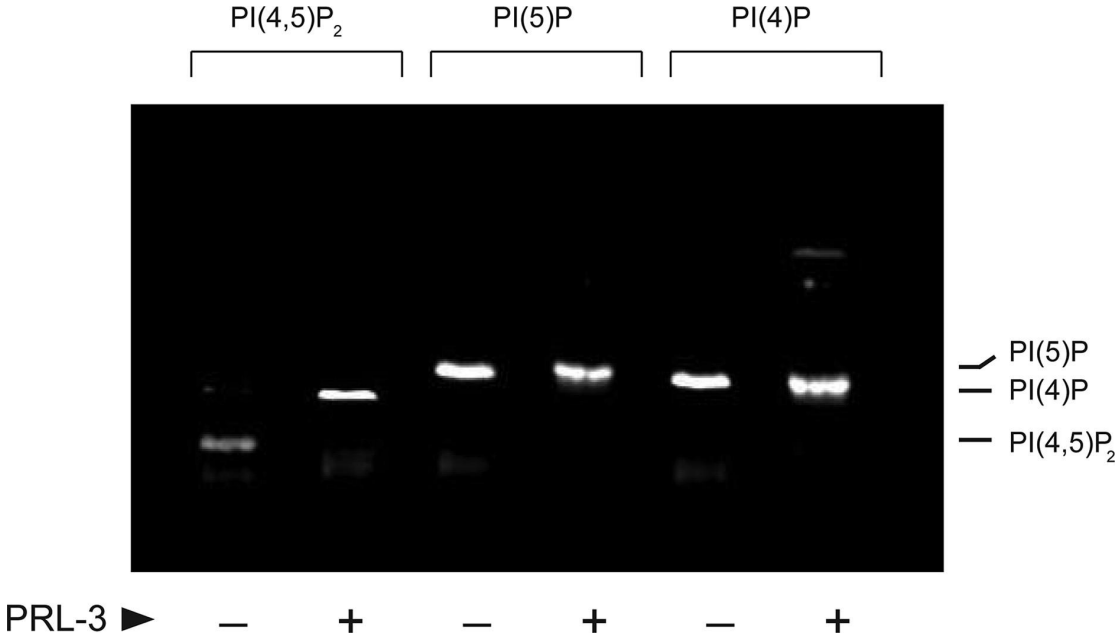

Figure III.7. Dephosphorylation of fluorescently labeled PI(4,5)P$_2$, PI(5)P, and PI(4)P by WT PRL-3. *Phosphatase assays containing 1.0 μg of fluorescent phosphoinositide substrate were conducted for 1 h at 37 °C with 9 μg of recombinant PRL-3 or in the presence of buffer only. Shown is a representative result of three experiments.*

Further, molecular modeling of PRL-3 with diC8-$PI(4,5)P_2$ can support the feasibility of PRL-3's 5-phosphatase activity. The aim of our model study was to find the highest-scoring docking solution containing either the 4- or the 5-phosphate pointing toward the catalytically active Cys. Because there is no structure available for PRL-3 bound to a ligand, we performed homology modeling and MD simulation for model refinement using the structure of PRL-1 bound to a sulfate ion (PDB entry 1XM2) as a template.[26] The 3D structural model of diC8-$PI(4,5)P_2$ in the deprotonated form for molecular docking was built on the basis of the structure of PI(3)P bound to MTMR2.[36] During the entire process, Cys 104 was considered to be

deprotonated and hence functions as a nucleophile in the catalytic reaction. Asp 72 was considered protonated and therefore able to act as a general acid in catalysis. One hundred docking solutions were generated and ranked by GoldScore. To select the possible binding mode, the complex structures of MTMR2 with PI(3)P (PDB entry 1ZSQ) and PI(3,5)P_2 (PDB entry 1ZVR)[36] were used for reference. A common feature of the binding mode in these two structures is that the hydrogen on the carbon atom that carries the phospho group pointing into the catalytic site is opposite to the "general acid" residue Asp 422. The highest-scoring docking solution satisfying this feature was selected as the initial predicted binding mode (Figure III.8A,B). In this docking solution, the 5-phosphate of diC8-PI(4,5)P_2 is dephosphorylated. To further test this preference, a constrained docking study was performed in which either the 4- or 5-phosphate was constrained in the catalytic pocket. Three parallel dockings were performed for each situation, and 10 docking solutions were generated in each run. Solutions satisfying the feature described above with the highest score in each run were selected for comparison. The results show that the scores for docking solutions in which the 5-phosphate points into the catalytic site are generally higher. The highest-scoring one, which also scores higher than the initial predicted binding mode, was selected as the final predicted binding mode (Figure III.8C,D). These theoretical studies further corroborate the hypothesis that PRL-3 could be a phosphatidylinositol 5-phosphatase.

III.4.3. Investigation of the Influence of the Mutations on PRL-3's Ability To Promote Cell Migration

Next, we determined the cellular phenotype of WT PRL-3 and its variants. PRL-3-overexpressing cells are reported to enhance cell migration in a wound healing assay.[3,17] Thus, we created stable cell lines of all PRL-3 variants as well as WT PRL-3 and a stable control cell line with the empty vector using the Flp-In 293 T-Rex cell line (Invitrogen). All PRL-3 proteins were triple FLAG-tagged at the N-terminus. Anti-FLAG Western blot analysis showed that all PRL-3 cell lines express the proteins in equal amounts (Figure III.9A), and immunofluorescence read-out with anti-FLAG antibodies shows that in all cell lines the proteins are localized equally to the plasma membrane as expected (shown for WT PRL-3 in Figure III.9B, data of the variants not shown). There was no expression of PRL-3 observed in the control cell line.

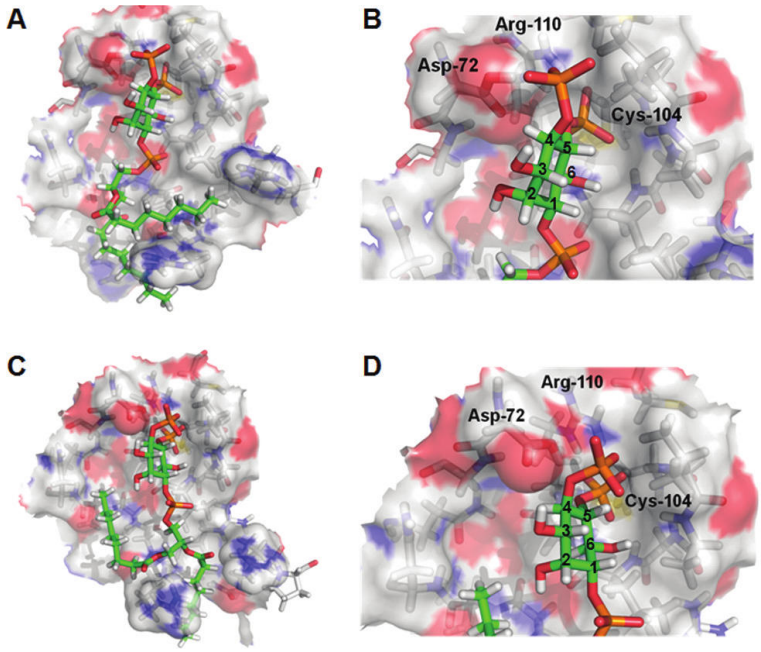

Figure III.8. Docking solution of PI(4,5)P_2 bound to PRL-3. *(A) Initial predicted binding mode. (B) Close-up of the catalytically active site of the structure in panel A. The 5-phosphate points toward Cys 104. (C) Final predicted binding mode, with the solution with the highest score. (D) Close-up of the catalytically active site of the structure in panel C.*

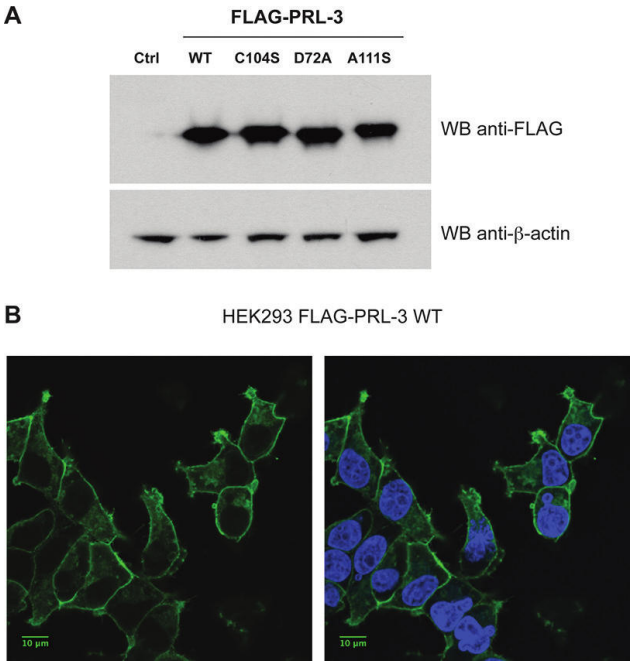

Figure III.9. Generation of stable Flp-In T-Rex 293 cells expressing FLAG-tagged WT PRL-3 or its mutants under the control of a tetracycline inducible promoter. *(A) Western blot (WB) analysis of cell lysates from stable cell lines expressing WT or mutant PRL-3. Cells were incubated overnight in medium containing 1 µg/mL tetracycline, harvested, lysed, and probed with an anti-FLAG antibody to assess the expression levels; an anti-β-actin antibody was used as a loading control. A control cell line was also generated by transfecting Flp-In 293 cells with the blank vector (Ctrl). (B) The stable cell lines were processed for indirect immunofluorescence using the FLAG antibody (left). Hoechst was used to stain the nuclei (right). Only WT PRL-3 is shown.*

We then conducted wound healing assays with all cell lines (Figure III.10). As expected, the WT PRL-3 cell line closes the wound faster than the empty vector control cell line, demonstrating that WT PRL-3 promotes cell migration. The phenotype of the C104S PRL-3 cell line is the same as that of the empty vector control cell line, which is in agreement with the fact that the C104S mutant is inactive in vitro, and it also agrees with reports in the literature.[3,46] This indicates that PRL-3 catalytic activity is required to promote cell migration. The D72A PRL-3 cell line exhibited the same phenotype as WT PRL-3 cells. This correlates with the residual lipid phosphatase activity detected for this variant (see above). As discussed above, the D to A mutation does not completely inactivate the phosphatase, and given that D72A PRL-3 is highly over-expressed in our system, the residual catalytic activity of this variant could be sufficient for promoting cell migration. Fiordalisi et al. reported the same observation using stably transfected SW480 cells.[17] In another report, D72A PRL-3 transiently transfected into mouse B16 cells showed that the extent of promotion of cell migration in a Transwell assay was greatly reduced. However, some residual activity was observed compared to that of the C104S mutant and mock vector control.[46]

We made an astonishing observation when monitoring the cellular phenotype of the A111S mutant: It showed the same lack of activity in accelerating cell migration as the empty vector and the C104S mutant cell line. To the best of our knowledge, this mutant has never been tested in a wound healing assay. The hyperactivity toward the unnatural substrate, OMFP, is thus not apparent in the context of a living cell. On the other hand, the inactivity of A111S PRL-3 toward $PI(4,5)P_2$ in our in vitro assays is in complete agreement with the observed phenotype. This finding provides evidence that the natural S111A mutation in PRL-3 is required for its function, and it might suggest that there are unknown mechanisms involved in the catalytic activity of the PRL family. It may also be that the A111S mutant no longer recognizes its natural substrate, which could potentially be due to structural perturbation in the variant. Importantly, our data clearly emphasize the need for caution when relating phosphatase activity with unnatural substrates such as OMFP to potential in cell activity.

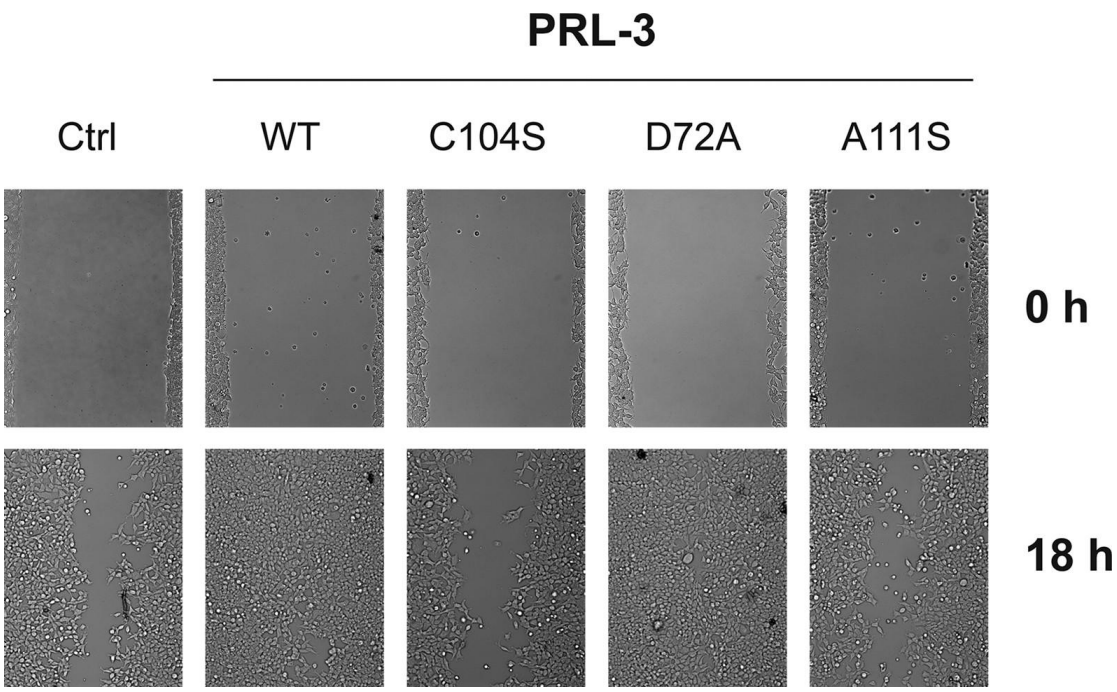

Figure III.10. Wound healing assay with stable HEK 293 cell lines expressing WT, C104S, D72A, and A111S PRL-3 as well as the empty vector control. *Stable cell lines were incubated overnight in medium containing 1 µg/mL tetracycline to induce PRL-3 protein expression. A cell-free gap of approximately 500 µm was created by removing the Culture-Insert. The dishes were filled with fresh DMEM supplemented with 5% FBS and 1 µg/mL tetracycline to maintain protein expression. The wounded areas were photographed at the beginning of the assay (0 h, top panels) and after 18 h (18 h, bottom panels). Shown is a representative result of three experiments.*

To ensure that the activity of the recombinant protein really correlates with the enzyme when it is stably expressed in cells, all four PRL-3 proteins were immunoprecipitated and their phosphatase activity was analyzed using the fluorescently labeled $PI(4,5)P_2$. Figure III.11 demonstrates that immunoprecipitated WT and D72A PRL-3 can dephosphorylate $PI(4,5)P_2$, whereas the C104S and A111S variants lack phosphatase activity toward this substrate. These results are in complete agreement with the observed activity of the recombinant variants and also correlate with the observed phenotypes in wound healing assays.

Taken together, the monitored cellular phenotypes of all PRL-3 variants in stable HEK293 cell lines are in complete agreement with their activity toward $PI(4,5)P_2$ measured using two completely different biochemical assays. This suggests that this activity can be correlated to PRL-3's function in vivo.

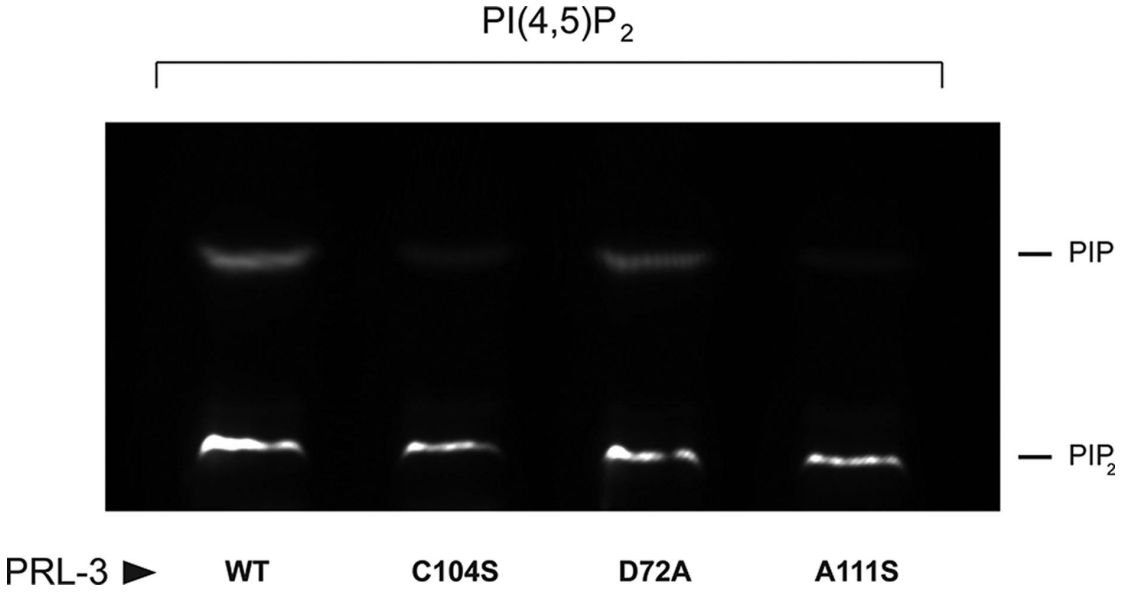

Figure III.11. Dephosphorylation of fluorescently labeled PI(4,5)P_2 using immunoprecipitated WT, D72A, C104S, and A111S PRL-3. *FLAG-tagged PRL-3 proteins were purified by immunoprecipitation with anti-FLAG affinity resin from HEK293 stable cell lines. Immunoprecipitates were incubated with 1.0 μg of fluorescently labeled PI(4,5)P_2 for 1 h at 37 °C, processed as described in Materials and Methods, and analyzed by TLC. Shown is a representative result of three experiments. Similar PIP background levels as in C104S and A111S PRL-3 lanes are also apparent in TLC read-outs using noninduced WT PRL-3 cells for immunoprecipitation (data not shown).*

III.5. Concluding remarks

PRL-3 overexpression affects the regulation of multiple proteins and pathways leading to several favorable conditions for cancer progression and invasiveness.[2] Intriguingly, PI(4,5)P_2 plays a role upstream of many of the described signaling networks in which overexpressed PRL-3 exerts its activity. PI(4,5)P_2 is an important modulator of cytoskeleton organization during diverse cellular functions such as focal adhesion formation and cell migration. These dynamic processes require rapid and highly localized changes in PI(4,5)P_2 content; therefore, PI(4,5)P_2 levels are spatially and temporally regulated by the action of PI(4)P 5-kinases, 5-phosphatases, and phospholipase C enzymes (PLC).[43,47,48] Sequestration or depletion of membrane PI(4,5)P_2 decreases the plasma membrane− cytoskeletal adhesion energy leading to changes in cell shape, reduction of cell−substrate adhesion, and formation of blebs.[49] Moreover, reduction of PI(4,5)P_2 levels through either hydrolysis by PLCγ or impairment of the PI(4,5)P_2-producing kinase PIPKIγ has been described as playing a role in cancer.[43] Depletion of PIPKIγ leads to a morphological transformation from an

epithelial to a mesenchymal phenotype.[50] Reduction of $PI(4,5)P_2$ levels by PLCγ activates Cofilin-mediated enhanced cell motility.[43,48] Thus hypothetically, the role of PRL-3 in cancer metastasis and progression could be mediated via an effect on $PI(4,5)P_2$ levels.

PRL-3 is suggested to reduce the number of focal adhesions and/or increase the rate of focal adhesion turnover in cells leading to enhanced cell migration.[2] Focal adhesions are sites where cellular contact with the extracellular matrix is mediated by Integrins, and focal adhesion complexes contain more than 150 components.[43] Levels of $PI(4,5)P_2$ at the cell membrane are crucial for regulating the dynamics of focal adhesion complexes.[43] A key component of focal adhesion complexes is focal adhesion kinase (FAK), which integrates external signals to promote cell motility via many different pathways involving the regulation of or interaction with proteins such as Cadherins, Src, p130Cas, Rho-family GTPases, and Ezrin,[51] many of which have been implicated as being affected by or interacting with PRL-3.[1,2,10,11,13,14,16–18,20] Therefore, our finding that PRL-3 is active toward $PI(4,5)P_2$ offers a reasonable link to described effects of PRL-3 overexpression.

Little is known regarding the physiological role of PRL-3. If PRL-3 is a phosphatidylinositol 5-phosphatase, it would have to be tightly regulated in healthy cells given the importance of its potential substrate $PI(4,5)P_2$. PRL-3 is expressed only in low levels in specific tissues (skeletal muscle and heart),[1,2] which could be a hint about it being tightly regulated. In addition, its tight regulation has been described in the context of a nuclear function.[52] PIPs exist in the nucleus and regulate a number of processes such as chromatin remodeling and DNA repair; however, only one 5-phosphatase (SHIP2) has been reported in the nucleus, and its function is unclear.[6] In general, 10 human 5-phosphatases have been discovered to date, but none of them belongs to the superfamily of PTPs.[6] They conduct a variety of different functions and are regulated and expressed distinctly; however, our knowledge of regulatory mechanisms is in general still limited.[6,43] Alterations in these phosphatases lead to a number of diseases.[6,43] Their roles in cancer are very diverse and controversial, and they can range from tumor suppressors to cancer-promoting proteins, which was generally investigated in relation to their ability to dephosphorylate $PI(3,4,5)P_3$ to $PI(3,4)P_2$.[43]

These considerations make our hypothesis that PRL-3 could be a phosphatidylinositol 5-phosphatase very reasonable. Currently, we are working on the

proof that PRL-3 has in vivo lipid phosphatase activity. Our results offer a new view of PRL-3's function and role and open up new lines of investigation for this important oncogene.

III.6. References

(1) Besette, D. C., Qiu, D., and Pallen, C. J. (2008) PRL PTPs: Mediators and markers of cancer progression. Cancer Metastasis Rev. 27, 231−252.

(2) Al-Aidaroos, A. Q., and Zeng, Q. (2010) PRL-3 phosphatase and cancer metastasis. J. Cell. Biochem. 111, 1087−1098.

(3) Zeng, Q., Dong, J. M., Guo, K., Li, J., Tan, H. X., Koh, V., Pallen, C. J., Manser, E., and Hong, W. (2003) PRL-3 and PRL-1 promote cell migration, invasion, and metastasis. Cancer Res. 63, 2716−2722.

(4) Matter, W. F., Estridge, T., Zhang, C., Belagaje, R., Stancato, L., Dixon, J., Johnson, B., Bloem, L., Pickard, T., Donaghue, M., Acton, S., Jeyaseelan, R., Kadambi, V., and Vlahos, C. J. (2001) Role of PRL-3, a human muscle-specific tyrosine phosphatase, in angiotensin-II signal- ling. Biochem. Biophys. Res. Commun. 283, 1061−1068.

(5) Saha, S., Bardelli, A., Buckhaults, P., Velculescu, V. E., St. Rago, C., Croix, B., Romans, K. E., Choti, M. A., Lengauer, C., Kinzler, K. W., and Vogelstein, B. (2001) A phosphatase associated with metastasis of colorectal cancer. Science 294, 1343−1346.

(6) Ooms, L. M., Horan, K. A., Rahman, P., Seaton, G., Gurung, R., Kethesparan, D. S., and Mitchell, C. A. (2009) The role of the inositol polyphosphate 5-phosphatases in cellular function and human disease. Biochem. J. 419, 29−49.

(7) Kim, K.-A., Song, J. S., Jee, J. G., Sheen, M. R., Lee, C., Lee, T. G., Ro, S., Cho, J. M., Lee, W., Yamazaki, T., Jeon, Y. H., and Cheong, C. (2004) Structure of human PRL-3, the phosphatase associated with cancer metastasis. FEBS Lett. 565, 181−187.

(8) Zeng, Q., Hong, W., and Tan, Y. H. (1998) Mouse PRL-2 and PRL-3, two potentially prenylated protein tyrosine phosphatases homologous to PRL-1. Biochem. Biophys. Res. Commun. 244, 421−427.

(9) Iwasaki, H., Murata, Y., Kim, Y., Hossain, Md. I., Worby, C. A., Dixon, J. E., McCormack, T., Sasaki, T., and Okamura, Y. (2008) A voltage-sensing phosphatase, Ci-VSP, which shares sequence identity with PTEN, dephosphorylates phosphatidylinositol 4,5-bisphosphate. Proc. Natl. Acad. Sci. U.S.A. 105, 7970−7975.

(10) Forte, E., Orsatti, L., Talamo, F., Barbato, G., De Francesco, R., and Tomei, L. (2008) Ezrin is a specific and direct target of protein tyrosine phosphatase PRL-3. Biochim. Biophys. Acta 1783, 334−344.

(11) Orsatti, L., Forte, E., Tomei, L., Caterino, M., Pessi, A., and Talamo, F. (2009) 2-D Difference in gel electrophoresis combined with Pro-Q Diamond staining: A successful approach for the identification of kinase/phosphatase targets. Electrophoresis 30, 2469−2476.

(12) Mizuuchi, E., Semba, S., Kodama, Y., and Yokozaki, H. (2009) Down-modulation of keratin 8 phosphorylation levels by PRL-3 contributes to colorectal carcinoma progression. Int. J. Cancer 124, 1802−1810.

(13) Peng, L., Jin, G., Wang, L., Guo, J., Meng, L., and Shou, C. (2006) Identification of integrin α1 as an interacting protein of protein tyrosine phosphatase PRL-3. Biochem. Biophys. Res. Commun. 342, 179−183.

(14) Peng, L., Xing, X., Li., W., Qu, L., Meng, L., Lian, S., Jiang, B., Wu, J., and Shou, C. (2009) PRL-3 promotes the motility, invasion, and metastasis of LoVo colon cancer cells through PRL-3-integrin β1- ERK1/2 and -MMP2 signaling. Mol. Cancer 8, 110−123.

(15) Zheng, P., Liu, Y.-X., Chen, L., Liu, X.-H., Xiao, Z.-Q., Zhao, L., Li, G.-Q., Zhou, J., Ding, Y.-Q., and Li, J. M. (2010) Stathmin, a new target of PRL-3 identified by proteomic methods, plays a key role in progression and metastasis of colorectal cancer. J. Proteome Res. 9, 4897−4905.

(16) Wang, H., Quah, S. Y., Dong, J. M., Manser, E., Tang, J. P., and Zeng, Q. (2007) PRL-3 down-regulates PTEN expression and signals through PI3K to promote epithelial-mesenchymal transition. Cancer Res. 67, 2922−2926.

(17) Fiordalisi, J. J., Keller, P. J., and Cox, A. D. (2006) PRL tyrosine phosphatases regulate rho family GTPases to promote invasion and motility. Cancer Res. 66, 3153−3161.

(18) Liang, F., Liang, J., Wang, W.-Q., Sun, J.-P., Udho, E., and Zhang, Z.-Y. (2007) PRL-3 Promotes Cell Invasion and Proliferation by Down-regulation of Csk Leading to Src Activation. J. Biol. Chem. 282, 5413−5419.

(19) Liang, F., Luo, Y., Dong, Y., Walls, C. D., Liang, J., Jiang, H.-Y., Sanford, J. R., Wek, R. C., and Zhang, Z.-Y. (2008) Translational control of C-terminal Src kinase (Csk) expression by PRL3 phosphatase. J. Biol. Chem. 283, 10339−10346.

(20) Liu, Y., Zhou, J., Chen, J., Gao, W., Le, Y., Ding, Y., and Li, J. (2009) PRL-3 promotes epithelial mesenchymal transition by regulating cadherin directly. Cancer Biol. Ther. 8, 1352−1359.

(21) Kozlov, G., Cheng, J., Ziomek, E., Banville, D., Gehring, K., and Ekiel, I. (2004) Structural Insights into Molecular Function of the Metastasis-associated Phosphatase PRL-3. J. Biol. Chem. 279, 11882− 11889.

(22) Greenfield, N. J. (2007) Using circular dichroism spectra to estimate protein secondary structure. Nat. Protoc. 1, 2876−2890.

(23) Sun, J.-P., Luo, Y., Yu, X., Wang, W.-Q., Zhou, B., Liang, F., and Zhang, Z.-Y. (2007) Phosphatase Activity, Trimerization, and the C- terminal Polybasic Region Are All Required for PRL1-mediated Cell Growth and Migration. J. Biol. Chem. 282, 29043−29051.

(24) Pascaru, M., Tanase, C., Vacaru, A. M., Boeti, P., Neagu, E., Popescu, I., and Szedlacsek, S. E. (2009) Analysis of molecular determinants of PRL-3. J. Cell. Mol. Med. 13, 3141−3150.

(25) Traynor-Kaplan, A. E., Thompson, B. L., Harris, A. L., Taujor, P., Omann, G. M., and Sklar, L. A. (1989) Transient increase in phosphatidylinositol 3,4-bisphosphate and phosphatidylinositol trisphosphate during activation of human neutrophils. J. Biol. Chem. 264, 15668−15673.

(26) Jeong, D. G., Kim, S. J., Kim, J. H., Son, J. H., Park, M. R., Lim, S. M., Yoon, T. S., and Ryu, S. E. (2005) Trimeric structure of PRL-1 phosphatase reveals an active enzyme conformation and regulation mechanisms. J. Mol. Biol. 345, 401−413.

(27) The UniProt Consortium (2011) Ongoing and future developments at the Universal Protein Resource. Nucleic Acids Res. 39, D214−D219.

(28) Larkin, M. A., Blackshields, G., Brown, N. P., Chenna, R., McGettigan, P. A., McWilliam, H., Valentin, F., Wallace, I. M., Wilm, A., Lopez, R., Thompson, J. D., Gibson, T. J., and Higgins, D. G. (2007) Clustal W and Clustal X version 2.0. Bioinformatics 23, 2947− 2948.

(29) Sun, J. P., Wang, W. Q., Yang, H., Liu, S., Liang, F., Fedorov, A. A., Almo, S. C., and Zhang, Z. Y. (2005) Structure and biochemical properties of PRL-1, a phosphatase implicated in cell growth, differentiation, and tumor invasion. Biochemistry 44, 12009−12021.

(30) Sali, A., and Blundell, T. L. (1993) Comparative protein modelling by satisfaction of spatial

restraints. J. Mol. Biol. 234, 779− 815.

(31) Zhou, H., and Zhou, Y. (2002) Distance-scaled, finite ideal-gas reference state improves structure-derived potentials of mean force for structure selection and stability prediction. Protein Sci. 11, 2714−2726.

(32) McGuffin, L. J. (2008) The ModFOLD server for the quality assessment of protein structural models. Bioinformatics 24, 586−587.

(33) Phillips, J. C., Braun, R., Wang, W., Gumbart, J., Tajkhorshid, E., Villa, E., Chipot, C., Skeel, R. D., Kale, L., and Schulten, K. (2005) Scalable molecular dynamics with NAMD. J. Comput. Chem. 26, 1781− 1802.

(34) Wang, J. M., and Kollman, P. A. (2001) Automatic parameterization of force field by systematic search and genetic algorithms. J. Comput. Chem. 22, 1219−1228.

(35) Jorgensen, W. L., Chandrasekhar, J., Madura, J. D., Impey, R. W., and Klein, M. L. (1983) Comparison of Simple Potential Functions for Simulating Liquid Water. J. Chem. Phys. 79, 926−935.

(36) Begley, M. J., Taylor, G. S., Brock, M. A., Ghosh, P., Woods, V. L., and Dixon, J. E. (2006) Molecular basis for substrate recognition by MTMR2, a myotubularin family phosphoinositide phosphatase. Proc. Natl. Acad. Sci. U.S.A. 103, 927−932.

(37) Guha, R., Howard, M. T., Hutchison, G. R., Murray-Rust, P., Rzepa, H., Steinbeck, C., Wegner, J., and Willighagen, E. L. (2006) The Blue Obelisk-interoperability in chemical informatics. J. Chem. Inf. Model. 46, 991−998.

(38) Verdonk, M. L., Cole, J. C., Hartshorn, M. J., Murray, C. W., and Taylor, R. D. (2003) Improved protein-ligand docking using GOLD. Proteins 52, 609−623.

(39) Stephens, B., Han, H., Gokhale, V., and Von Hoff, D. (2005) PRL phosphatases as potential molecular targets in cancer. Mol. Cancer Ther. 4, 1653−1661.

(40) Jia, Z., Barford, D., Flint, A. J., and Tonks, N. K. (1995) Structural basis for phosphotyrosine peptide recognition by protein tyrosine phosphatase 1B. Science 268, 1754−1758.

(41) Rudolph, J., Epstein, D. M., Parker, L., and Eckstein, J. (2001) Specificity of natural and artificial substrates for human Cdc25A. Anal. Biochem. 28, 43−51.

(42) Wiland, A. M., Denu, J. M., Mourey, R. J., and Dixon, J. E. (1996) Purification and kinetic characterization of the mitogen- activated protein kinase phosphatase rVH6. J. Biol. Chem. 271, 33486− 33492.

(43) Bunney, T. D., and Katan, M. (2010) Phophoinositide signalling in cancer: Beyond PI3K and PTEN. Nat. Rev. Cancer 10, 342−352.

(44) Kisseleva, M. V., Wilson, M. P., and Majerus, P. W. (2000) The Isolation and Characterization of a cDNA Encoding Phospholipid- specific Inositol Polyphosphate 5-Phosphatase. J. Biol. Chem. 275, 20110−20116.

(45) Blanchetot, C., Chagnon, M., Dubé, N., Hallé, M., and Tremblay, M. L. (2005) Substrate-trapping techniques in the identification of cellular PTP targets. Methods 35, 44−53.

(46) Wu, X., Zeng, H., Zhang, X., Zhao, Y., Sha, H., Ge, X., Zhang, M., Gao, X., and Xu, Q. (2004) Phosphatase of regenerating liver-3 promotes motility and metastasis of mouse melanoma cells. Am. J. Pathol. 164, 2039−2054.

(47) McLaughlin, S., Wang, J., Gambhir, A., and Murray, D. (2002) PIP(2) and proteins: Interactions, organization, and information flow. Annu. Rev. Biophys. Biomol. Struct. 31, 151−175.

(48) Saarikangas, J., Zhao, H., and Lappalainen, P. (2010) Regulation of the actin cytoskeleton-plasma membrane interplay by phosphoinositides. Physiol. Rev. 90, 259−289.

(49) Raucher, D., Stauffer, T., Chen, W., Shen, K., Guo, S., York, J. D., Sheetz, M. P., and Meyer, T. (2000) Phosphatidylinositol 4,5- bisphosphate functions as a second messenger that regulates cytoskeleton-plasma membrane adhesion. Cell 100, 221−228.

(50) Ling, K., Bairstow, S. F., Carbonara, C., Turbin, D. A., Huntsman, D. G., and Anderson, R. A. (2007) Type Iγ phosphatidylinositol phosphate kinase modulates adherens junction and E-cadherin trafficking via a direct interaction with μ1B adaptin. J. Cell Biol. 176, 343−353.

(51) Mitra, S. K., Hanson, D. A., and Schlaepfer, D. D. (2005) Focal adhesion kinase: In command and control of cell motility. Nat. Rev. Mol. Cell Biol. 6, 56−68.

(52) Basak, S., Jacobs, S. B. R., Krieg, A. J., Pathak, N., Zeng, Q., Kaldis, P., Giaccia, A. J., and Attardi, L. D. (2008) The metastasis- associated gene Prl-3 is a p53 target involved in cell-cycle regulation. Mol. Cell 30, 303−314.

Chapter IV: The Metastasis-Promoting Phosphatase PRL-3 affects epithelial cell polarization by altering post-mitotic midbody fate

Derived from:

Giulia Varsano and Maja Köhn.

Manuscript ready for submission

IV.1. Abstract

Epithelial organs are typically organized in elongated tubules and lumen-containing spherical cysts. Apical cell polarity specification and coordinated lumen formation require a complex crosstalk between the trafficking machinery and polarity complex proteins. Here we show that over-expression of the metastasis-associated phosphatase PRL-3 significantly affects epithelial morphogenesis by interfering with the fate of post-mitotic midbodies. We identified the post-mitotic midbody as the first polarization signal during cyst development, defining the apical domain and the lumen position. PRL-3 over-expression promotes intracellular as well as lateral plasma membrane retention of post-mitotic midbodies, generating cysts with ectopic lumens that arise at the sites where post-mitotic midbodies are retained. These results define a critical function of post-mitotic midbodies in the establishment and maintenance of the axis of polarity, reveal that PRL-3 can regulate post-mitotic midbody fate and show that PRL-3 aberrant expression is associated with major defects in epithelial cell polarization, suggesting a novel mechanism for epithelial tumorigenesis.

IV.2. Introduction

Polarized epithelial cells are characterized by the asymmetric distribution of both proteins and lipids across the plasma membrane[1]. This asymmetry is required to generate apico-basal polarity[1,2]. The process of epithelial polarization and *de novo* lumen formation has been extensively studied in the three dimensional (3D) MDCK cell system, an excellent in vitro model of epithelial morphogenesis[3,4]. MDCK cells, in contact with extracellular matrix, form polarized lumen-enclosing spherical cysts with the apical membrane facing a hollow central lumen and a basal surface attached to a layer of extracellular matrix. Recently, important insights into the early stages of lumenogenesis have been described [3,5,6]. *De Novo* lumen formation in MDCK cysts requires polarized exocytosis of membrane vesicles at specific sites of cell-cell contact in the core region of the cysts. This region is specified as a specialized membrane domain called the “apical membrane initiation site” (AMIS) and is the site where the lumen will open. The polarization process in MDCK cysts starts at a very early stage with the selective localization of key polarity and trafficking proteins to the AMIS[5–7]. However, how the AMIS and subsequently the lumen position are specified exactly in center of the cysts is still an open question.

Epithelial tissue is the source of more than 80% of human cancers such as colorectal cancer, and the loss of apico-basal polarity in epithelial cells is considered a fundamental event during malignant tumor progression and metastasis[8,9]. Phosphatase of Regenerating Liver-3 (PRL-3) is a metastasis-associated phosphatase and an emerging prognostic marker for prediction of human colorectal cancer progression[10]. PRL-3 belongs to the family of Dual Specificity Phosphatases (DSPs), consists only of a single domain and carries a C-terminal prenylation motif. The C-terminal lipid prenyl group is essential for PRL-3 subcellular localization, anchoring the protein to membrane compartments such as the plasma membrane[11,12]. Although the correlation between aberrant PRL-3 expression and the acquisition of a migratory and invasive cell phenotype is well established, the molecular basis of PRL-3 function is unclear[12]. Here, we show that the overexpression of PRL-3 in MDCK cysts significantly affects epithelial morphogenesis. Moreover, we demonstrate that a remnant of the cytokinesis process, the post-mitotic midbody[13], defines the position where the AMIS and thus the lumen will be positioned. Finally, we demonstrate that PRL-3 overexpression affects apical lumen formation in MDCK cysts by promoting intracellular or lateral plasma membrane retention of post-mitotic midbodies. In summary, we describe a novel role of midbody remnants in cell polarity, identify the metastasis-associated phosphatase PRL-3 as a protein involved in the determination of midbody fate and we show that this PRL-3 disregulation is associated with major defects in epithelial cell polarization in a non-cancerous background.

IV.3. Results

IV.3.1. PRL-3 overexpression affects the formation of a single apical lumen in epithelial cells

Several reports over the past few years have suggested a correlation between high PRL-3 expression and metastatic progression of epithelial cancers[10–12] but the effect of PRL-3 overexpression on cellular polarity has not been examined[11,12]. To determine if PRL-3 overexpression affects epithelial cell polarity in MDCK cysts, we stably expressed the WT version of PRL-3 fused to GFP (GFP-PRL-3 WT) in MDCK cells. The resulting cell lines showed a heterogeneous expression of PRL-3 allowing us to compare, in the same sample, the effect of PRL-3 in MDCK cystogenesis with respect to cells with low or no expression. As previously reported, MDCK cells form spherical cysts in Matrigel characterized by a central hollow lumen surrounded by one

layer of polarized cells[7,14]. In these cysts (Fig. IV.1a, arrowhead), F-actin is enriched at the apical membrane facing the central lumen[15]. By contrast, PRL-3 overexpressing cysts are frequently abnormal with multiple lumens positive for F-actin (Fig. IV.1a, arrows; Fig. IV.1d,f,g). Interestingly, mosaic cysts, where only few cells express PRL-3, are also abnormal (Fig. IV.1b), with PRL-3 expressing cells extended from the monolayer to the lumenal space. These defects are attributable to PRL-3 catalytic activity because MDCK cysts stably expressing the catalytic inactive mutant of PRL-3 (GFP-PRL-3-C104S) show a normal phenotype comparable to parental cysts[15] (Fig. IV.1c,e,g). Furthermore, in PRL-3 WT overexpressing cysts intracellular lumen-like structures are frequently observed that are not connected with cell-cell contact regions (Fig. IV.1d,e arrows). These results suggest that enhanced PRL-3 catalytic activity causes the formation of multiple lumens in MDCK cysts.

IV.3.2. PRL-3- induced ectopic lumens preserve key luminal marks

As reported previously, MDCK cells establish apicobasal polarity at a very early stage of cystogenesis when the membranes that face the lumen acquire a clear apical identity and well-defined tight junctions are formed[5–7]. To further characterize PRL-3-induced ectopic lumens, we investigated the localization of tight junction proteins and apical markers in PRL-3 WT cysts. The tight junction markers ZO-1 and Par3 localize to the apical sites of cell-cell contact adjacent to the central lumen in PRL-3 C104S cysts (Fig. IV.2a,c) as previously reported for parental cysts[5,16]. Interestingly, PRL-3-induced ectopic lumens are still flanked by tight junctions (Fig. IV.2b,d). Moreover, PRL-3 WT cysts are still able to polarize apical markers, generating ectopic lumens where key apical surface determinants are maintained. To this end, ectopic lumens are PI(4,5)P_2 and Annexin2 positive (Fig. IV.S1b,d) like the central lumen in PRL-3 C104S cysts (Fig. IV.S1a,c and see ref. 16) and enriched in phosphorylated Ezrin (Fig. IV.2e,f). Taken together these results indicate that enhanced PRL-3 catalytic activity leads to a failure in the specification of the lumen position rather than a disruption in overall cell polarity, giving rise to fully polarized lumens in ectopic positions.

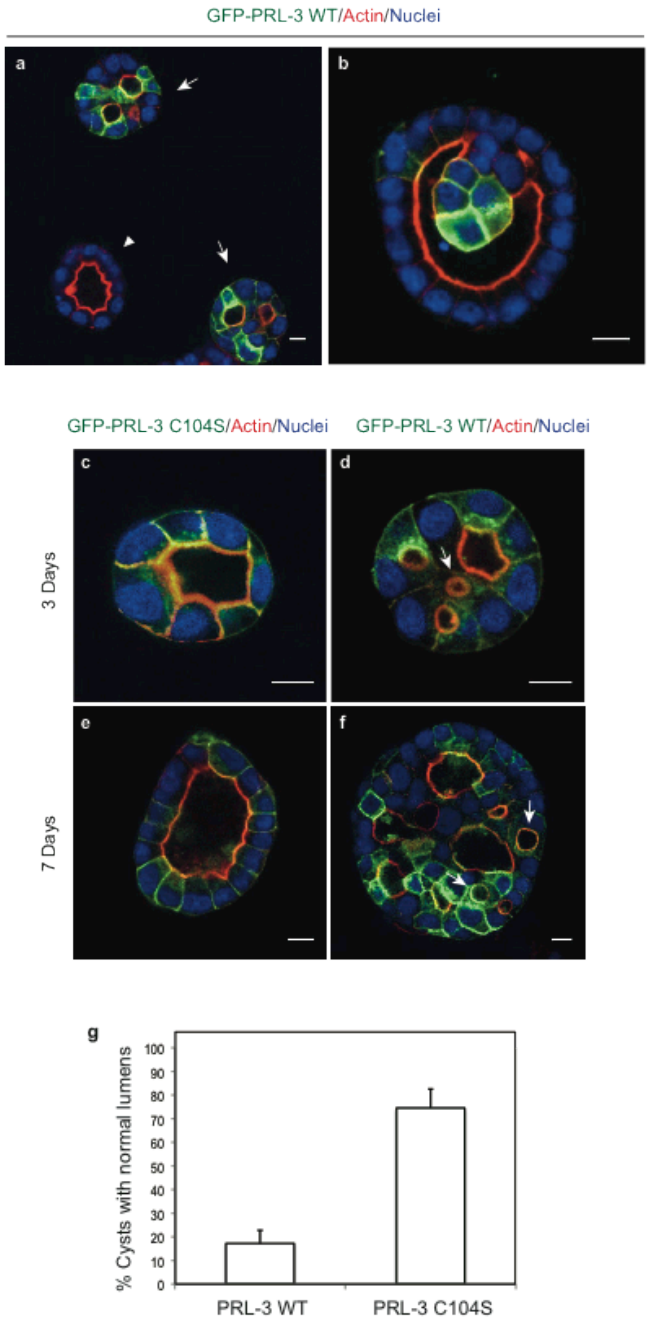

Figure IV.1. PRL-3 overexpressing MDCK cells fail to form normal cysts with an integrated single lumen. *(**a**) Representative confocal microscopy images of cysts expressing GFP-PRL-3 WT (green) at 72-96 h after plating and incubated with Hoechst (blue) to visualize nuclei and with phalloidin (red) to visualize actin. Arrowheads indicate parental MDCK cyst, arrows indicate GFP-PRL-3 WT overexpressing cysts. (**b**) Representative confocal microscopy images of hybrid cysts formed by parental and PRL-3 WT overexpressing MDCK cells, stained as in **a**. (**c-f**) MDCK cysts expressing GFP-PRL-3 (C104S catalytically inactive substitution mutant (**c**,**e**) or wild-type PRL-3, WT (**d**,**f**); both green) were grown for 3 days (**c**,**d**) or 7 days (**e**,**f**) and stained as in **a** and **b**. Arrows indicate intracellular lumens (**d**,**f**). (**g**) Proportion of cysts with a single lumen in MDCK cysts stably expressing GFP-PRL-3 WT or GFP-PRL-3 C104S. Values represent the means plus standard deviation of three experiments. GFP-PRL-3 WT n=158, GFP-PRL-3 C104S n=103. Scale bars 10 μm.*

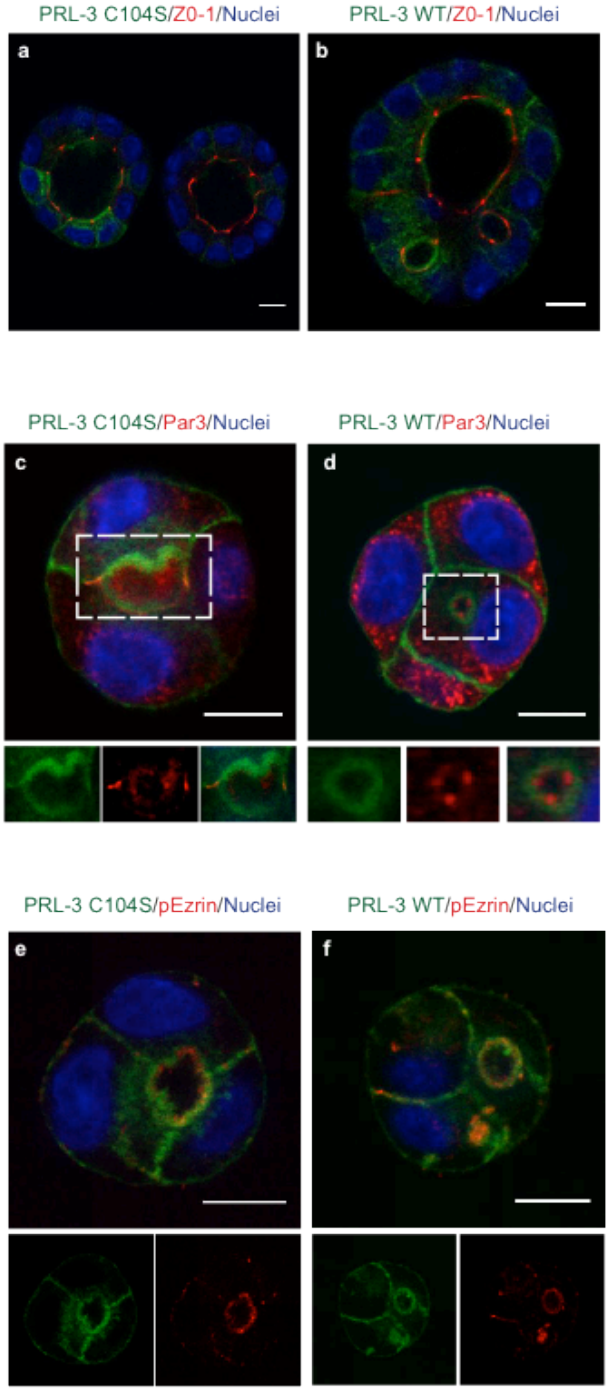

Figure IV.2. PRL-3 overexpressing cysts show fully specified lumens in ectopic positions. *(**a-b**) Representative images of cysts either expressing GFP-PRL-3 WT (**b**) or expressing the catalytically inactive mutant GFP-PRL-3 C104S (**a**) (both green) incubated with Hoechst (blue) and with antibodies against ZO-1 (red) at 96 h after plating. (**c-d**) Experiments performed as in **a** and **b** except cysts were analyzed 48 h after seeding and cells were incubated with antibodies against Par3 (red). Bottom: higher magnification images of the indicated regions showing GFP-PRL-3 (C104S in **c** and WT in **d**; left), Par3 (middle) and a merge of these two images (right). (**e-f**) Experiments performed as in **c** and **d** except cysts were stained with an antibody against threonine-phosphorylated ERM (ezrin/radixin/moesin) proteins (pEzrin) shown in red, further details about the antibody are described in the methods section. Bottom: separate fluorescent channels showing localization of individual proteins, GFP-PRL-3 (C104S in **e** and WT in **f**; left) and pEzrin (right). Scale bars 10 μm.*

IV.3.3. PRL-3-induced ectopic lumens arise from incorrectly localized and PRL-3 enriched apical membrane initiation sites

The process of polarization in MDCK cysts begins soon after the first cell division when apical polarity and trafficking proteins, such as Par3 and Sec8 (also known as EXOC4), are delivered to a specialized zone of cell-cell contact, the AMIS[5,17] (see also Fig. IV.3b and Fig. IV.3d). AMIS specification is one of the earliest steps in lumenogenesis and precedes the formation of a tight junction-delimited lumen[5,6]. To gain further insight into the defect in cystogenesis of PRL-3 overexpressing cells, we analyzed the process of ectopic lumen formation by live cell imaging. Figure IV.3a shows that ectopic lumens arise from intracellular PRL-3-rich patch-like structures (Fig. IV.3a arrow and movie1). Furthermore, PRL-3-induced intracellular lumens are not stable but seem to be dynamically opened and absorbed during time (Fig. IV.3a and Movie1). These PRL-3 intracellular patches stain positive for the AMIS markers Par3 (Fig. IV.3c) and Sec8 (Fig. IV.3e, see below). In addition, in PRL-3 WT cysts the normal staining of the AMIS at cell-cell contacts in the center of the cysts is lost (Fig. IV.3c, IV.3e). The PRL-3-rich patch-like structures are $PI(4,5)P_2$ positive intracellular membrane compartments (Fig. IV.S2a) and are surrounded by phosphorylated Ezrin (Fig. IV.S2c), which is only found in the central AMIS in normal PRL-3 C104S cysts (Fig. IV.S2b).

In MDCK cysts the delivery of apical determinants to the AMIS requires polarized vesicular trafficking, a process that is dependent on the exocyst complex[5]. Sec8 is a key component of the exocyst complex and is one of the first detectable proteins that shows an asymmetric distribution, concentrating to the AMIS together with Par3[5]. Considering that Sec8 surrounds these PRL-3-rich patch-like structures (Fig. IV.3e) we tested the hypothesis that PRL-3 overexpression could redirect vesicle trafficking to PRL-3 induced ectopic lumens rather than to the cysts core where the central lumen would normally open. Figure IV.3f shows that exocytic vesicles, labeled with BODIPY-Tr-Ceramide[18], are indeed delivered to nascent PRL-3- induced intracellular lumens (see also movie 2). Taken together, these results indicate that PRL-3-induced ectopic lumens arise from fully specified apical membrane initiation sites. However, these AMIS appear to be incorrectly localized and PRL-3 enriched.

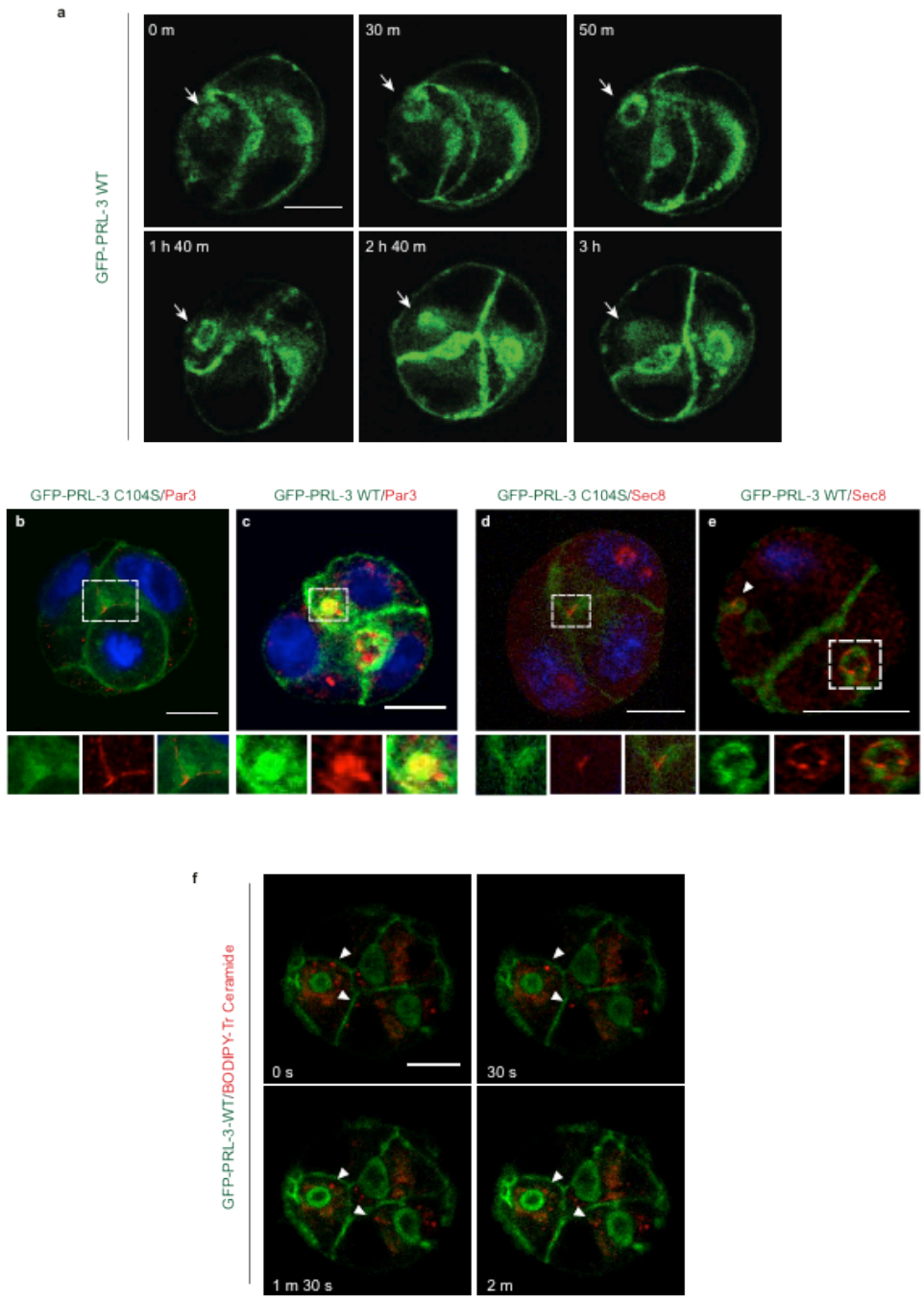

Figure IV.3. PRL-3 overexpressing cysts form incorrectly localized and PRL-3 enriched apical membrane initiation sites. *(**a**) Selected time points of time-lapse live-cell imaging of a 45 h GFP-PRL-3 WT cyst. Arrow indicates PRL-3 accumulation in an intracellular patch that gives rise to an intracellular lumen, which is subsequently reabsorbed. (**b-e**) Representative images of cysts at 45 h stably expressing either PRL-3 WT (**c**, **e**) or PRL-3 C104S (**b**, **d**) treated with Hoechst (blue) and antibodies against Par3 (**b**, **c**) or Sec8 (**d**, **e**) shown in red. PRL-3 WT intracellular patches are Par3 positive (**c**) and surrounded by Sec8 (**e**). Bottom, higher magnification images of the indicated regions showing GFP-PRL-3 (left), Par3 or Sec8 (middle) and a merge of these two images (right). Arrowhead in **e** indicates an additional PRL-3 patch surrounded by Sec8. (**f**) Selected pictures of time-lapse live-cell imaging of 48 h GFP-PRL-3 WT cysts showing vesicles trafficking to ectopic AMIS. Cysts were pretreated with the red-fluorescent BODIPY-TR ceramide (5μM final concentration) at 4 C° for 30 minutes. Cells were let to recover at 37 C° for 20 minutes before starting the image acquisition. Scale bars 10 μm.*

IV.3.4. PRL-3 interacts with polarity and trafficking proteins

The above data suggest that PRL-3 could associate with Par3 and Sec8. To address this hypothesis, GFP-PRL-3, transiently expressed in HEK293 cells, was immunoprecipitated. All three isoforms of endogenous Par3 (Fig. IV.4a) and also endogenous Sec8 (Fig. IV.4d) specifically and reproducibly co-precipitated with GFP-PRL-3. Reciprocal co-immunoprecipitation experiments further validated these interactions (Fig. IV.S3). GFP-PRL-3 C104S was also able to interact with endogenous Sec8 (Fig. IV.4d). Since the catalytically inactive mutant of PRL-3 does not affect the normal cyst phenotype when overexpressed in MDCK cysts, we can exclude that the PRL-3 induced multi-lumen phenotype is simply due to trapping of critical lumen determinants such as Sec8 in ectopic positions.

To test whether PRL-3 binds directly to Par3, recombinant purified PRL-3 was incubated with GST-protein fusions of Par3 fragments (Fig. IV.4b). PRL-3 binds most strongly to the Par-3 fragment containing the aPKC-binding region (Par3 C) but does not detectably bind the N-terminal fragments of Par3 (Fig. IV.4c).

Par3 is an evolutionarily conserved cell polarity protein and is part of a ternary complex consisting of Par3, Par6 and aPKC[19]. The interaction between Par3 and aPKC is essential for apical membrane formation in MDCK cells, while tight junction maturation is not strictly dependent on this interaction[15]. Since PRL-3 binds Par3 on the aPKC-binding region, we investigated if PRL-3 overexpression could interfere with Par3-aPKC binding. The results show that the fraction of aPKC bound to Par3 is not reduced by PRL-3 overexpression, and we thus conclude that overexpression of PRL-3 does not interfere with the formation of the Par3-aPKC complex. Additionally, neither the overexpression of PRL-3 C104S nor WT perturbs tight junction *de novo* formation, as measured using a classical calcium switch assay (Fig. IV.S4b,c)[20].

In conclusion, PRL-3 is able to interact with the polarity and trafficking proteins Par3 and Sec8. However, it neither interferes with Par3-aPKC interaction nor with the tight junction formation pathway.

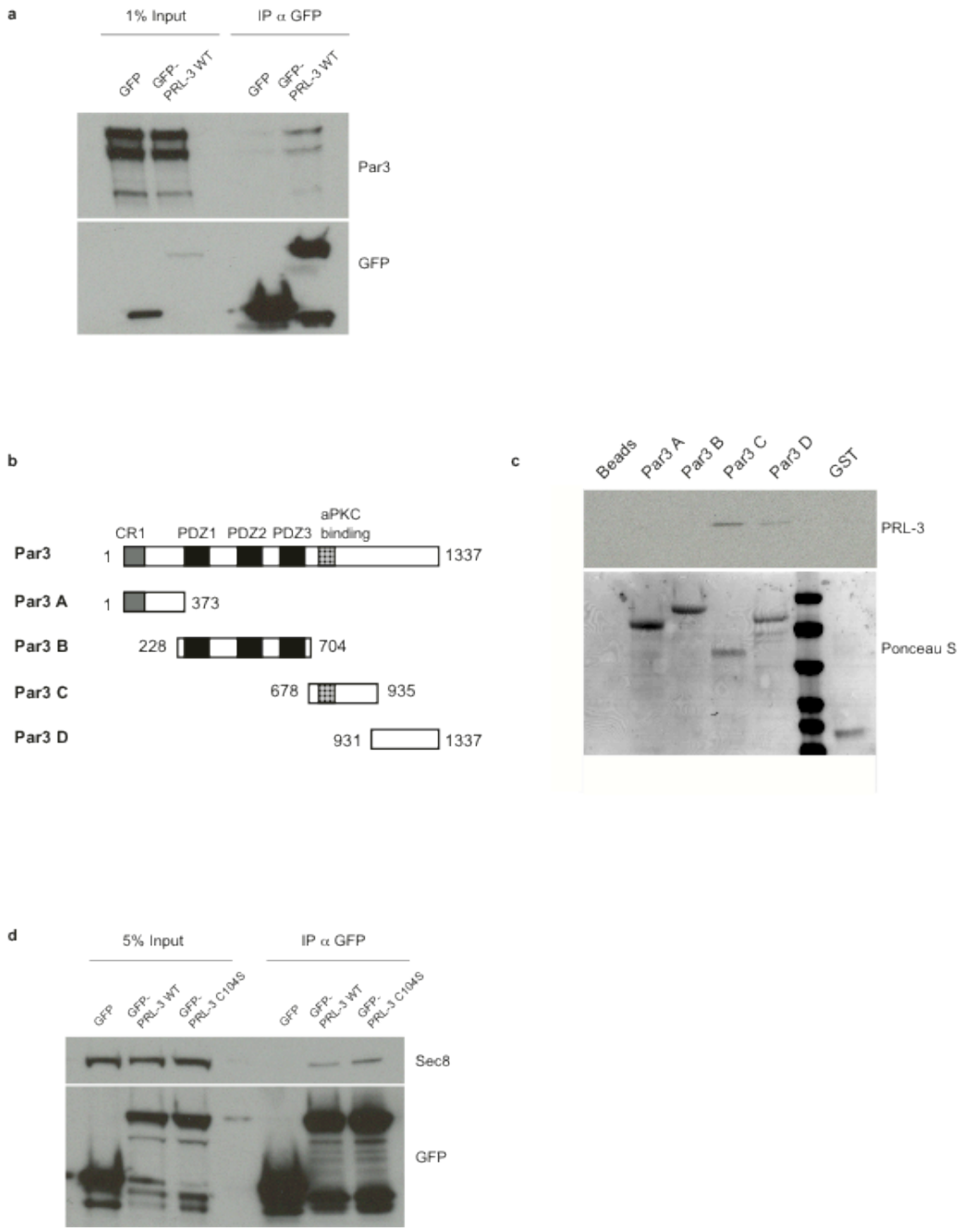

Figure IV.4. PRL-3 interacts with Par3 and Sec8. ***(a)*** *Endogenous Par3 co-immunoprecipitated with GFP-PRL-3 in HEK293 cells. Lysates from HEK293 transfected with GFP control vector or vector encoding GFP-PRL-3 WT were immunoprecipitated using GFP-TRAP beads. Immunoprecipitates were immunoblotted with antibodies against Par3 (top) and GFP (bottom).* ***(b)*** *Schematic diagram showing the domain organizations of Par-3 as well as the various Par-3 fragments used to construct GST fusion proteins for the pulldown experiments in* ***c****.* ***(c)*** *PRL-3 directly binds to the C-terminus of Par3 in vitro. GST and GST–Par3 fragments were used as bait in pulldown experiments adding recombinant PRL-3. PRL-3 binding was detected by immunoblot (top). GST fusion proteins were resolved by SDS–PAGE and Ponceau S staining (bottom).* ***(d)*** *Endogenous Sec8 co-immunoprecipitated with GFP-PRL-3 (either WT or C104S mutant) in HEK293 cells. Lysates from HEK293 cells transfected with GFP control vector or a plasmid encoding GFP PRL-3 WT or C104S were subjected to immunoprecipitation with GFP-TRAP beads. Immunoprecipitates were immunoblotted with antibodies against Sec8 (top) and GFP (bottom).*

IV.3.5. Midbody remnants define the apical domain during cyst development

PRL-3 overexpression led to mislocalization of the AMIS in MDCK cysts. AMIS specification is one of the first steps in lumenogenesis in MDCK cysts[5,6], but currently the signal that specifies the AMIS position is not known. Since polarization in MDCK cysts begins immediately after the first cytokinesis[17], we hypothesized that a remnant of the final stage of cytokinesis (abscission) defines the AMIS position. The midbody is the structure that connects the two daughter cells at this stage and that is required for their final separation[21,22]. Recent studies have shown that midbodies can persist in post-mitotic cells and participate in functions unrelated with cytokinesis[13,23–25]. To test the idea that midbody remnants could specify the AMIS position, we examined midbody marker staining in parental MDCK cysts at different stages. At an early stage, when the lumen is still not physically opened, the midbody ring markers MKLP1 (also known as KIF23), γ-tubulin and Cep55 stain the center of the cysts (Fig. IV.5a,b,c). Interestingly, midbody remnants persist long after lumen opening where they can be found to delineate the edge of the lumen (Fig. IV.5d,e,f). Staining with Aurora B, an additional midbody marker, further validates these results. Aurora B also forms foci in the cyst core at an early stage of cystogenesis (Fig. IV.5g,h). However, at later stages, when the lumen is completely opened, Aurora B is mainly dispersed in the lumenal space (Fig. IV.5i arrow), in contrast to MKLP1 that remains associated with the midbody (Fig. IV.5i arrowhead). This observation can be explained by the fact that aged, post-mitotic midbodies can lose some components[26]. In vitro as well in vivo studies in other cell types have shown that after cytokinesis midbodies can either be released into the extracellular space or retained by one of the daughter cells. Retained midbodies can either be immediately degraded or persist in the cytoplasm for extended periods of time[13]. In MDCK cysts, midbody remnants after cytokinesis were still adjacent to the apical membrane through the half-disassembled intercellular bridge (Fig. IV.5a arrow) and were subsequently released into the lumenal space (Fig. IV.5d, see also Fig. IV.6b,c). Taken together, these results suggest that midbody remnants could define the AMIS position in MDCK cysts and consequently the site of lumen opening.

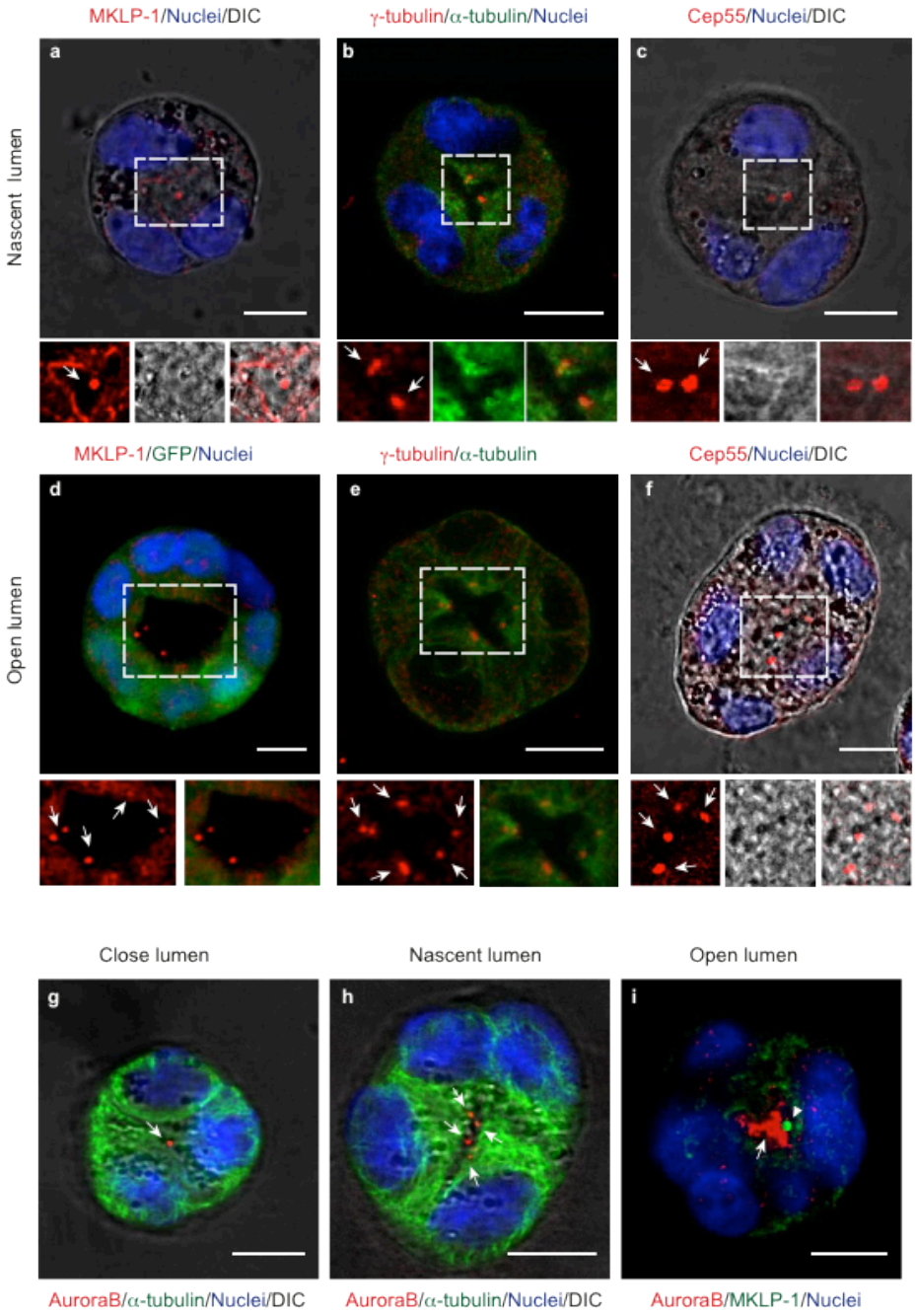

Figure IV.5. Midbody remnants define the lumen position in MDCK cysts. *(**a-c**) Representative images of parental MDCK cysts at 45 h after plating (initial stages of lumen formation) stained with Hoechst (blue) to visualize nuclei and antibodies against midbody remnants proteins (red); MKLP-1 in (**a**), γ-tubulin in (**b**) and Cep55 in (**c**). Cysts in **b** were additionally stained with α-tubulin to visualize microtubules (green) in order to exclude cytokinesis events. Bottom: higher magnification images of the indicated regions showing individual channels (left, middle) and a merge of these two images (right). Arrows indicate midbody remnants marking the nascent lumen position. (**d-f**) Experiments performed as in **a, b** and **c** except cysts were analyzed 72/96 h after seeding (open lumen stage). Arrows in the higher magnification images indicate midbody remnants at the edges of the lumen. (**g-i**) AuroraB localization during lumen morphogenesis. Representative parental MDCK cysts at different stages during lumen initiation stained with antibody against AuroraB (red) and α-tubulin (green) in **g** and **h** or MKLP-1 (green) in **i**. Arrows indicate AuroraB localization, arrowhead in **i** indicate MKLP-1 positive midbody remnant. Scale bars 10 μm.*

IV.3.6. PRL-3 overexpression affects apical lumen formation by altering post-mitotic midbody fate

Since PRL-3 overexpression led to the formation of cysts with incorrectly localized and frequently intracellular AMISs (Fig. IV.3c,e), we tested the hypothesis that in PRL-3 WT cysts the fate of midbody remnants is altered from release into the lumenal space to retention. As expected, MKLP1 staining in morphologically normal PRL-3 C104S cysts resembled that in parental cysts, with midbody remnants defining the AMIS (Fig. IV.6a) and later being adjacent to the lumen (Fig. IV.6b, see also Fig. IV.S5h,i,l for additional midbodies staining). Remarkably, in PRL-3 WT overexpressing cysts, midbody remnants were mainly retained either on the lateral plasma membrane or in the cytoplasm. MKLP1 staining shows that at an early stage the midbody remnants are in the PRL-3 intracellular patches we previously characterized as mislocalized AMIS (Fig. IV.6d). Moreover, at later cystogenesis stages, we found midbody remnants associated with ectopic lumens (Fig. IV.6e). Similar results were obtained by co-transfecting mKATE-PRL-3 WT and YFP-MKLP1 in MDCK cells (Fig. IV.S5a) as well as by staining with additional antibodies directed against midbody remnant proteins such as γ–tubulin, Aurora B and Cep55 (Fig. IV.S5b,c,d). In agreement with the observations in parental cysts, Aurora B was dispersed in the central lumen in PRL-3 C104S normal cysts and also in the ectopic lumens that arise in PRL-3 WT cysts (Fig. IV.S5f,i).

We also analyzed mosaic cysts, which revealed that PRL-3 WT-expressing cells extending into the lumenal space have lost midbody remnants. This contrasts with the observation made with parental cells in the same mosaic cysts, which maintained midbody remnants facing a small lumen. Similarly, in PRL-3 C104S expressing mosaic cysts the lumen edge was marked by midbody remnants (Fig. IV.6f,c).

Next, we carried out live cell imaging experiments using YFP-MKLP1 as a midbody remnant marker, to follow the fate of post-mitotic midbody over time in morphologically normal PRL-3 C104S cysts and in PRL-3 WT cysts. Figure IV.6g shows that at the two-cell stage, normal PRL-3 C104S cysts maintained the post-mitotic midbody at their center (Fig. IV.6g arrow). Moreover, this first midbody was maintained over time and marked the edge of the lumen when it finally opened (Fig. IV.6g arrow). The movie also showed that at the following division, the new post-mitotic midbody was positioned at the apical surface that later delimited, together with the older midbody, the nascent lumen (Fig. IV.6g arrowhead). In contrast,

midbody remnants in PRL-3 WT cysts followed a different fate and this was associated with phenotypic alterations. PRL-3 WT overexpression altered the post-mitotic midbody fate from release to retention (Fig. IV.6h). Retained post-mitotic midbodies either gave rise to ectopic lumens (Fig. IV.6h arrow) or disappeared with time (Fig. IV.6h arrowhead).

In summary, these results show that PRL-3 overexpression in MDCK cysts alters post-mitotic midbody fate from release in the luminal space to intracellular or intercellular retention. Retained midbodies can either persist or become undetectable, possibly through degradation. In the first case ectopic lumens arise at the site where the midbodies are retained, in the second case cells appear to lose a fundamental polarization signal and extend into the luminal space.

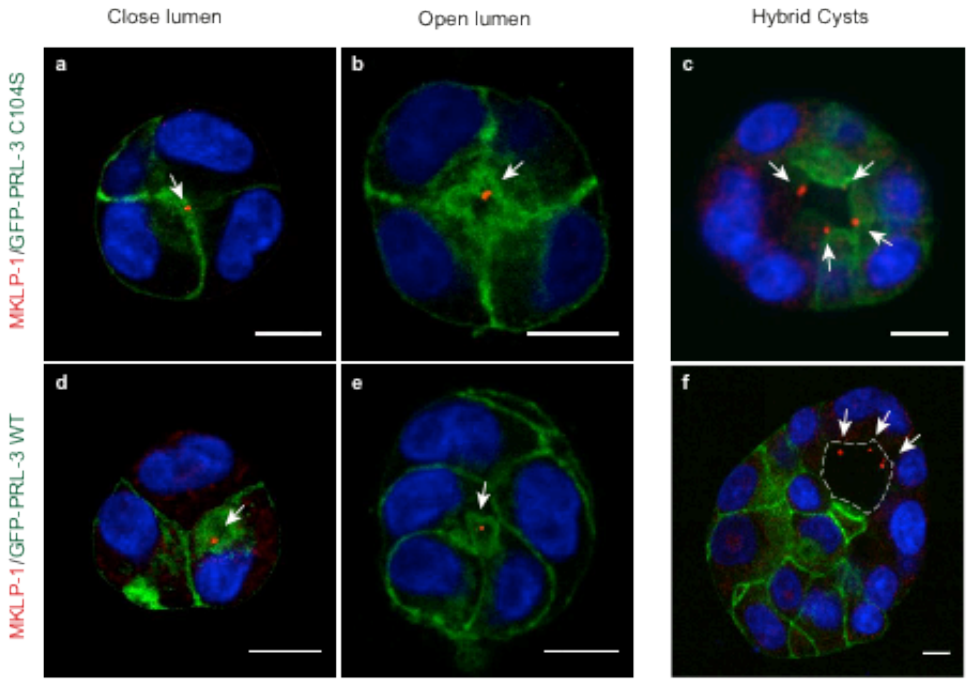

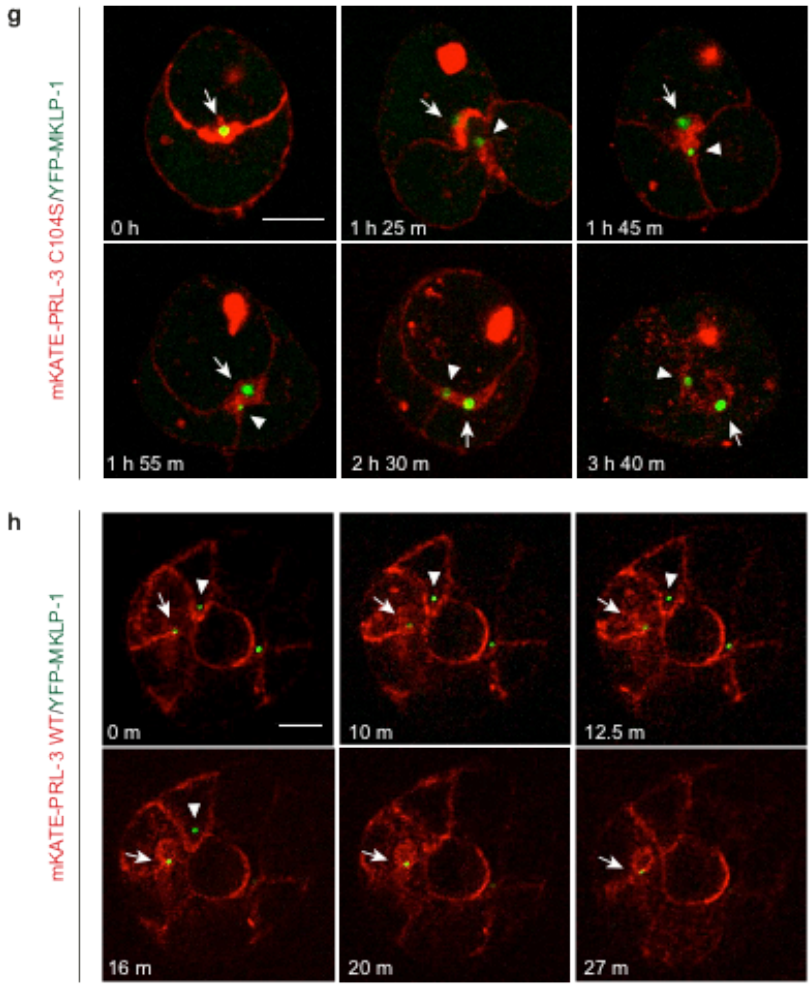

Figure IV.6. PRL-3 overexpression induces a multi-lumen phenotype in MDCK cysts by altering post-mitotic midbody fate. *(**a-c**) Representative confocal microscopy images of cysts expressing GFP-PRL-3 C104S (green) at 45 h (close lumen) or 72 h (open lumen and hybrid cysts) after plating and incubated with Hoechst (blue) to visualize nuclei and with MKLP-1 antibody (red) to visualize midbody remnants. Arrows indicate midbody remnants marking the center of the cysts in **a** and facing the lumen in **b** and **c**. Note that in **c** half of the cells in the cysts are not expressing GFP-PRL-3 C104S. (**d-f**) Representative images of cysts expressing GFP-PRL-3 WT at 45 h (close lumen), 72 h (open lumen) or 5 day (hybrid cysts) after plating stained as described in **a-c**. Arrows indicate cytoplasmic retained midbody remnants marking wrong localized AMIS in **d** and facing an ectopic lumen in **e**. Note that in **f** only the cells in the cysts that are not expressing PRL-3 WT show midbdody remnants (highlighted with arrows) facing the lumen. (**g-h**) Selected time points of time-lapse live-cell imaging of 45 h cysts stably expressing either GFP-PRL-3 C104S (**g**) or GFP-PRL-3 WT (**h**) transfected with YFP-MKLP-1. Arrow in **g** highlights the first midbody remnant; arrowhead highlights the midbody remnant coming from the second cytokinesis. Arrow in **h** indicates a midbody remnant that gets internalized with subsequent ectopic lumen formation; arrowhead highlights a midbody remnant that disappears with time. Scale bars 10 μm.*

IV.4. Discussion

Understanding how epithelial cells establish and maintain the axis of polarity is a fundamental issue for our comprehension of how epithelial tissue organize themselves into tubes and cysts. In the present study, we have demonstrated that in MDCK cysts the midbody remnant of the first cellular division is the earliest polarization signal (Model in Fig. IV.7a). The position of the first post-mitotic midbody defines the location of lumen formation and establishes the axis of polarity, converting the membrane where it is positioned into the AMIS. Moreover, midbody remnants are also maintained in the following division, marking the edge of the lumen when it physically opens. It has been shown that the resolution of the membrane connection between two daughter cells, during abscission, requires targeting and fusion of exocyst vesicles with the intracellular-bridge plasma membrane[27]. Several subunits of the exocyst complex, including Sec8, localized to the midbody ring during abscission and formed a ring-like structure[27]. Thus, the selective localization of key tethering factors (such as Sec8) of the exocyst complex at the midbody during abscission could be the link between midbody remnant and AMIS specification via polarized exocytosis.

We provide evidence for this model by showing that a perturbation of midbody remnant fate is associated with major defects in MDCK cyst morphogenesis. The overexpression of the phosphatase PRL-3 alters the fate of the post-mitotic midbody from release into the lumenal space to cytoplasmic or lateral plasma membrane retention (Model in Fig. IV.7b). The site where the midbody remnant is retained became first an ectopic AMIS, enriched in Par3 and surrounded by Sec8, and later on an ectopic lumen that stained positive for all the classical luminal markers (Model in Fig. IV.7b). Together, our results show that midbody remnants themselves are a signal sufficient to drive the entire pathway of *de novo* lumen formation, leading to the opening of completely specified lumens, independently of the position where they are located.

Recently, it has been suggested that midbody remnants could participate in non-cytokinetic functions, such as cell fate determination and cell polarity specification[13,23,25]. In particular, it has been shown that cytokinesis remnants are the earliest landmarks of neuronal polarity in Drosophila melanogaster *in vivo*[24]. Moreover, in *Drosophila* follicular epithelium, apical midbody localization provides a positional cue critical for the formation of the apico-basal axis of the tissue, as

confirmed by disruption of the epithelial architecture in case of midbody ectopic localization[25]. Our results strongly support a function of midbody remnants in polarization, showing that during cystogenesis, midbody remnants are the earliest signal of polarization. Interestingly, a link between cytokinesis and polarization has been also described in unicellular organisms, such as budding yeast, where the post-mitotic bud scar contributes to cell polarity and to establishing the division axis for the next cell division[28].

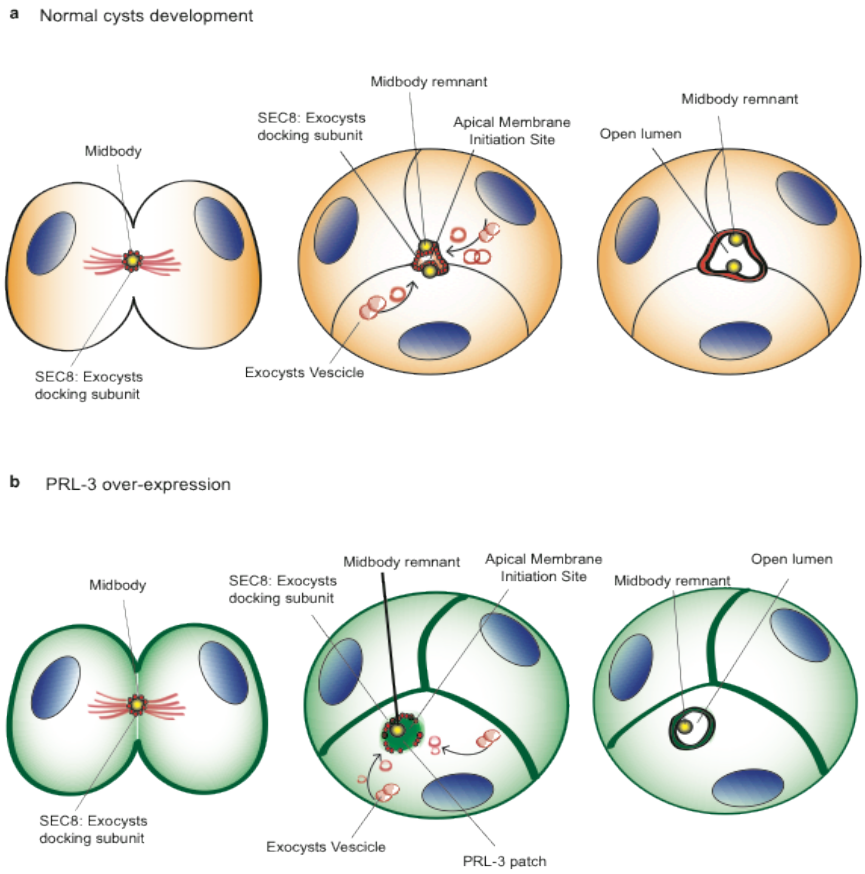

Figure IV.7. Midbody remnants are the earliest signal of polarization, determining intrinsically the lumen position. *(**a**) Schematic representation of different stages of lumenogenesis in MDCK cysts. During the first cytokinesis, members of the exocysts complex are delivered to the midbody to complete the abscission. Midbody remnants define the AMIS (apical membrane initiation site) that is established by polarized exocytosis. Expansion then allows opening of the luminal space, midbody remnants mark the edge of the lumen. (**b**) PRL-3 overexpression affects lumenogenesis by altering post-mitotic midbody fate. After the first cytokinesis the post-mitotic midbody is internalized and retained in the cytoplasm. This site becomes a wrongly localized and PRL-3 enriched AMIS where apical determinants are delivered by exocytosis. Expansion then allows opening of ectopic lumens in the position where the midbody remnant is retained. Red lines, microtubules; yellow circles, midbody and midbody remnants; small red circles, exocysts subunits; blue ovals, nuclei; empty red circles, exocysts vescicles.*

Molecular details of how the fate of midbody remnants is determined will be illuminated by the identification of the PRL-3 substrate in this process, which could be a key player in the establishment the lumen. Thus far, several protein substrates and a non-protein substrate have been suggested, but none has been confirmed yet as the substrate that accounts for the pleiotropic effects on cellular signaling caused by PRL-3 overexpression[12]. Indeed, the identification of PRL-3 substrates has remained extremely challenging since its discovery over a decade ago[11,12]. In the context of lumen formation, the suggested PRL-3 substrates $PI(4,5)P_2$ and Ezrin are particularly attractive candidates as they are known determinants of cellular polarity[16]. We did not observe significant changes in the phosphorylation status of either one of these proposed substrates with the methods applied here. Rapid changes of tightly controlled phosphorylation levels may however be difficult to detect, and it will take the development of elaborate, sensitive methods such as phosphoproteomics at distinct time points in 3D cell culture to make progress in this area. Acute changes, for example in the concentration of $PI(4,5)P_2$ at relevant locations as seen in other processes such as endocytosis and exocytosis[29], could account for the alteration of midbody fate with its dramatic phenotypic consequences. Alternatively, hitherto unknown effects caused by protein-protein interactions that depend on the intact WT phosphatase (as opposed to the C104S mutant, which seems to be structurally less stable[30]) could be the critical factor in altering midbody fate.

The question of whether PRL-3 is a bona-fide oncogene has not yet been addressed in detail. In a recent report[31], the authors observed elevated expression of PRL-3 in the colon of WT mice immediately following the treatment with a carcinogen. In addition, WT mice expressed PRL-3 at an elevated level in primary tumors and PRL-3 knock out mice developed 50% fewer tumors following treatment with carcinogens[31]. These findings suggest strongly that PRL-3 could play a role in colon tumorigenesis, aside from its known role in the progression of late stage cancer and metastasis[11,12]. Our data strongly support these findings in that the simple over-expression of PRL-3 in a non-cancerous background causes detrimental disorganization of epithelial structures. Moreover, it is known that one of the earliest events following the acquisition of oncogenic mutations by an epithelial cell is the formation of multilayered and disorganized structures[8]. This resembles the phenotype exhibited by PRL-3 overexpressing multilayered cells that grow into the cyst lumen in a disorganized way. In addition to the disruption of cell-cell contacts, cell-matrix

adhesion and spindle orientation[8], switching the fate of midbody remnants could therefore be another reason for loss of epithelial organization in cancer.

We identified midbody remnants as the earliest signal of polarization in cystogenesis, and that PRL-3 overexpression alters the fate of the midbody remnants. These findings not only offer an explanation for the long unanswered question of how the position of the AMIS is specified, but also suggest a novel mechanism for the loss of epithelial organization in cancer, including the identification of PRL-3 as an enzyme involved in this mechanism. Studying these mechanisms in vivo in epithelial organ formation and cancers originating from epithelial tissues will be major challenges in developmental and cancer cell biology in the future.

IV.5. Methods

IV.5.1. Cells

MDCK cells were grown in Minimum Essential Medium (MEM) containing 10% fetal bovine serum (FBS), (both from Gibco, Life Technologies), 100 U/ml penicillin and 100 μg/mL streptomycin (Sigma) and 2 mM L-glutamine (Sigma). MDCK stably expressing GFP-PRL-3 WT and GFP-PRL-3 C104S were made by transfection (Lipofectamine LTX, Life Technologies) of pEGFP-C1-PRL-3 WT and pEGFP-C1-PRL-3 C104S respectively, and selection with 4mg/ml of Geneticin (Gibco, Life Technologies) for 2 weeks. MDCK cells stably co-expressing GFP-PH PLCδ and mKATE-PRL-3 (either WT or C104S) were generated by transfection of MDCK GFP-PH-PLCδ (provided by F.M. Belmonte, CBMSO, Spain) with pmKATE2-C PRL-3 (WT or C104S) and double selection with 4mg/ml of Geneticin and 5 μg/ml of Blasticidin S (Invitrogen) for 2 weeks. Transfected cells underwent fluorescence activated cell sorting (FACS) after selection. HEK 293 kidney epithelial cells were cultured in Dulbecco's Modified Eagle's Medium (DMEM) supplemented with 10% (v/v) FBS, 100 U/ml penicillin and 100 μg/mL streptomycin and 2 mM L-glutamine.

IV.5.2. 3D culture

MDCK cell cyst formation was performed as described previously[16]. Briefly, to prepare cysts in Matrigel (BD Bioscience) cells were trypsinized to a single cell suspension of $4x10^4$ cells/ml in complete medium containing 2% Matrigel. Suspensions (250μl) were plated into 8-well coverglass chambers (Nunc), pre-coated

with Matrigel diluted 1:10 (v/v) in MEM serum free. Cells were grown for the indicated times before fixation in 4% paraformaldehyde (PFA) or for live cell imaging experiments. For Annexin-A2-mRFP and YFP-MKLP1 expression, cells in 2D were transiently transfected (Lipofectamine LTX, Life Technologies) before plating into 3D.

IV.5.3. Plasmids

Vectors pEGFP-C1, pmKATE2-C, pCMV-3-FLAG were used to overexpress WT human PRL-3. PRL-3 C104S mutant was generated by site-directed mutagenesis[30]. Annexin-A2-mRFP construct in clontech N1 vector was obtained from Dr. Carsten Schultz (EMBL, Heidelberg). pEGFP-C1 Par3 and pdEYFP-Sec8[32] were obtained from Dr. Rainer Pepperkok (EMBL, Heidelberg). Par3 fragments (Par3A, Par3B, Par3C, Par3D) tagged with GST were generated by PCR amplification and cloned into pGEX-6P-2rbs vector. In detail, Par3A residues 1-373, Par3B residues 228-704, Par3C residues 678-935, Par3D residues 931-1337.

IV.5.4. Antibodies and immunolabelling

Primary mouse antibodies used were: anti-Sec8 (Immunofluorescence, 1:100; Enzo Life Sciences; western blot, 1:300; Santa Cruz Biotechnology); anti-ZO-1-Alexa Fluor 594 (1:50; Invitrogen); anti-FLAG M2 (1:1000; Sigma); anti-GFP (1:1000; Roche); anti-AuroraB (1:200; BD Transduction Laboratories clone 6/AIM-1); anti-gamma-tubulin (1:100; Sigma, clone GTU-88); anti-Cep55 (1:100; Abnova). Primary rabbit antibodies used were: anti-MKLP1 (1:1000; Santa Cruz Biotechnology); anti-Par3 (Immunofluorescence, 1:100, western blot, 1:1000; Millipore); anti-alpha-tubulin (1:500; Millipore, clone EP1332Y); anti-phospho-ERM detecting phosphorylation of Ezrin (Thr-567)/Radixin (Thr-564)/Moesin (Thr-558) (1:100; Cell signaling Technology), in the experiments was used to detect phosphorylated Ezrin considering that MDCK cells express mainly Ezrin of ERM family proteins[33]. Primary sheep antibody used was: anti PKC iota/lambda/zeta (1:000; LifeSpan Biosciences). Mouse monoclonal antibody against human PRL-3 (clone 1E7) was generated using His-tagged recombinant PRL-3 produced in bacteria and purified using nickel resin as immunogen. Specificity of the anti-PRL-3 antibody was evaluated by ELISA assays and western immunoblotting using recombinant PRL-1

and PRL-3. Alexa fluorophore-conjugated secondary antibodies (1:1000 for all secondary antibodies; Invitrogen) or Phalloidin (1:400; Invitrogen) and Hoechst to label nuclei (10 mg/ml), were utilized. The procedure for the immunofluorescence staining of cysts was previously described in detail[34]. Briefly, samples were rinsed with phosphate-buffered saline (PBS) twice quickly and fixed with 4% PFA for 30 min. Cells were quenched with 0,1 M glycin in PBS for 20 min, permeabilized with 0.5% Triton X-100 in PBS for 10 min and blocked with 10% FBS in PBS/0.5% Triton for 30 min. Samples were then incubated with primary antibodies in blocking solution at 4°C overnight, followed by washing and incubation with Alexa Fluor - conjugated secondary antibody for 1 hour. To stain Cep55 cells were permeabilized in digitonin solution (50mg/ml digitonin in PBS) at 37°C for 5 min, excess of digitonin was quenched with 50mM NH4Cl in PBS at 37°C for 5 min, then cells were blocked with 2% bovine serum albumin (BSA; Sigma), 5% FBS in PBS at 37°C for 30 min. Primary antibody was diluted in blocking solution, cells were incubated for 1 hour at 37°C.

IV.5.5. Immunoprecipitation and immunoblotting

Cells were lysed on ice in HNTG (50 mM Hepes, pH 7.5, 150 mM NaCl, 10% glycerol, 5 mM EGTA, and 1% Triton X-100) containing complete protease inhibitors (Roche). After centrifugation at $12\times10^3\times g$ for 15 min, the protein concentration was measured, and equal amounts of lysate were used for immunoprecipitation. Immunoprecipitations were performed with GFP-Trap beads (ChromoTek) overnight at 4 °C. Thereafter, the precipitants were washed three times with lysis buffer and the immune complexes eluted with sample buffer containing 1% SDS for 5 min at 95 °C. The immunoprecipitated proteins were then separated by SDS–PAGE. Western blotting was performed with specific antibodies and secondary anti-mouse or anti-rabbit antibodies conjugated to horseradish peroxidase (Sigma and Amersham Biosciences respectively). Visualization was achieved with the Amersham Biosciences ECL (Enhanced Chemiluminescence)

IV.5.6. Purification of recombinant proteins and GST-pulldown

Plasmids expressing GST–Par3 fragments were used to transform the *Escherichia coli* strain BL21. Cultures were grown overnight at 37 °C. The next day, cultures were diluted 1:10 in fresh LB medium and grown at 37 °C to an optical density of 0.6 at

600 nm. Protein expression was then induced for 3 hours at 37 °C in the presence of 0.1 mM isopropyl- β-D-thiogalactopyranoside (IPTG). For GST pull-down assays the bacteria pellets were resuspended in NETN buffer (20 mM Tris-HCl, pH 8.0, 100 mM NaCl, 1 mM EDTA, and 0.5% NP-40) supplemented with complete protease inhibitors (Roche). After sonication the supernatants of the cell lysates were incubated with glutathione magnetic beads (Thermo scientific Pierce) for 1 hour at 4 °C. To test direct binding between GST-Par3 fragments and PRL-3, 5mg of GST fusion protein bound onto glutathione magnetic beads were incubated for 1 hour at 4 °C in HNTG buffer with 100 ng of recombinant PRL-3, purified as described previously[30]. Beads were extensively washed with HNTG, bound protein were eluted with sample buffer containing 1% SDS for 5 min at 95 °C and processed for immunoblot analysis.

IV.5.7. Vesicles trafficking

To label exocysts vesicles cells were treated with 5μM of the red-fluorescent BODIPY-TR ceramide complexed to BSA (Invitrogen) at 4 C° for 30 minutes. Samples were then rinsed several times with ice-cold medium and incubated in fresh medium at 37 C° for further 20 minutes before starting the image acquisition.

IV.5.8. Calcium Switch Assay

Calcium switch experiments were performed as described previously[20]. Briefly, MDCK cells were plated in eight-well Lab-Tek II chambers with complete growth medium (normal calcium medium, HCM). After 24 hr cells were switched into low calcium medium (LCM). LCM was prepared by supplementing MEM with 2% FBS which was dialysed against 150mM NaCl overnight. After 16 hr incubation in LCM, cells were switched back to HCM for the indicated times.

IV.6. References

1. St Johnston, D. & Ahringer, J. Cell polarity in eggs and epithelia: parallels and diversity. *Cell* **141,** 757–74 (2010).

2. Datta, A., Bryant, D. M. & Mostov, K. E. Molecular regulation of lumen morphogenesis. *Curr Biol* **21,** R126–36 (2011).

3. Schlüter, M. A. & Margolis, B. Apical Lumen Formation in Renal Epithelia. *J Am Soc Nephrol* **20,** 1444–1452

4. Brien, L. E. O., Zegers, M. M. P. & Mostov, K. E. Building epithelial architecture: insight from three-dimensional culture models. *Nat. Rev. Mol. Cell Biol.* **3,** 1–7 (2002).

5. Bryant, D. M. *et al.* A molecular network for de novo generation of the apical surface and lumen. *Nat. Cell Biol.* **12,** 1035–45 (2010).

6. Apodaca, G. Opening ahead: early steps in lumen formation revealed. *Nat. Cell Biol.* **12,** 1026–8 (2010).

7. Apodaca, G., Gallo, L. I. & Bryant, D. M. Role of membrane traffic in the generation of epithelial cell asymmetry. *Nat. Cell Biol.* **14,** 1235–43 (2012).

8. McCaffrey, L. M. & Macara, I. G. Epithelial organization, cell polarity and tumorigenesis. *Trends Cell Biol* **21,** 727–35 (2011).

9. Aranda, V., Nolan, M. E. & Muthuswamy, S. K. Par complex in cancer: a regulator of normal cell polarity joins the dark side. *Oncogene* **27,** 6878–87 (2008).

10. Guzińska-Ustymowicz, K. & Pryczynicz, A. PRL-3, an emerging marker of carcinogenesis, is strongly associated with poor prognosis. *Anticancer Agents Med Chem* **11,** 99–108 (2011).

11. Al-Aidaroos, A. Q. O. & Zeng, Q. PRL-3 phosphatase and cancer metastasis. *J Cell Biochem* **111,** 1087–98 (2010).

12. Rios, P., Li, X. & Köhn, M. Molecular mechanisms of the PRL phosphatases. *FEBS J.* **280,** 505–24 (2013).

13. Chen, C.-T., Ettinger, A. W., Huttner, W. B. & Doxsey, S. J. Resurrecting remnants: the lives of post-mitotic midbodies. *Trends Cell Biol* **23,** 118–28 (2013).

14. Debnath, J. & Brugge, J. S. Modelling glandular epithelial cancers in three-dimensional cultures. *Nat. Rev. Cancer* **5,** 675–88 (2005).

15. Horikoshi, Y. *et al.* Interaction between PAR-3 and the aPKC – PAR-6 complex is indispensable for apical domain development of epithelial cells. *J. Cell Sci.* **122,** 1595–1606 (2009).

16. Martin-belmonte, F. *et al.* PTEN-Mediated Apical Segregation of Phosphoinositides Controls Epithelial Morphogenesis through Cdc42. *Cell* **128,** 383–397 (2007).

17. Schlu, M. A. *et al.* Trafficking of Crumbs3 during Cytokinesis Is Crucial for Lumen Formation. *Mol. Biol. Cell* **20,** 4652–4663 (2009).

18. Van der Sluijs, P., Bennett, M. K., Antony, C., Simons, K. & Kreis, T. E. Binding of exocytic vesicles from MDCK cells to microtubules in vitro. *J. Cell Sci.* **95 (Pt 4),** 545–53 (1990).

19. Suzuki, A. & Ohno, S. The PAR-aPKC system: lessons in polarity. *J. Cell Sci.* **119,** 979–87 (2006).

20. Chen, X. & Macara, I. G. Par-3 controls tight junction assembly through the Rac exchange factor Tiam1. *Nat. Cell Biol.* **7,** (2005).

21. Neto, H. & Gould, G. W. The regulation of abscission by multi-protein complexes. *J. Cell Sci.* **124,** 3199–207 (2011).

22. Steigemann, P. & Gerlich, D. W. Cytokinetic abscission: cellular dynamics at the midbody. *Trends Cell Biol* **19,** 606–16 (2009).

23. Kuo, T.-C. *et al*. Midbody accumulation through evasion of autophagy contributes to cellular reprogramming and tumorigenicity. *Nat. Cell Biol.* **13,** 1214–23 (2011).

24. Pollarolo, G., Schulz, J. G., Munck, S. & Dotti, C. G. Cytokinesis remnants define first neuronal asymmetry in vivo. *Nat. Neurosci.* **14,** 1525–33 (2011).

25. Morais-de-Sá, E. & Sunkel, C. Adherens junctions determine the apical position of the midbody during follicular epithelial cell division. *EMBO Rep.* **14,** 1–8 (2013).

26. Joseph, N., Hutterer, A., Poser, I. & Mishima, M. ARF6 GTPase protects the post-mitotic midbody from 14-3-3-mediated disintegration. *EMBO J.* **31,** 2604–14 (2012).

27. Gromley, A. *et al*. Centriolin anchoring of exocyst and SNARE complexes at the midbody is required for secretory-vesicle-mediated abscission. *Cell* **123,** 75–87 (2005).

28. Nelson, W. J. Adaptation of core mechanisms to generate cell polarity. *Nature* **422,** 766–74 (2003).

29. McLaughlin, S., Wang, J., Gambhir, A. & Murray, D. PIP2 and proteins: interactions, organization, and information flow. *Annu. Rev. Biophys. Biomol. Struct.* **31,** 151–75 (2002).

30. McParland, V. *et al*. The metastasis-promoting phosphatase PRL-3 shows activity toward phosphoinositides. *Biochemistry* **50,** 7579–90 (2011).

31. Zimmerman, M. W., Homanics, G. E. & Lazo, J. S. Targeted deletion of the metastasis-associated phosphatase Ptp4a3 (PRL-3) suppresses murine colon cancer. *PLOS ONE* **8,** e58300 (2013).

IV.7. Supplementary Figures

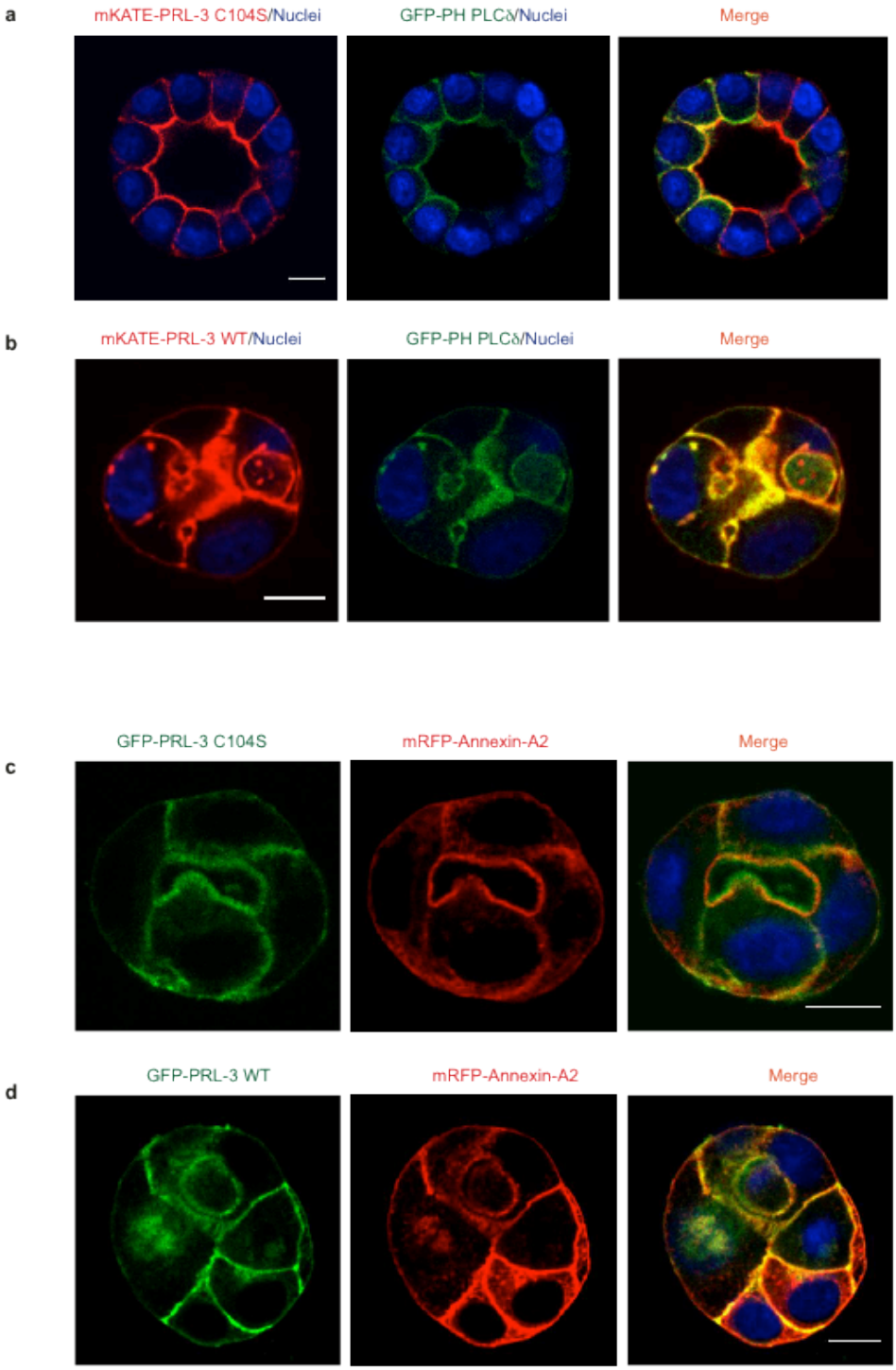

Figure IV.S1. Ectopic lumens in PRL-3 WT cysts are positive for apical determinants. *(**a-b**) Representative images of 72 h cysts either stably expressing the catalytically inactive mutant mKATE-PRL-3 C104S (**a**) or mKATE PRL-3 WT (**b**) (both red) and the PI(4,5)P_2 sensor GFP-PH PLCδ (green). Nuclei were stained with Hoechst (blue). (**c-d**) Representative images of 72 h cysts either stably expressing GFP-PRL-3 C104S (**c**) or GFP PRL-3 WT (**d**) (both green) transiently transfected with mRFP-Annexin2 (red). Nuclei were stained with Hoechst (blue). Scale bars 10 μm.*

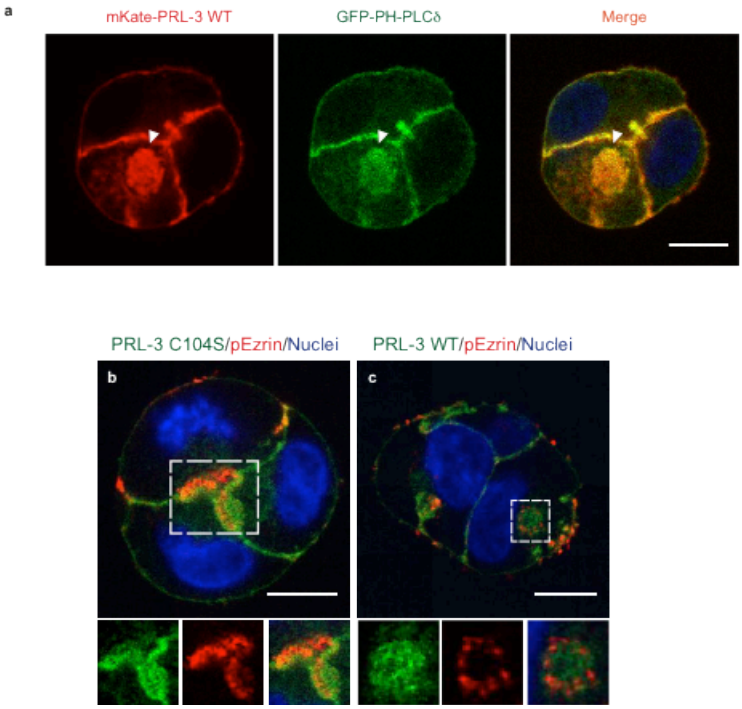

Figure IV.S2. PRL-3 intracellular patches are positive for apical determinants. *(**a**) Representative images of 45 h cysts stably expressing mKATE PRL-3 WT (red) and the PI(4,5)P_2 sensor GFP-PH PLCδ (green). Nuclei were stained with Hoechst (blue). Arrowhead indicates a PI(4,5)P_2 positive PRL-3 patch. (**b-c**) Representative images of cysts either expressing the catalytically inactive mutant GFP-PRL-3 C104S (**b**) or expressing GFP-PRL-3 WT (**c**) (both green) incubated with Hoechst (blue) and with antibodies against threonine-phosphorylated ERM (ezrin/radixin/moesin) proteins (pEzrin) shown in red at 45 h after plating. Bottom: higher magnification images of the indicated regions showing individual channels (left, middle) and a merge of these two images (right). Note in **c** a PRL-3 patch surrounded by phosphorylated Ezrin. Scale bars 10 μm.*

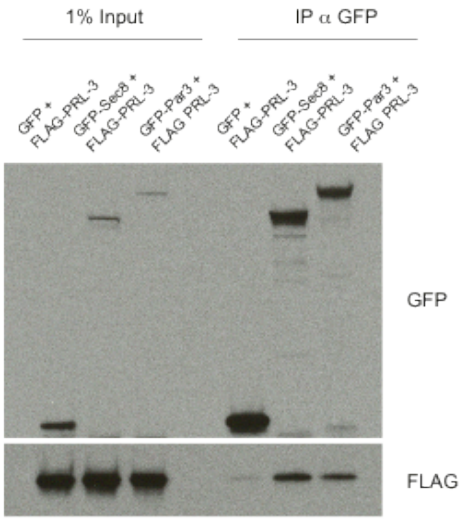

Figure IV.S3. PRL-3 interacts with Par3 and Sec8. *FLAG- tagged PRL-3 co-immunoprecipitated with GFP-Par3 or GFP-Sec8 in HEK293 cells. Lysates from HEK293 co-transfected with FLAG-PRL-3 and GFP control vector or vectors encoding either GFP-Par3 or GFP-Sec8 were immunoprecipitated using GFP-TRAP beads. Immunoprecipitates were immunoblotted with antibodies against GFP (top) and FLAG (bottom).*

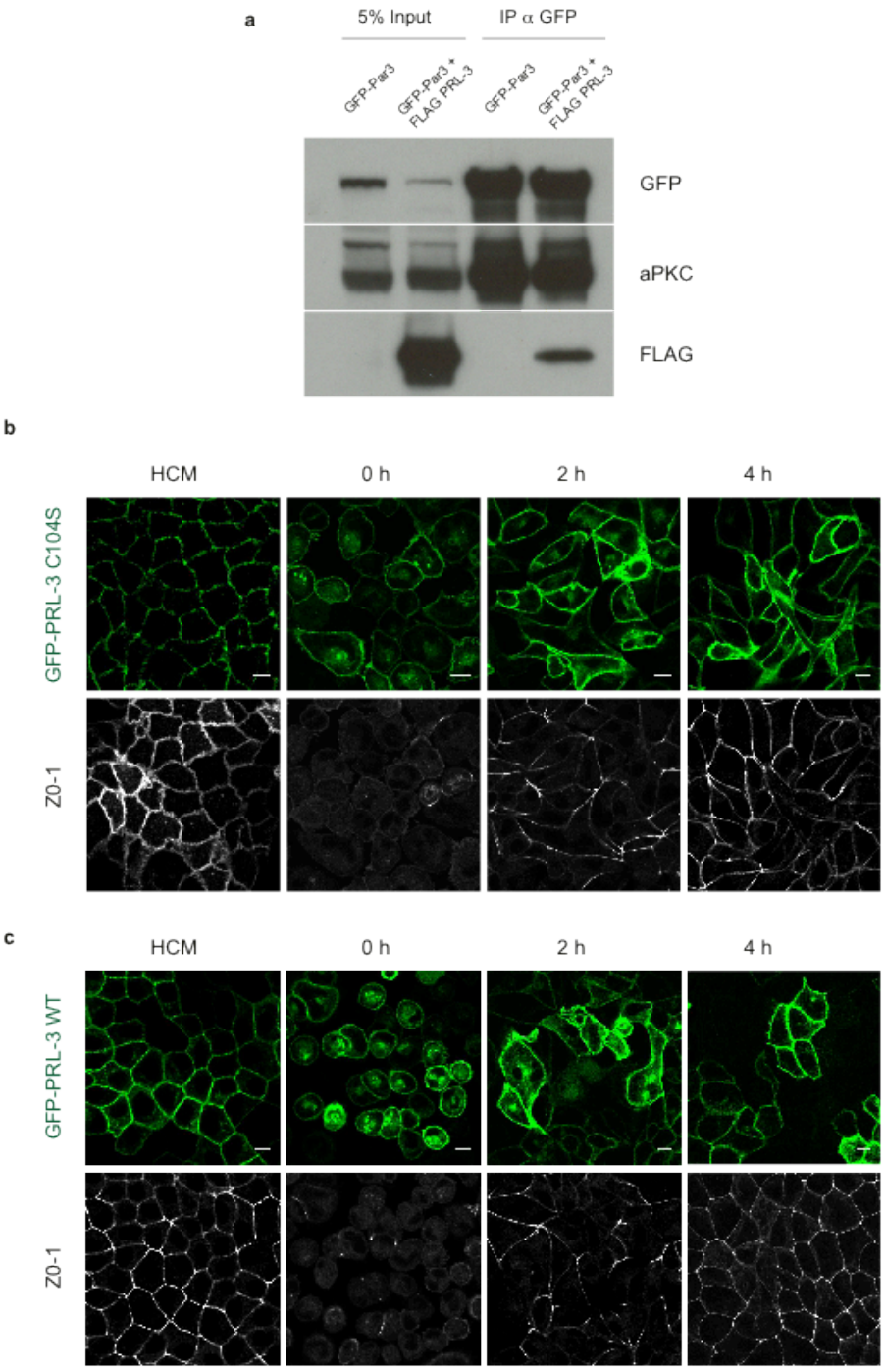

Figure IV.S4. PRL-3 overexpression is interfering neither with Par3-aPKC interaction nor with de novo tight junction formation. *(**a**) GFP-Par3 co-immunoprecipitated endogenous aPKC and also FLAG-PRL-3 in HEK293 cells. Lysates from HEK293 transfected with GFP-Par3 or co-transfected with GFP-Par3 and FLAG-PRL-3 were immunoprecipitated using GFP-TRAP beads. Immunoprecipitates were immunoblotted with antibodies against GFP (top), aPKC (middle) and FLAG (bottom). In the anti aPKC immunoblot, two bands, corresponding to the isoforms PKCζ and PKCι, can be noted (**b-c**) PRL-3 overexpression did not disrupt the relocalization of ZO-1 to cell borders during a calcium switch assay. Control GFP-PRL-3 C104S (**b**) or GFP-PRL-3 WT (**c**) MDCK cells were subjected to a calcium switch. Cells were fixed at the indicated time points after restoring normal Ca^{2+} levels to the growth media and stained with antibodies against ZO-1. HCM, normal calcium-containing medium. Scale bars 10 μm.*

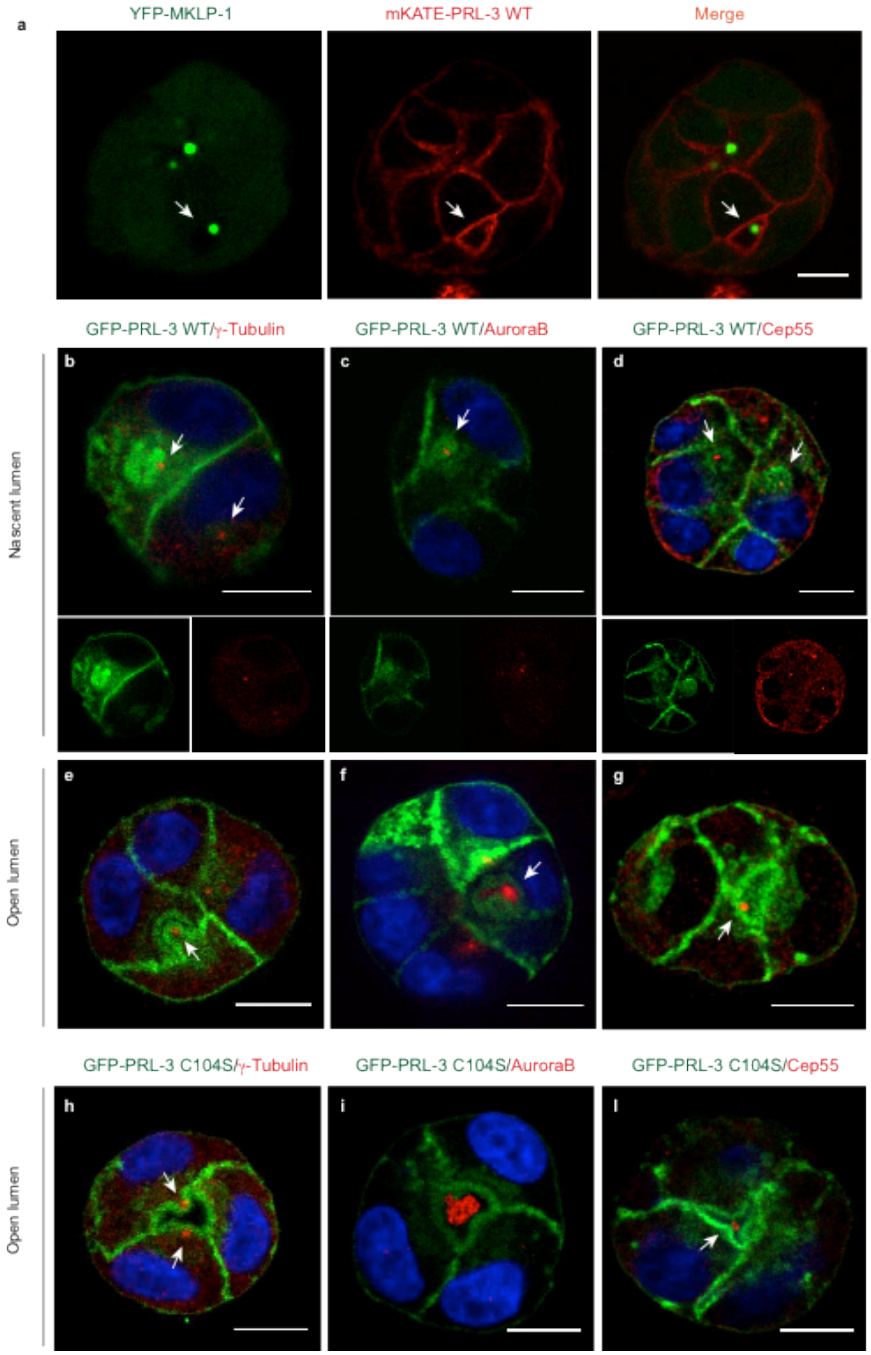

Figure IV.S5. PRL-3 overexpression induces a multi-lumen phenotype in MDCK cysts by promoting midbody remnants retention. *(**a**) Representative image of 72 h cysts expressing YFP-MKLP-1 and mKATE-PRL-3 WT. Arrow indicate a midbody remnant associated with an ectopic lumen. (**b-g**) Representative confocal microscopy images of cysts expressing GFP-PRL-3 WT (green) at 45 h (close lumen) or 72 h (open lumen) after plating and incubated with Hoechst (blue) to visualize nuclei and with antibodies against midbody remnants proteins (red); γ-tubulin in (**b,e**), AuroraB in (**c,f**), Cep55 in (**d,g**). Bottom in (**b-d**): separate fluorescent channels showing localization of individual proteins. Arrows indicate midbody remnants associated with PRL-3 intracellular patches previously characterized as ectopic AMIS (**b-d**) or with ectopic lumens (**e-f**). (**h-l**) midbody remnants define the central lumen in morphologically normal PRL-3 C104S cysts. Representative confocal microscopy images of cysts expressing GFP-PRL-3 C104S (green) at 72 h (open lumen) after plating and incubated with Hoechst (blue) to visualize nuclei and with antibodies against midbody remnants proteins (red); γ-tubulin in (**h**), AuroraB in (**i**) Cep55 in (**l**). Arrows indicate midbody remnants marking the central lumen. Scale bars 10 μm.*

Chapter V: General discussion and perspectives

V.1. Identification of PRL-3 substrates

PRL-3 belongs to the family of dual specificity phosphatase and its expression appears highly restricted and tightly regulated. In agreement with these observations, the aberrant expression of PRL-3 is associated with pathological conditions and, in particular, correlates with cancer progression, poor prognostic outcome and probably with primary tumor development (Rios et al., 2013; Zimmerman et al., 2013). Although in the last decade numerous clinical studies have extensively validated the role of PRL-3 in cancer, to date its substrate(s) and the direct downstream transduction pathways affected by PRL-3 overexpression are still elusive (Bessette et al., 2007). The identification of substrates of PRL-3 turned out to be extremely challenging, taking into account its extremely low activity in vitro and the tremendous pleiotropic effects that its overexpression generates in stable cell lines (Rios et al., 2013).

For example, recently a study was published concerning a tyrosine-specific phosphoproteomic analysis of squamous epithelial HEK293 cells overexpressing PRL-3 (Walls et al., 2013). Phosphoproteomic data revaled a global enhancement in tyrosine phosphorylation, similar to the cellular response obtained by transmembrane growth factor receptor activation. The authors could not explain the data identifying the central "hub" whose phosphorylation was directly affected by PRL-3 overexpression, but they could only confirm previous observations regarding PRL-3-dependent Src tyrosine kinase activation. Notably, Src activation itself seems not to be directly related with PRL-3 phosphatase activity but is an indirect effect due to PRL-3 dependent downregulation of the kinase Csk, a negative regulator of Src (Liang et al., 2007).

On the other hand, also the generation of a PRL-3 knockout mouse has not given any clue regarding physiological roles and substrates of PRL-3 (Zimmerman et al., 2013). Indeed, the lack of a clear phenotype opens the possibility that PRL-3 physiological functions can be redundant and overcome by other enzymes *in vivo*. Thus, to date, the molecular basis of PRL-3 function remains an enigma. However, the identification of PRL-3 substrates is still considered a fundamental goal, not only

to provide information about its physiological functions, but also to facilitate the development of specific inhibitors possibly useful for clinical purposes.

Here we show that PRL-3 does not hydrolyze any of a large number of tested phosphopeptides. However, we cannot exclude that the phosphatase needs the native 3D-dimensional structure of the substrates for their recognition or that PRL-3 needs co-factors to be fully catalytically competent. On the contrary, we show that PRL-3 dephosphorylates PtdIns(4,5)P_2 *in vitro* using two distinct biochemical assays. Moreover, we provide evidence that PRL-3 could be a 5-phosphatase, hydrolyzing PtdIns(4,5)P_2 into PtdIns(4)P.

Notably, additional members of the class of dual specificity phosphatases are primarily lipid phosphatases, namely PTEN and the phosphatases of the myotubularin family. These enzymes fulfill their functions by dephosphorylating PtdIns(3,4,5)P_3 and PtdIns(3)P, respectively (Pulido et al., 2013).

Fluctuations in PtdIns(4,5)P_2 levels or its compartmentalization in plasma membrane microdomains directly regulate a multitude of cellular responses, including exo- and endocytosis, ion channel transport, cytokinesis, cell shape, motility, polarity and adhesion (McLaughlin et al., 2002). Thus, PRL-3 activity against PtdIns(4,5)P_2 could partially explain the drastic effects observed when PRL-3 is overexpressed. However, to date, we still miss a clear proof that PRL-3 functions as a lipid phosphatase activity in cells although several technical approaches, including live cell imaging and phosphate radioactive labeling have been attempted (data not shown).

In addition to the *in vitro* characterization of PRL-3 phosphatase activity, we have also studied the effect of PRL-3 aberrant expression in an organotypic 3D-culture system, potentially mimicking the in vivo cancer progression scenario. The results show that PRL-3 overexpression, in a 3D model of glandular epithelium, is on its own sufficient to perturb dramatically epithelial architecture, with the phosphatase behaving as a classical oncogene and consequently reinforcing its pathological relevance. From the substrates point of view, we tested in this system two putative substrates, Thr567 phosphorylated ezrin and PtdIns(4,5)P_2. Unfortunately, we did not detect any substantial change in the overall phosphorylation of these two molecules. However, we cannot exclude a correlation between the observed phenotype and PRL-3 lipid phosphatase activity. Indeed, although in PRL-3 overexpressing cysts the apical domain is still PtdIns(4,5)P_2 enriched, transient and local PtdIns(4,5)P_2

fluctuations in defined plasma membrane domains could be still behind the phenotypic alterations observed.

Furthermore, we identified the post-mitotic midbody, a remnant organelle from cytokinesis, as the first polarization signal during cystogenesis and we prove that PRL-3 overexpression disrupts cysts overall epithelial architecture by interfering with the fate of post-mitotic midbodies. Three distinct fates of post-mitotic midbodies have been described, i.e. their release into the extracellular space or their cytoplasmic retention followed or not by degradation through autophagy(Chen et al., 2013). We proved that, during cysts development, post-mitotic midbodies are committed to only one fate that is apical release, specifying intrinsically the lumen position. Moreover, we described that the aberrant expression of PRL-3 alters the fate of post-mitotic midbodies by interfering with their release. Finally, we correlate the multi-lumen phenotype, observed in PRL-3 overexpressing cysts, with the PRL-3-induced alteration of post-mitotic midbodies fate.

Recently, multiple lines of evidence have been forwarded to support the notion that midbody remnants could participate in functions unrelated to cytokinesis, such as, for example, the establishment of neuronal asymmetry (Pollarolo et al., 2011). Moreover, it seems that the fate of post-mitotic midbodies could be rigorously cell or tissue-type specific. Indeed, it has recently been shown that stem cells are characterized by the accumulation of cytoplasmic midbody remnants, a characteristic that is lost when stem cells proceed to differentiation (Kuo et al., 2011). In agreement with these observations the authors have also shown that the accumulation of aberrant midbody remnants through evasion of autophagy is associated with cellular reprogramming and an increased tumorigenic potential of selected cell lines.

Although several non-cytokinetic roles of midbody remnants have been recently described, to date, the signaling pathways governing midbody remnants fate are entirely unknown. Thus, to identify and characterize how PRL-3 overexpression alters midbody fate determination is extremely challenging.

At the moment, we are planning to use two distinct strategies to answer this question, considering screening-based methods as well as candidate-based approaches. In the first case, we are setting the conditions to perform complete lipidomic and phosphoproteomic studies of cysts at different stages, in order to compare the overall changes induced by PRL-3 overexpression in a 3D model of glandular epithelium. In the second case, from a lipid perspective we are planning to

investigate a possible role of PtdIns(4,5)P_2 immediately after cytokinesis at the moment of midbody remnants sorting, whereas from a protein perspective, we are mainly focused on GTPases regulating proteins, in particular guanine nucleotide exchange factors (GEFs). Indeed, a complex signaling crosstalk between GTPases and phosphoinositides at the cleavage furrow during cytokinesis has been recently described (Field et al., 2005; Logan and Mandato, 2006).

It has been suggested that PtdIns(4,5)P_2 progressively concentrates at the cleavage furrow of dividing cells, facilitating the attachment of the plasma membrane to structural components of the actomyosin ring. Interestingly, it seems that during furrow progression PtdIns(4,5)P_2 levels are not constant but cycle through bursts of synthesis and PLC-mediated hydrolysis (Field et al., 2005; Logan and Mandato, 2006).

In addition to PtdIns(4,5)P_2, an intriguing hypothesis worthy of further investigation is the possible involvement of the GEF Ect2 (epithelial cell transforming sequence 2 oncogene) in the PRL-3 mediated phenotype. Ect2 is a component of the centralspindlin complex, a multiprotein complex required for the myosin contractile ring formation during cytokinesis. It has been reported that Ect2 localizes at the midbody during abscission and that the interactions between components of the centralspindlin complex, including Ect2, RacGAP and MKLP1, are regulated by dynamic events of phosphorylation/dephosphorylation (Saito et al., 2004; Yüce et al., 2005). Moreover, Ect2 is a Par6/aPKC interacting protein and a direct substrate of aPKC (Liu et al., 2006). Although Ect2 knockdown in MDCK cysts is not associated with any phenotype, the overexpression of a constitutively active mutant significantly affects epithelial morphogenesis, leading to formation of cysts with multiple abnormal lumens (Liu et al., 2006; Qin et al., 2010). Ect2 stimulates the activity of members of the Rho GTPase family, including RhoA and Cdc42, and most of its biological functions described are related to the regulation of cytokinesis (Oceguera-Yanez et al., 2005; Yüce et al., 2005). From a pathological perspective, Ect2 is found highly overexpressed and mislocalized in several human tumors and its overexpression correlates with poor prognosis in patients (Saito et al., 2004). We have identified Ect2 as a weak PRL-3 interacting protein in a screening for new PRL-3 binding proteins (data not shown). We are planning to investigate a possible involvement of Ect2 in post-mitotic midbodies fate determination. Indeed, considering the role of this protein in cytokinesis as well as its effect on cell polarity, Ect2 is a good candidate-substrate

for PRL-3 and could be the direct link between PRL-3 overexpression, alteration of the fate of midbody remnants and disruption of epithelial architecture.

V.2. From 3D cell culture models to *in vivo* studies

In this work we provide evidence for an important role of post-mitotic midbodies in the establishment and maintenance of the axis of polarity and consequently for lumen positioning. Moreover, we show that alteration in the position of post-mitotic midbodies is associated with ectopic lumen formation whereas their loss, probably by degradation, generates a phenotype that resembles luminal filling. Extremely attractive is the hypothesis that post-mitotic midbodies could behave as polarity landmark *in vivo* during epithelial tubular organ morphogenesis. Recently, a comprehensive study was published on kinesin motor proteins in which the localization of the midbody remnant marker MKLP1 has been analyzed in different tissues using transgenic mice expressing GFP-labeled MKLP1 (Maliga et al., 2013). The figures show multiple midbody remnants facing the luminal space in the embryonic neuroepithelium and in the intestinal crypt (Fig. V.1A,B). However, post-mitotic midbodies were undetectable in other tissues such as liver and kidney (Fig. V.1C,D). Moreover the authors did not contextualize the data in reference to epithelial cell polarity.

To confirm if the mechanism of midbody-determined lumen localization is relevant during mammalian epithelial tubulogenesis and to test the attractive hypothesis that PRL-3 overexpression could drive epithelial tumor formation by altering post-mitotic midbodies fate, we are planning to use in vivo and ex vivo mouse-derived models. To this end, we are going to generate PRL-3 overexpressing mice, in which the transgene expression is under the control of an inducible promoter and can be selectively activated in defined epithelial tissues. These experiments will probably answer if PRL-3 is a classical oncogene and could reveal a completely new mechanism of tumorigenesis based on midbody remnants fate alteration.

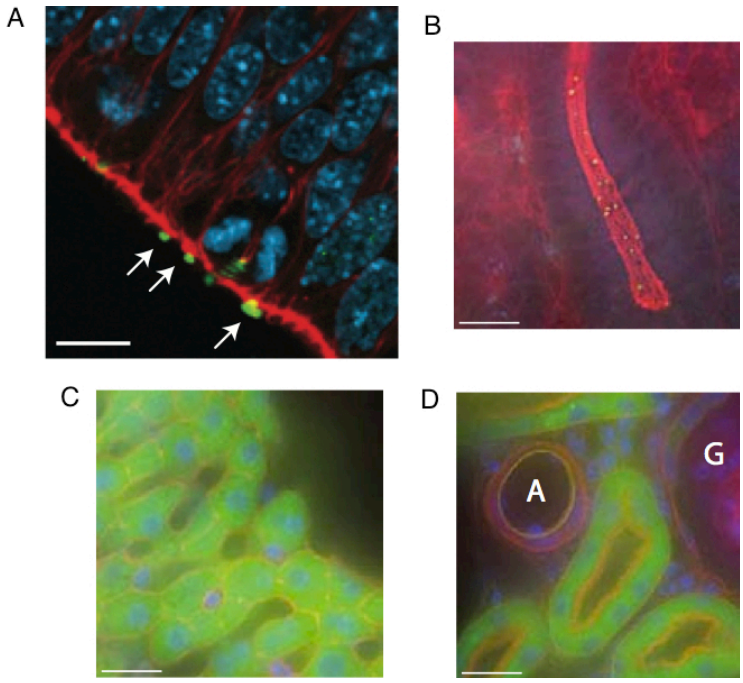

Figure V.1. Midbody remnants localizazion and tissue distrubution in MKLP1-GFP transgenic mice. *(**A**) Confocal image of mouse embryonic neuroepithelium stained for DNA (blue) and actin (red). Native GFP-MKLP1 staining (green) shows multiple midbody remnants facing the extracellular space (arrows). (**B**) Section of intestinal crypt stained for actin (red) and GFP-MKLP1 (green). (**C**,**D**) Tissue sections of liver and kidney with artery (A) and glomerulus (G) labeled. MKLP1 staining (green) results diffuse with undetectable midbody remnants. Reprinted by permission from Macmillan Publishers Ltd: Maliga et al., copyright 2013, Nature Publishing Group.*

Summary

Dynamic events of protein and lipid phosphorylation and dephosphorylation are involved virtually in all cellular signaling networks and transduction pathways. Kinases are the enzymes that catalyze phosphorylation reactions, while phosphatases are responsible for phosphate hydrolysis from the substrates. Defective or inappropriate activity of phosphatases contributes to the development of many human diseases, including cancer. PRL-3 is a plasma membrane-associated dual specificity phosphatase that exhibits a highly restricted and tightly regulated expression pattern. Additionally, PRL-3 is an emerging prognostic marker for cancer progression and a promising therapeutic target. Although in the last decade numerous clinical studies have extensively validated the causative role of PRL-3 in cancer metastasis, to date its substrate(s) and the direct downstream transduction pathways affected by PRL-3 overexpression are still elusive.

The first part of this work concerns the *in vitro* characterization of PRL-3 phosphatase activity towards phosphopeptides and phosphoinositides. We show that PRL-3 does not present any activity against the library of phosphopeptides tested, while it robustly dephosphorylates the phosphoinositide PtdIns(4,5)P_2. Moreover, our experimental results and molecular docking studies suggest that PRL-3 is a phosphatidylinositol 5-phosphatase. Finally, structure-activity relationship studies correlate the PRL-3 phosphatase activity toward PI(4,5)P_2 with its ability to promote cell migration.

The second part of this work concerns the characterization of PRL-3 oncogenic activity with respect to epithelial cell polarity. Using an organotypic 3D-culture system, in which epithelial cells form highly organized spherical cysts, we show that overexpression of PRL-3 significantly affects epithelial morphogenesis leading to the development of cysts with ectopic lumens. Moreover, we prove that a remnant organelle from the cytokinesis process, the post-mitotic midbody, is the first polarization signal during cyst development. Finally, we show that PRL-3 over-expression generates major defects in epithelial cell polarization by interfering with the fate of post-mitotic midbodies.

In conclusion, we show that PRL-3 could be a new phosphoinositide phosphatase and that its overexpression affects epithelial cell polarization by altering post-mitotic midbody fate, suggesting a novel mechanism for epithelial tumorigenesis.

Samenvatting

Dynamische fosforylering en de-fosforylering van eiwitten en vetten liggen ten grondslag aan vrijwel alle cellulaire signalerings routes. Kinases zijn de enzymen die fosforylering katalyseren, terwijl fosfatases zorg dragen voor de hydrolysering van fosfaat-groepen van substraten. Verstoorde activiteit van fosfatases dragen bij aan de ontwikkeling van verscheidene ziektes, waaronder kanker. PRL-3 is een bi-specifiek fosfatase dat gebonden is aan de cel membraan, en waarvan de expressie strikt gereguleerd is. Daarnaast wordt PRL-3 in toenemende mate beschouwd als een indicator voor kanker progressie, en daarmee als een veelbelovende target voor mogelijke therapie. Hoewel een groot aantal klinische studies gedurende de laatste 10 jaar het causale verband hebben aangetoond tussen PRL-3 en metastase, is tot op heden onbekend welke substraten en signaleringsroutes gereguleerd worden door over-expressie van PRL-3.

Het eerste deel van dit werk betreft de karakterisatie van de enzymatische activiteit van PRL-3 ten opzichte van fosfopeptiden en fosfoinositiden. We tonen aan dat PRL-3 geen activiteit vertoont voor de groep fosfopeptiden die we hebben getest, maar dat het zeer actief het fosfoinositide PtdIns(4,5)P_2 defosforyleert. Bovendien suggereren onze experimenten en docking studies dat PRL-3 een fosfatidylinositol 5-fosfatase is. Ten slotte tonen structuur-activiteitsstudies aan dat de fosfatase activiteit van PRL-3 ten opzichte van PI(4,5)P_2 correleert met bevordering van cel migratie.

Het tweede deel van dit werk betreft de karakterisatie van de oncogene activiteit van PRL-3 met betrekking tot polariteit van epitheel cellen. Met behulp van een organotypisch 3-dimensionaal cultuur systeem, waarin epitheel cellen zich organiseren in bolvormige cysten, tonen we aan dat over-expressie van PRL-3 de morfogenese van deze cellen beinvloedt, wat leidt tot de vorming van cysten met een ectopisch lumen. Bovendien tonen we aan dat een deel van het orgaan dat onstaat bij celdeling, de post-mitotische midbody, het eerste signaal is voor polarisatie gedurende ontwikkeling van de cyste. Ten slotte laten we zien dat over-expressie van PRL-3 leidt tot sterke afwijkingen in polarisatie van epitheel cellen door aan te grijpen op post-mitotische midbodies.

Concluderend hebben we aangetoond dat PRL-3 een nieuw fosfoinositide-fosfatase is, en dat de verhoogde concentratie ervan polarisatie van epitheel cellen verstoort door mis-localisatie van de midbody. Dit veronderstelt een nieuw mechanisme van tumor vorming.

References (for Chapters I and V)

Al-Aidaroos, A.Q.O., and Zeng, Q. (2010). PRL-3 phosphatase and cancer metastasis. Journal of Cellular Biochemistry *111*, 1087–1098.

Alonso, A., Sasin, J., Bottini, N., Friedberg, I., Friedberg, I., Osterman, A., Godzik, A., Hunter, T., Dixon, J., and Mustelin, T. (2004). Protein tyrosine phosphatases in the human genome. Cell *117*, 699–711.

Apodaca, G. (2010). Opening ahead: early steps in lumen formation revealed. Nature Cell Biology *12*, 1026–1028.

Apodaca, G., Gallo, L.I., and Bryant, D.M. (2012). Role of membrane traffic in the generation of epithelial cell asymmetry. Nature Cell Biology *14*, 1235–1243.

Aranda, V., Nolan, M.E., and Muthuswamy, S.K. (2008). Par complex in cancer: a regulator of normal cell polarity joins the dark side. Oncogene *27*, 6878–6887.

Bagnat, M., Cheung, I.D., Mostov, K.E., and Stainier, D.Y.R. (2007). Genetic control of single lumen formation in the zebrafish gut. Nature Cell Biology *9*, 954–960.

Balla, T. (2013). Phosphoinositides: tiny lipids with giant impact on cell regulation. Physiological Reviews *93*, 1019–1137.

Basak, S., Jacobs, S.B.R., Krieg, A.J., Pathak, N., Zeng, Q., Kaldis, P., Giaccia, A.J., and Attardi, L.D. (2008). The metastasis-associated gene Prl-3 is a p53 target involved in cell-cycle regulation. Molecular Cell *30*, 303–314.

Baum, B., and Georgiou, M. (2011). Dynamics of adherens junctions in epithelial establishment, maintenance, and remodeling. The Journal of Cell Biology *192*, 907–917.

Berridge, M.J., and Irvine, R.F. (1987). Inositol trisphosphate as a second messenger in signal transduction. Nature *494*, 39–51.

Bessette, D.C., Wong, P.C.W., and Pallen, C.J. (2007). PRL-3: a metastasis-associated phosphatase in search of a function. Cells, Tissues, Organs *185*, 232–236.

Bessette, D.C., Qiu, D., and Pallen, C.J. (2008). PRL PTPs: mediators and markers of cancer progression. Cancer Metastasis Reviews *27*, 231–252.

Boivin, B., and Tonks, N.K. (2010). Analysis of the redox regulation of protein tyrosine phosphatase superfamily members utilizing a cysteinyl-labeling assay. Methods in Enzymology *474*, 35–50.

Brautigan, D.L. (2013). Protein Ser/Thr phosphatases--the ugly ducklings of cell signalling. The FEBS Journal *280*, 324–345.

Brien, L.E.O., Zegers, M.M.P., and Mostov, K.E. (2002). Building epithelial architecture: insights from three-dimensional culture models. Nature Reviews Molecular Cell Biology *3*, 1–7.

Bryant, D.M., and Mostov, K.E. (2008). From cells to organs: building polarized tissue. Nature Reviews. Molecular Cell Biology *9*, 887–901.

Bryant, D.M., Datta, A., Rodríguez-Fraticelli, A.E., Peränen, J., Martín-Belmonte, F., and Mostov, K.E. (2010). A molecular network for de novo generation of the apical surface and lumen. Nature Cell Biology *12*, 1035–1045.

Bunney, T.D., and Katan, M. (2010). Phosphoinositide signalling in cancer: beyond PI3K and PTEN. Nature Reviews. Cancer *10*, 342–352.

Burstein, H.J., Polyak, K., Wong, J.S., Lester, S.C., and and Kaelin, C.M. (2004). Ductal Carcinoma in Situ of the Breast. The New England Journal of Medicine 1430–1441.

Carracedo, A., and Pandolfi, P.P. (2008). The PTEN-PI3K pathway: of feedbacks and cross-talks. Oncogene *27*, 5527–5541.

Chen, X., and Macara, I.G. (2005). Par-3 controls tight junction assembly through the Rac exchange factor Tiam1. Nature Cell Biology *7*, 262 – 269.

Chen, C.-T., Ettinger, A.W., Huttner, W.B., and Doxsey, S.J. (2013). Resurrecting remnants: the lives of post-mitotic midbodies. Trends in Cell Biology *23*, 118–128.

Choi, M.-S., Min, S.-H., Jung, H., Lee, J.D., Lee, T.H., Lee, H.K., and Yoo, O.-J. (2011). The essential role of FKBP38 in regulating phosphatase of regenerating liver 3 (PRL-3) protein stability. Biochemical and Biophysical Research Communications *406*, 305–309.

Cohen, P. (2002). The origins of protein phosphorylation. Nature Cell Biology *4*, 127–130.

Cohen, D., Rodriguez-Boulan, E., and Müsch, A. (2004). Par-1 promotes a hepatic mode of apical protein trafficking in MDCK cells. Proceedings of the National Academy of Sciences of the United States of America *101*, 13792–13797.

Comer, F.I., and Parent, C.A. (2007). Phosphoinositides specify polarity during epithelial organ development. Cell *128*, 239–240.

Craene, B. De, and Berx, G. (2013). Regulatory networks defining EMT during cancer initiation and progression. Nat Rev Cancer *13*, 97–110.

Czech, M.P. (2000). PIP2 and PIP3: complex roles at the cell surface. Cell *100*, 603–606.

Datta, A., Bryant, D.M., and Mostov, K.E. (2011). Molecular regulation of lumen morphogenesis. Current Biology *21*, R126–36.

Debnath, J., and Brugge, J.S. (2005). Modelling glandular epithelial cancers in three-dimensional cultures. Nature Reviews Cancer *5*, 675–688.

Debnath, J., Mills, K.R., Collins, N.L., Reginato, M.J., Muthuswamy, S.K., and Brugge, J.S. (2002). The role of apoptosis in creating and maintaining luminal space within normal and oncogene-expressing mammary acini. Cell *111*, 29–40.

Di Paolo, G., and De Camilli, P. (2006). Phosphoinositides in cell regulation and membrane dynamics. Nature *443*, 651–657.

Dong, Y., Zhang, L., Zhang, S., Bai, Y., Chen, H., Sun, X., Yong, W., Li, W., Colvin, S.C., Rhodes, S.J., et al. (2012). Phosphatase of regenerating liver 2 (PRL2) is essential for placenta development by downregulating PTEN (phosphatase and tensin homologue deleted on chromosome 10) and activating Akt. The Journal of Biological Chemistry *2*, 11–15.

Dumaual, C.M., Sandusky, G.E., Crowell, P.L., and Randall, S.K. (2006). Cellular localization of PRL-1 and PRL-2 gene expression in normal adult human tissues. The Journal of Histochemistry and Cytochemistry : Official Journal of the Histochemistry Society *54*, 1401–1412.

Feng, W., Wu, H., Chan, L.-N., and Zhang, M. (2008). Par-3-mediated junctional localization of the lipid phosphatase PTEN is required for cell polarity establishment. The Journal of Biological Chemistry *283*, 23440–23449.

Field, S.J., Madson, N., Kerr, M.L., Galbraith, K.A.A., Kennedy, C.E., Tahiliani, M., Wilkins, A., and Cantley, L.C. (2005). PtdIns(4,5)P2 functions at the cleavage furrow during cytokinesis. Current Biology *15*, 1407–1412.

Fiordalisi, J.J., Keller, P.J., and Cox, A.D. (2006). PRL tyrosine phosphatases regulate rho family GTPases to promote invasion and motility. Cancer Research *66*, 3153–3161.

Fiordalisi, J.J., Dewar, B.J., Graves, L.M., Madigan, J.P., and Cox, A.D. (2013). Src-mediated phosphorylation of the tyrosine phosphatase PRL-3 is required for PRL-3 promotion of Rho activation, motility and invasion. PloS One *8*, e64309.

Forte, E., Orsatti, L., Talamo, F., Barbato, G., De Francesco, R., and Tomei, L. (2008). Ezrin is a specific and direct target of protein tyrosine phosphatase PRL-3. Biochimica et Biophysica Acta *1783*, 334–344.

Gassama-Diagne, A., Yu, W., ter Beest, M., Martin-Belmonte, F., Kierbel, A., Engel, J., and Mostov, K. (2006). Phosphatidylinositol-3,4,5-trisphosphate regulates the formation of the basolateral plasma membrane in epithelial cells. Nature Cell Biology *8*, 963–970.

Gromley, A., Yeaman, C., Rosa, J., Redick, S., Chen, C.-T., Mirabelle, S., Guha, M., Sillibourne, J., and Doxsey, S.J. (2005). Centriolin anchoring of exocyst and SNARE complexes at the midbody is required for secretory-vesicle-mediated abscission. Cell *123*, 75–87.

Guo, K., Li, J., Wang, H., Osato, M., Tang, J.P., Quah, S.Y., Gan, B.Q., and Zeng, Q. (2006). PRL-3 initiates tumor angiogenesis by recruiting endothelial cells in vitro and in vivo. Cancer Research *66*, 9625–9635.

Guzińska-Ustymowicz, K., and Pryczynicz, A. (2011). PRL-3, an emerging marker of carcinogenesis, is strongly associated with poor prognosis. Anti-Cancer Agents in Medicinal Chemistry *11*, 99–108.

He, B., and Guo, W. (2009). The exocyst complex in polarized exocytosis. Current Opinion in Cell Biology *21*, 537–542.

Humphreys, R.C., Krajewska, M., Krnacik, S., Jaeger, R., Weiher, H., Krajewski, S., Reed, J.C., and Rosen, J.M. (1996). Apoptosis in the terminal endbud of the murine mammary gland: a mechanism of ductal morphogenesis. Development *122*, 4013–4022.

Jacoby, M., Cox, J.J., Gayral, S., Hampshire, D.J., Ayub, M., Blockmans, M., Pernot, E., Kisseleva, M. V, Compère, P., Schiffmann, S.N., et al. (2009). INPP5E mutations cause primary cilium signaling defects, ciliary instability and ciliopathies in human and mouse. Nature Genetics *41*, 1027–1031.

Jaulin, F., and Kreitzer, G. (2010). KIF17 stabilizes microtubules and contributes to epithelial morphogenesis by acting at MT plus ends with EB1 and APC. The Journal of Cell Biology *190*, 443–460.

Jaulin, F., Xue, X., Rodriguez-Boulan, E., and Kreitzer, G. (2007). Polarization-dependent selective transport to the apical membrane by KIF5B in MDCK cells. Developmental Cell *13*, 511–522.

Jiang, Y., Liu, X.-Q., Rajput, A., Geng, L., Ongchin, M., Zeng, Q., Taylor, G.S., and Wang, J. (2011). Phosphatase PRL-3 is a direct regulatory target of TGFbeta in colon cancer metastasis. Cancer Research *71*, 234–244.

Kato, H., Semba, S., Miskad, U. a, Seo, Y., Kasuga, M., and Yokozaki, H. (2004). High expression of PRL-3 promotes cancer cell motility and liver metastasis in human colorectal cancer: a predictive molecular marker of metachronous liver and lung metastases. Clinical Cancer Research *10*, 7318–7328.

Kisseleva, M. V, Wilson, M.P., and Majerus, P.W. (2000). The isolation and characterization of a cDNA encoding phospholipid-specific inositol polyphosphate 5-phosphatase. The Journal of Biological Chemistry *275*, 20110–20116.

Kolmodin, K., and Aqvist, J. (2001). The catalytic mechanism of protein tyrosine phosphatases revisited. FEBS Letters *498*, 208–213.

Krndija, D., Münzberg, C., Maass, U., Hafner, M., Adler, G., Kestler, H. a, Seufferlein, T., Oswald, F., and von Wichert, G. (2012). The phosphatase of regenerating liver 3 (PRL-3) promotes cell migration through Arf-activity-dependent stimulation of integrin α5 recycling. Journal of Cell Science *125*, 3883–3892.

Kuo, T.-C., Chen, C.-T., Baron, D., Onder, T.T., Loewer, S., Almeida, S., Weismann, C.M., Xu, P., Houghton, J.-M., Gao, F.-B., et al. (2011). Midbody accumulation through evasion of autophagy contributes to cellular reprogramming and tumorigenicity. Nature Cell Biology *13*, 1214–1223.

Kutateladze, T.G. (2010). Translation of the phosphoinositide code by PI effectors. Nature Chemical Biology *6*, 507–513.

Lanier, L.M., and Gertler, F.B. (2000). Actin cytoskeleton: thinking globally, actin' locally. Current Biology *10*, R655–R657.

Le Roy, C., and Wrana, J.L. (2005). Clathrin- and non-clathrin-mediated endocytic regulation of cell signalling. Nature Reviews. Molecular Cell Biology *6*, 112–126.

Leung, C.T., and Brugge, J.S. (2012). Outgrowth of single oncogene-expressing cells from suppressive epithelial environments. Nature *482*, 410–413.

Li, X., Wilmanns, M., Thornton, J., and Köhn, M. (2013). Elucidating human phosphatase-substrate networks. Science Signaling *6*, rs10.

Liang, F., Liang, J., Wang, W.-Q., Sun, J.-P., Udho, E., and Zhang, Z.-Y. (2007). PRL3 promotes cell invasion and proliferation by down-regulation of Csk leading to Src activation. The Journal of Biological Chemistry *282*, 5413–5419.

Lin, D., Edwards, a S., Fawcett, J.P., Mbamalu, G., Scott, J.D., and Pawson, T. (2000). A mammalian PAR-3-PAR-6 complex implicated in Cdc42/Rac1 and aPKC signalling and cell polarity. Nature Cell Biology *2*, 540–547.

Liu, X.F., Ohno, S., and Miki, T. (2006). Nucleotide exchange factor ECT2 regulates epithelial cell polarity. Cell Signaling.

Liu, Y., Zhou, J., Chen, J., Gao, W., Le, Y., Ding, Y., and Li, J. (2009). PRL-3 promotes epithelial mesenchymal transition by regulating cadherin directly. Cancer Biology & Therapy *8*, 1352–1359.
Logan, M.R., and Mandato, C. a (2006). Regulation of the actin cytoskeleton by PIP2 in cytokinesis. Biology of the Cell *98*, 377–388.

Lubarsky, B., and Krasnow, M.A. (2003). Tube morphogenesis: making and shaping biological tubes. Cell *112*, 19–28.

Maehama, T. (1998). The Tumor Suppressor, PTEN/MMAC1, Dephosphorylates the Lipid Second Messenger, Phosphatidylinositol 3,4,5-Trisphosphate. Journal of Biological Chemistry *273*, 13375–13378.

Mailleux, A.A., Overholtzer, M., Schmelzle, T., Bouillet, P., Strasser, A., and Brugge, J.S. (2007). BIM regulates apoptosis during mammary ductal morphogenesis, and its absence reveals alternative cell death mechanisms. Developmental Cell *12*, 221–234.

Majerus, P.W., and York, J.D. (2009). Phosphoinositide phosphatases and disease. Journal of Lipid Research *50 Suppl*, S249–54.

Maliga, Z., Junqueira, M., Toyoda, Y., Ettinger, A., Mora-Bermúdez, F., Klemm, R.W., Vasilj, A., Guhr, E., Ibarlucea-Benitez, I., Poser, I., et al. (2013). A genomic toolkit to investigate kinesin and myosin motor function in cells. Nature Cell Biology *15*, 325–334.

Martin-belmonte, F., Gassama, A., Datta, A., Yu, W., Rescher, U., Gerke, V., and Mostov, K. (2007). PTEN-Mediated Apical Segregation of Phosphoinositides Controls Epithelial Morphogenesis through Cdc42. Cell *128*, 383–397.

Matter, K., and Balda, M.S. (2003). Signalling to and from tight junctions. Nature Reviews Molecular Cell Biology *4*, 225–236.

Matter, W.F., Estridge, T., Zhang, C., Belagaje, R., Stancato, L., Dixon, J., Johnson, B., Bloem, L., Pickard, T., Donaghue, M., et al. (2001). Role of PRL-3, a human muscle-specific tyrosine phosphatase, in angiotensin-II signaling. Biochemical and Biophysical Research Communications *283*, 1061–1068.

McCaffrey, L.M., and Macara, I.G. (2009). Widely conserved signaling pathways in the establishment of cell polarity. Cold Spring Harbor Perspectives in Biology *1*, a001370.

McLaughlin, S., Wang, J., Gambhir, A., and Murray, D. (2002). PIP2 and proteins: interactions, organization, and information flow. Annual Review of Biophysics and Biomolecular Structure *31*, 151–175.

Meder, D., Shevchenko, A., Simons, K., and Füllekrug, J. (2005). Gp135/podocalyxin and NHERF-2 participate in the formation of a preapical domain during polarization of MDCK cells. The Journal of Cell Biology *168*, 303–313.

Min, S.-H., Kim, D.M., Heo, Y.-S., Kim, H.M., Kim, I.-C., and Yoo, O.-J. (2010). Downregulation of p53 by phosphatase of regenerating liver 3 is mediated by MDM2 and PIRH2. Life Sciences *86*, 66–72.

Ming, J., Liu, N., Gu, Y., Qiu, X., and Wang, E.-H. (2009). PRL-3 facilitates angiogenesis and metastasis by increasing ERK phosphorylation and up-regulating the levels and activities of Rho-A/C in lung cancer. Pathology *41*, 118–126.

Mizuno, K., Suzuki, A., Hirose, T., Kitamura, K., Kutsuzawa, K., Futaki, M., Amano, Y., and Ohno, S. (2003). Self-association of PAR-3-mediated by the conserved N-terminal domain contributes to the development of epithelial tight junctions. The Journal of Biological Chemistry *278*, 31240–31250.

Mizuuchi, E., Semba, S., Kodama, Y., and Yokozaki, H. (2009). Down-modulation of keratin 8 phosphorylation levels by PRL-3 contributes to colorectal carcinoma progression. International Journal of Cancer *124*, 1802–1810.

Nagai-tamai, Y., Mizuno, K., Hirose, T., Suzuki, A., and Ohno, S. (2002). Regulated protein – protein interaction between aPKC and PAR-3 plays an essential role in the polarization of epithelial cells. Genes to Cells 1161–1171.

Nakayama, M., Goto, T.M., Sugimoto, M., Nishimura, T., Shinagawa, T., Ohno, S., Amano, M., and Kaibuchi, K. (2008). Rho-kinase phosphorylates PAR-3 and disrupts PAR complex formation. Developmental Cell *14*, 205–215.

Neisch, A.L., and Fehon, R.G. (2011). Ezrin, Radixin and Moesin: key regulators of membrane-cortex interactions and signaling. Current Opinion in Cell Biology *23*, 377–382.

Neto, H., and Gould, G.W. (2011). The regulation of abscission by multi-protein complexes. Journal of Cell Science *124*, 3199–3207.

Nishimura, A., and Linder, M.E. (2013). Identification of a novel prenyl, palmitoyl CaaX modification of Cdc42 that regulates RhoGDI binding. Molecular and Cellular Biology *33*, 1417–1429.

Noda, Y., Okada, Y., Saito, N., Setou, M., Xu, Y., Zhang, Z., and Hirokawa, N. (2001). KIFC3, a microtubule minus end-directed motor for the apical transport of annexin XIIIb-associated Triton-insoluble membranes. The Journal of Cell Biology *155*, 77–88.

O'Brien, L.E., Jou, T.S., Pollack, a L., Zhang, Q., Hansen, S.H., Yurchenco, P., and Mostov, K.E. (2001). Rac1 orientates epithelial apical polarity through effects on basolateral laminin assembly. Nature Cell Biology *3*, 831–838.

Oceguera-Yanez, F., Kimura, K., Yasuda, S., Higashida, C., Kitamura, T., Hiraoka, Y., Haraguchi, T., and Narumiya, S. (2005). Ect2 and MgcRacGAP regulate the activation and function of Cdc42 in mitosis. The Journal of Cell Biology *168*, 221–232.

Ooms, L.M., Horan, K. a, Rahman, P., Seaton, G., Gurung, R., Kethesparan, D.S., and Mitchell, C. a (2009). The role of the inositol polyphosphate 5-phosphatases in cellular function and human disease. The Biochemical Journal *419*, 29–49.

Orsatti, L., Forte, E., Tomei, L., Caterino, M., Pessi, A., and Talamo, F. (2009). 2-D Difference in gel electrophoresis combined with Pro-Q Diamond staining: a successful approach for the identification of kinase/phosphatase targets. Electrophoresis *30*, 2469–2476.

Paris, L., Tonutti, L., Vannini, C., and Bazzoni, G. (2008). Structural organization of the tight junctions. Biochimica et Biophysica Acta *1778*, 646–659.

Patterson, K.I., Brummer, T., Brien, P.M.O., and Daly, R.J. (2009). Dual-specificity phosphatases : critical regulators with diverse cellular targets. Biochemstry Journal *418*, 475–489.

Peng, L., Jin, G., Wang, L., Guo, J., Meng, L., and Shou, C. (2006). Identification of integrin alpha1 as an interacting protein of protein tyrosine phosphatase PRL-3. Biochemical and Biophysical Research Communications *342*, 179–183.

Peng, L., Xing, X., Li, W., Qu, L., Meng, L., Lian, S., Jiang, B., Wu, J., and Shou, C. (2009). PRL-3 promotes the motility, invasion, and metastasis of LoVo colon cancer cells through PRL-3-integrin β1-ERK1/2 and-MMP2 signaling. Molecular Cancer *8*, 110.

Pollarolo, G., Schulz, J.G., Munck, S., and Dotti, C.G. (2011). Cytokinesis remnants define first neuronal asymmetry in vivo. Nature Neuroscience *14*, 1525–1533.

Pulido, R., Stoker, A.W., and Hendriks, W.J.A.J. (2013). PTPs emerge as PIPs: protein tyrosine phosphatases with lipid-phosphatase activities in human disease. Human Molecular Genetics 1–11.

Qian, F., Li, Y.-P., Sheng, X., Zhang, Z.-C., Song, R., Dong, W., Cao, S.-X., Hua, Z.-C., and Xu, Q. (2007). PRL-3 siRNA inhibits the metastasis of B16-BL6 mouse melanoma cells in vitro and in vivo. Molecular Medicine Cambridge Mass *13*, 151–159.

Qin, Y., Meisen, W.H., Hao, Y., and Macara, I.G. (2010). Tuba, a Cdc42 GEF, is required for polarized spindle orientation during epithelial cyst formation. The Journal of Cell Biology *189*, 661–669.

Ridley, A.J. (2012). Historical overview of Rho GTPases. Methods in Molecular Biology Clifton NJ *827*, 3–12.

Rios, P., Li, X., and Köhn, M. (2013). Molecular mechanisms of the PRL phosphatases. FEBS Journal *280*, 505–524.

Roignot, J., Peng, X., and Mostov, K. (2013). Polarity in mammalian epithelial morphogenesis. Cold Spring Harbor Perspectives in Biology *5*, a013789.

Roskoski, R. (2004). Src protein-tyrosine kinase structure and regulation. Biochemical and Biophysical Research Communications *324*, 1155–1164.

Saarikangas, J., Zhao, H., and Lappalainen, P. (2010). Regulation of the actin cytoskeleton-plasma membrane interplay by phosphoinositides. Physiological Reviews *90*, 259–289.

Saha, S., Bardelli, A., Buckhaults, P., Velculescu, V.E., Rago, C., St Croix, B., Romans, K.E., Choti, M.A., Lengauer, C., Kinzler, K.W., et al. (2001). A Phosphatase Associated with Metastasis of Colorectal Cancer formed global gene expression profiles of. Science *294*, 1343–1346.

Saito, S., Liu, X.-F., Kamijo, K., Raziuddin, R., Tatsumoto, T., Okamoto, I., Chen, X., Lee, C.-C., Lorenzi, M. V, Ohara, N., et al. (2004). Deregulation and mislocalization of the cytokinesis regulator ECT2 activate the Rho signaling pathways leading to malignant transformation. The Journal of Biological Chemistry *279*, 7169–7179.

Schlu, M.A., Pfarr, C.S., Pieczynski, J., Whiteman, E.L., Hurd, T.W., Fan, S., Liu, C., and Margolis, B. (2009). Trafficking of Crumbs3 during Cytokinesis Is Crucial for Lumen Formation. Mol. Biol. Cell *20*, 4652–4663.

Schlüter, M. a, and Margolis, B. (2009). Apical lumen formation in renal epithelia. Journal of the American Society of Nephrology *20*, 1444–1452.

Schulzke, J.-D., and Fromm, M. (2009). Tight junctions: molecular structure meets function. Annals of the New York Academy of Sciences *1165*, 1–6.

Seifried, A., Schultz, J., and Gohla, A. (2013). Human HAD phosphatases: structure, mechanism, and roles in health and disease. The FEBS Journal *280*, 549–571.

Semba, S., Mizuuchi, E., and Yokozaki, H. (2010). Requirement of phosphatase of regenerating liver-3 for the nucleolar localization of nucleolin during the progression of colorectal carcinoma. Cancer Science *101*, 2254–2261.

Sharma, N., Low, S.H., Misra, S., Pallavi, B., and Weimbs, T. (2006). Apical targeting of syntaxin 3 is essential for epithelial cell polarity. The Journal of Cell Biology *173*, 937–948.

Shattil, S.J., Kim, C., and Ginsberg, M.H. (2010). The final steps of integrin activation: the end game. Nature Reviews Molecular Cell Biology *11*, 288–300.

Shewan, A., Eastburn, D.J., and Mostov, K. (2011). Phosphoinositides in cell architecture. Cold Spring Harbor Perspectives in Biology *3*, a004796.

Shin, K., Fogg, V.C., and Margolis, B. (2006). Tight junctions and cell polarity. Annual Review of Cell and Developmental Biology *22*, 207–235.

Sit, S.-T., and Manser, E. (2011). Rho GTPases and their role in organizing the actin cytoskeleton. Journal of Cell Science *124*, 679–683.

Skinner, A.L., Vartia, A. a, Williams, T.D., and Laurence, J.S. (2009). Enzyme activity of phosphatase of regenerating liver is controlled by the redox environment and its C-terminal residues. Biochemistry *48*, 4262–4272.

Song, M.S., Salmena, L., and Pandolfi, P.P. (2012). The functions and regulation of the PTEN tumour suppressor. Nature Reviews Molecular Cell Biology *13*, 283–296.

St Johnston, D., and Ahringer, J. (2010). Cell polarity in eggs and epithelia: parallels and diversity. Cell *141*, 757–774.

Stephens, B.J., Han, H., Gokhale, V., and Von Hoff, D.D. (2005). PRL phosphatases as potential molecular targets in cancer. Molecular Cancer Therapeutics *4*, 1653–1661.

Sun, J.-P., Luo, Y., Yu, X., Wang, W.-Q., Zhou, B., Liang, F., and Zhang, Z.-Y. (2007). Phosphatase activity, trimerization, and the C-terminal polybasic region are all required for PRL1-mediated cell growth and migration. The Journal of Biological Chemistry *282*, 29043–29051.

Suzuki, A., and Ohno, S. (2006). The PAR-aPKC system: lessons in polarity. Journal of Cell Science *119*, 979–987.

Takada, Y., Ye, X., and Simon, S. (2007). The integrins. Genome Biology *8*, 215.

Tamguney, T., and Stokoe, D. (2007). New insights into PTEN. Journal of Cell Science *120*, 4071–4079.

Thomas, J.E., Soriano, P., and Brugge, J.S. (1991). Phosphorylation of c-Src on tyrosine 527 by another protein tyrosine kinase. Science *254*, 568–571.

Tian, W., Qu, L., Meng, L., Liu, C., Wu, J., and Shou, C. (2012). Phosphatase of regenerating liver-3 directly interacts with integrin β1 and regulates its phosphorylation at tyrosine 783. BMC Biochemistry *13*, 22.

Tonks, N.K. (2003). PTP1B: From the sidelines to the front lines! FEBS Letters *546*, 140–148.

Tonks, N.K. (2006). Protein tyrosine phosphatases: from genes, to function, to disease. Nature Reviews. Molecular Cell Biology *7*, 833–846.

Tonks, N.K. (2013). Protein tyrosine phosphatases--from housekeeping enzymes to master regulators of signal transduction. The FEBS Journal *280*, 346–378.

Torkko, J.M., Manninen, A., Schuck, S., and Simons, K. (2008). Depletion of apical transport proteins perturbs epithelial cyst formation and ciliogenesis. Journal of Cell Science *121*, 1193–1203.

Treyer, A., and Müsch, A. (2013). Hepatocyte Polarity. Comprehensive Physiology *3*, 243–287.

Walls, C.D., Iliuk, A., Bai, Y., Wang, M., Tao, W.A., and Zhang, Z.-Y. (2013). Phosphatase of Regenerating Liver 3 (PRL3) provokes a tyrosine phosphoproteome to drive pro-metastatic signal transduction. Molecular & Cellular Proteomics *3*.

Wang, H., Quah, S.Y., Dong, J.M., Manser, E., Tang, J.P., and Zeng, Q. (2007). PRL-3 down-regulates PTEN expression and signals through PI3K to promote epithelial-mesenchymal transition. Cancer Research *67*, 2922–2926.

Wang, H., Vardy, L.A., Tan, C.P., Loo, J.M., Guo, K., Li, J., Lim, S.G., Zhou, J., Chng, W.J., Ng, S.B., et al. (2010). PCBP1 suppresses the translation of metastasis-associated PRL-3 phosphatase. Cancer Cell *18*, 52–62.

Wu, H., Feng, W., Chen, J., Chan, L., Huang, S., and Zhang, M. (2007). PDZ Domains of Par-3 as Potential Phosphoinositide Signaling Integrators. Molecular Cell 886–898.

Wu, X., Zeng, H., Zhang, X., Zhao, Y., Sha, H., Ge, X., Zhang, M., Gao, X., and Xu, Q. (2004). Phosphatase of regenerating liver-3 promotes motility and metastasis of mouse melanoma cells. The American Journal of Pathology *164*, 2039–2054.

Xu, J., Cao, S., Wang, L., Xu, R., Chen, G., and Xu, Q. (2011). VEGF promotes the transcription of the human PRL-3 gene in HUVEC through transcription factor MEF2C. PLoS ONE *6*, e27165.

Yu, W., Datta, A., Leroy, P., O'Brien, L.E., Mak, G., Jou, T.-S., Matlin, K.S., Mostov, K.E., and Zegers, M.M.P. (2005). Beta1-integrin orients epithelial polarity via Rac1 and laminin. Molecular Biology of the Cell *16*, 433–445.

Yuan, T.L., and Cantley, L.C. (2008). PI3K pathway alterations in cancer: variations on a theme. Oncogene *27*, 5497–5510.

Yüce, O., Piekny, A., and Glotzer, M. (2005). An ECT2-centralspindlin complex regulates the localization and function of RhoA. The Journal of Cell Biology *170*, 571–582.

Zegers, M.M.P., O'Brien, L.E., Yu, W., Datta, A., and Mostov, K.E. (2003). Epithelial polarity and tubulogenesis in vitro. Trends in Cell Biology *13*, 169–176.

Zeng, Q., Si, X., Horstmann, H., Xu, Y., Hong, W., and Pallen, C.J. (2000). Prenylation-dependent association of protein-tyrosine phosphatases PRL-1, -2, and -3 with the plasma membrane and the early endosome. The Journal of Biological Chemistry *275*, 21444–21452.

Zeng, Q., Dong, J.-M., Guo, K., Li, J., Tan, H.-X., Koh, V., Pallen, C.J., Manser, E., and Hong, W. (2003). PRL-3 and PRL-1 promote cell migration, invasion, and metastasis. Cancer Research *63*, 2716–2722.

Zhang, X.C., Piccini, A., Myers, M.P., Van Aelst, L., and Tonks, N.K. (2012). Functional analysis of the protein phosphatase activity of PTEN. The Biochemical Journal *444*, 457–464.

Zhao, W.-B., Li, Y., Liu, X., Zhang, L.-Y., and Wang, X. (2008). Evaluation of PRL-3 expression, and its correlation with angiogenesis and invasion in hepatocellular carcinoma. International Journal of Molecular Medicine *22*, 187–192.

Zheng, P., Liu, Y.-X., Chen, L., Liu, X.-H., Xiao, Z.-Q., Zhao, L., Li, G.-Q., Zhou, J., Ding, Y.-Q., and Li, J.-M. (2010). Stathmin, a new target of PRL-3 identified by proteomic methods, plays a key role in progression and metastasis of colorectal cancer. Journal of Proteome Research *9*, 4897–4905.

Zheng, P., Meng, H.-M., Gao, W.-Z., Chen, L., Liu, X.-H., Xiao, Z.-Q., Liu, Y.-X., Sui, H.-M., Zhou, J., Liu, Y.-H., et al. (2011). Snail as a key regulator of PRL-3 gene in colorectal cancer. Cancer Biology & Therapy *12*, 742–749.

Zimmerman, M.W., Homanics, G.E., and Lazo, J.S. (2013). Targeted deletion of the metastasis-associated phosphatase Ptp4a3 (PRL-3) suppresses murine colon cancer. PLOS ONE *8*, e58300.

Zuo, X., Guo, W., and Lipschutz, J.H. (2009). The exocyst protein Sec10 is necessary for primary ciliogenesis and cystogenesis in vitro. Molecular Biology of the Cell *20*, 2522–2529.

List of publications

Peer reviewed papers:

Frosi Y, Anastasi S, Ballaro C, **Varsano G**, Castellani L, Maspero E, Polo S, Alema S, and Segatto O (2010) A two-tiered mechanism of EGFR inhibition by RALT/MIG6 via kinase suppression and receptor degradation. *The Journal of Cell Biology,* **189,** 557-571.

McParland V,* **Varsano G**,* Li X, Thornton J, Baby J, Aravind A, Meyer C, Pavic K, Rios P and Köhn M (2011) The metastasis-promoting phosphatase PRL-3 shows activity toward phosphoinositides. *Biochemistry,* **50,** 7579–7590.

Abstracts:

Rios P, **Varsano G** and Köhn M (2012) A chemical biology approach to study PRL-3-induced cell migration in mammalian cells. EMBO Chemical Biology, EMBL Heidelberg, Germany, 27-29 September 2012.

* Victoria McParland and Giulia Varsano contributed equally to this work.

Curriculum Vitae

PERSONAL INFORMATION

Name and Surname	Giulia Varsano	Work Address	EMBL Meyerhofstr. 1 69117 Heidelberg Germany
Date of Birth	21 December 1983	E-mail address	Varsano@embl.de
Nationality	Italian	Marital status	Not married
Telephone number	+49/062213878117	Children	None

EDUCATION

Bachelor Degree	Name Diploma: Genetics and Molecular Biology Date: July 2006 University: Sapienza Rome University Final dissertation: Neurotrophin and MicroRNA Promoter: Dr. S. Nasi
Master Degree	Name Diploma: Genetics and Molecular Biology Date: February 2009 University: Sapienza Rome University Final dissertation: Role of RALT/MIG6 in EGFR endocytosis Promoter: Dr. O. Segatto

EMPLOYMENT HISTORY

April 2009- December 2009	Research collaborator at the Italian National Cancer Institute Regina Elena (IFO-IRE), Department of Immunology, Rome, Italy. (Dr. O. Segatto Lab.) Research topic: Role of RALT/MIG6 in EGFR endocytosis
Since January 2010	Graduate student at the European Molecular Biology Laboratories (EMBL), Heidelberg, Germany. (Dr. M. Köhn Lab.) Research topic: Investigations towards understanding the molecular mechanisms that underlie PRL-3's role in tumorigenesis

License agreement

Rightslink Printable License

NATURE PUBLISHING GROUP LICENSE
TERMS AND CONDITIONS

Oct 29, 2013

This is a License Agreement between Giulia Varsano ("You") and Nature Publishing Group ("Nature Publishing Group") provided by Copyright Clearance Center ("CCC"). The license consists of your order details, the terms and conditions provided by Nature Publishing Group, and the payment terms and conditions.

All payments must be made in full to CCC. For payment instructions, please see information listed at the bottom of this form.

License Number	3258260176367
License date	Oct 29, 2013
Licensed content publisher	Nature Publishing Group
Licensed content publication	Nature Cell Biology
Licensed content title	A genomic toolkit to investigate kinesin and myosin motor function in cells
Licensed content author	Zoltan Maliga, Magno Junqueira, Yusuke Toyoda, Andreas Ettinger, Felipe Mora-Bermúdez, Robin W. Klemm
Licensed content date	Feb 17, 2013
Volume number	15
Issue number	3
Type of Use	reuse in a thesis/dissertation
Requestor type	academic/educational
Format	print
Portion	figures/tables/illustrations
Number of figures/tables /illustrations	2
High-res required	no
Figures	Figure 3, Figure S3
Author of this NPG article	no
Your reference number	
Title of your thesis / dissertation	Investigations towards understanding the molecular basis underlying PRL-3's role in tumorigenesis
Expected completion date	Dec 2013
Estimated size (number of pages)	100
Total	0.00 EUR
Terms and Conditions	

Rightslink Printable License

NATURE PUBLISHING GROUP LICENSE
TERMS AND CONDITIONS

Oct 29, 2013

This is a License Agreement between Giulia Varsano ("You") and Nature Publishing Group ("Nature Publishing Group") provided by Copyright Clearance Center ("CCC"). The license consists of your order details, the terms and conditions provided by Nature Publishing Group, and the payment terms and conditions.

All payments must be made in full to CCC. For payment instructions, please see information listed at the bottom of this form.

License Number	3258220437740
License date	Oct 29, 2013
Licensed content publisher	Nature Publishing Group
Licensed content publication	Nature
Licensed content title	Outgrowth of single oncogene-expressing cells from suppressive epithelial environments
Licensed content author	Cheuk T. Leung, Joan S. Brugge
Licensed content date	Feb 8, 2012
Volume number	482
Issue number	7385
Type of Use	reuse in a thesis/dissertation
Requestor type	academic/educational
Format	print
Portion	figures/tables/illustrations
Number of figures/tables /illustrations	1
High-res required	no
Figures	Figure 1.C
Author of this NPG article	no
Your reference number	
Title of your thesis / dissertation	Investigations towards understanding the molecular basis underlying PRL-3's role in tumorigenesis
Expected completion date	Dec 2013
Estimated size (number of pages)	100
Total	0.00 EUR